Spring 1-1-2010

Pointwise Extensions to the Zienkiewicz-Zhu Adaptive Refinement Procedure

Ryan Clarke Anderson
University of Colorado at Boulder, rcanderson3@gmail.com

POINTWISE EXTENSIONS TO THE ZIENKIEWICZ-ZHU ADAPTIVE REFINEMENT PROCEDURE

by

RYAN CLARKE ANDERSON

B.S., University of Colorado, 2010

M.S., University of Colorado, 2010

A thesis submitted to the Faculty of the Graduate School of the University of Colorado in partial fulfillment of the requirement for the degree of

Master of Science

Department of Civil, Environmental, and Architectural Engineering

2010

This thesis entitled:
Pointwise Extensions to the Zienkiewicz-Zhu Adaptive Refinement Procedure
written by Ryan Clarke Anderson
has been approved for the Department of Civil, Environmental, and Architectural Engineering

_____
Committee Chair: John O Dow

_____
Committee Member: Siva Mettupalayam

Date: _____

The final copy of this thesis has been examined by the signatories, and we find that both the content and the form meet acceptable presentation standards of scholarly work in the above mentioned discipline.

Anderson, Ryan Clarke (M.S., Civil, Environmental, and Architectural Engineering)

Pointwise Extensions to the Zienkiewicz-Zhu Adaptive Refinement Procedure

Thesis directed by Associate Professor John O. Dow

ABSTRACT

The two primary components of the Zienkiewicz and Zhu (ZZ) adaptive refinement procedure for upgrading finite element models are improved in this work. A new approach for identifying the improvements needed to produce a more accurate model that is based on determining the *in situ* modeling deficiencies contained in the individual elements is developed. A pointwise error estimator that has the same basis as the integrated error estimator that is used in the current form of the ZZ approach is presented.

The relative importance of the two primary components of the adaptive refinement process is reversed because of these developments. The refinement guide becomes the primary component, instead of the error estimator, because the new refinement guide is based on first principles instead of being a heuristic function of the error estimator.

The identified *in situ* modeling deficiencies of the individual elements is combined with the modeling capabilities of the element and the termination criterion to estimate the number of elements needed to improve the model to the desired level of accuracy. This reduces the role of the error estimator to satisfying the termination criterion.

The integrated error estimator in the existing form of the ZZ adaptive refinement procedure estimates the error in the strain energy content of the individual elements. The pointwise error estimator developed here is based on the inter-element jumps at the nodes in the finite element strain representations. This pointwise error estimator is simpler to compute and is

expressed in terms of the strain components. This type of metric is more useful to the analyst because the estimated error is expressed in terms of quantities that are central to solid mechanics.

The smoothed solution that is central to the ZZ approach is given a solid theoretical basis in this work. It is shown that the inter-element jumps are identical to the residuals produced by the failure of the finite element solution to satisfy the governing differential equation being solved. This means the smoothed solution definitively adds a portion of the discretization errors to the existing finite element solution. Thus, the smoothed solution is an improved solution.

DEDICATION

This work is dedicated to Danace, who has been with me through every step of this process. Danace, your presence in my life is the most amazing thing to happen to me. You are the steadying influence that has made this work a reality. I am lucky to have you by my side. Words could never fully express the depth of my love for you, or everything that your presence in my life means to me.

ACKNOWLEDGEMENTS

The author acknowledges John O Dow and his graduate students over the years. It is their work that laid the foundation for the insights upon which this thesis is built.

CONTENTS

TABLES

Table

FIGURES

Figure

CHAPTER 1

INTRODUCTION

A comprehensive overview of error estimation procedures in the finite element method is presented in Chapter 13 of reference 1 with a bibliography containing 77 references. The error estimation procedures are broadly categorized as recovery techniques and residual techniques.

Starting in 1988, Zienkiewicz and Zhu published a series of papers that contained the first practical approach to error analysis and adaptive refinement [2]. In the final version of this procedure, a smoothed solution is formed by averaging the finite element nodal strains at the inter-element nodes. The smoothed solution is considered to be a better solution than the discontinuous finite element strain distribution because it is continuous. In Chapter 6, the improvement in the smoothed solution is identified using results from the residual approach.

After the smoothed solution is formed, the strain energy contained in the difference between the smoothed and the discontinuous strain distribution is computed by integrating over the domain of the individual elements. This strain energy quantity is taken as an estimate of the error in the element. Then, a heuristic estimate of the number of elements needed to improve the solution to the desired level of accuracy is made [1]. In Chapter 8 of this work, new approaches for estimating the degree of refinement needed for the individual elements so the overall finite element model rapidly converges to a result that satisfies the termination criterion are presented.

The residual approach to error analysis is presented most cogently by Kelly in reference 3. In this presentation, Kelly assumes that any finite element solution, no matter how badly it represents the problem being analyzed, is the exact solution to some problem. Specifically, this

finite element solution, with its discontinuous strain distribution, is the exact solution to the problem being modeled that has been augmented with a fictitious set of distributed applied loads.

The fictitious distributed loads are taken to be equal to the residuals that exist on the domain of the individual elements when the finite element solution is substituted into the governing differential equation being solved. Furthermore, Kelly argues, the inter-element jumps in the discontinuous finite element strain distribution are due to these fictitious loads acting as equivalent nodal loads. This contention is derived and demonstrated in Chapter 4.

The objective of this work is to develop pointwise extensions to the Zienkiewicz-Zhu approaches to error analysis and model refinement.

In this work, improvements are made to both the error estimation process and the development of refinement guides. The error estimation process is given a stronger theoretical basis by integrating the recovery and residual approaches to error estimation to explain why the smoothed solution is a better solution than the finite element solution. The error estimator is functionally improved because it is a pointwise quantity. No integration is required in its computation. Furthermore, the pointwise error estimator is expressed in terms of strain quantities instead of strain energy quantities. As a result, the termination criterion can be directly related to failure criteria.

A new type of refinement guides is developed and demonstrated that estimates the number of subdivisions that must be given to each element, i.e., h-refinement, to satisfy the specified level of accuracy. This refinement guide identifies the modeling deficiencies in the individual elements by comparing smoothed solutions to the modeling capabilities of the element being evaluated. As such, this approach is a recovery technique.

The advantage of the refinement guides developed here is that they are not heuristic. They have a rational basis because they are based on first principles. The *in situ* performance of the individual elements is estimated by comparing the characteristics of an improvement to the finite element solution to the strain distribution that actually exists in the element being evaluated. Then, the estimated modeling deficiencies in the individual elements identified by this process are related to the termination criterion to identify the required level of refinement to produce an acceptable solution.

The developments presented here are based on the use of a physically interpretable notation that was introduced in 1983 [4]. This self-referential notation is the basis of procedures that were initially developed to evaluate lattice structures for the international space station [5, 6, 7]. The objective of this evaluation was to identify coupling between the various deformation patterns with the specific goal of eliminating truss configurations that coupled flexure with torsion. This was important to eliminate rotations when the Space Shuttle docked.

The evaluation of the trusses essentially inverted the finite element method. That is to say, the stiffness matrix is reduced in size and the independent variables are expressed in terms of strain components, i.e., ε_x , ε_y , and γ_{xy} . In a series of papers that culminated in a book, procedures for evaluating the modeling characteristics of individual elements were developed, alternate formulation procedures for forming finite element stiffness matrices were presented, and the finite element and finite difference methods were integrated. All of these advances are used in this work. [8 - 24]

The succeeding Chapters contain the following. Chapter 2 provides an intuitive introduction to the errors and their source in finite element models. The errors are seen as inter-

element jumps in the strain and they are shown to decrease when the finite element model is improved.

Chapter 3 introduces the physically interpretable notation that serves as the basis of this work. This notation is used to replace the standard displacement interpolation polynomials. This notation is superior to the standard notation in two ways. The arbitrary coefficients of the standard notation are replaced with coefficients that are expressed in terms of rigid body motions, the strain components, and gradients of the strain components. Furthermore, the interpolation polynomials are clearly Taylor series expansions. As a result of these two improvements to the notation, the interpolation polynomials can be used in the developments presented here to evaluate the modeling capabilities of individual finite elements, to provide an alternate approach for forming element stiffness matrices and to form finite difference templates.

Chapter 4 demonstrates the theoretical basis for the residual approach to error analysis. The failure of the finite element solution to satisfy the governing differential equations on the domains of the individual elements is shown to be the source of the inter-element jumps in finite element solutions that do not capture the exact solution. In addition, the identification of the source of the inter-element jumps means that the smoothed solution formed by nodal averaging used here and in the ZZ approach to error estimation are definitively closer to the exact solution than the discontinuous finite element solution. As discussed in Chapter 6, the smoothing adds a component of the error in the finite element model to the finite element solution. Therefore, the smoothed solution is closer to the exact solution than the finite element solution.

Chapter 5 introduces and applies the adaptive refinement process. The results of adaptive refinement are contrasted to the results of uniform refinement. It is seen that uniform refinement introduces unneeded elements in regions of low error, rendering the model inefficient. The three

necessary components of adaptive refinement are identified, namely: 1) an error estimator, 2) a termination criterion and 3) a refinement strategy. In this introduction, the inter-element jumps, which are pointwise quantities, provide the basis for each of the three components needed for adaptive refinement.

Chapter 6 introduces and demonstrates the Zienkiewicz and Zhu (ZZ) error estimation process. This approach is an example of the recovery approach to error estimation. The ZZ approach differs from the residual approach presented in Chapter 4 by estimating the error in the strain energy content on the individual elements. In this approach, the strain energy contained in the difference between a smoothed solution, which is taken to be an improvement on the discontinuous finite element solution, and the finite element solution is used as the error estimator. In this work, the differences between the strains in the smoothed solution and the inter-element nodal strains are taken as the error estimators. As such, these error estimators integrate the recovery and the residual approaches to error analysis because the inter-element jumps, which are due to residual quantities, are used to improve the finite element solution and to estimate the errors in the finite element model.

Chapter 7 extends the pointwise error estimator introduced in Chapter 5 with one-dimensional problems to two dimensions. The error estimator is demonstrated with two loading conditions. The first loading condition is a uniform load over the domain of the problem. This example demonstrates that the error estimator based on inter-element jumps approaches zero when the finite element solution approaches an exact solution. The second loading condition is a complex loading condition that produces a result that cannot be represented exactly by a polynomial representation. The pointwise error estimator is demonstrated by uniformly reforming the model. As the model is improved, the error estimates are reduced, thus,

demonstrating their efficacy for a complex loading condition. As an aside, the six-node linear strain elements used in the examples presented in this Chapter are formed using the alternate element formulation procedure mentioned in Chapter 3.

Chapter 8 demonstrates a new approach for identifying the level of refinement needed in an adaptive refinement scheme for a finite element model to rapidly converge. This approach uses the physically interpretable notation introduced in Chapter 3 to evaluate the modeling deficiencies in the individual elements in a finite element model. This approach compares the complexity of an improved strain distribution on the domain of an element to the strain distribution actually contained in the element being evaluated. This approach uses pointwise quantities in the evaluation. It is demonstrated with one-dimensional problems, but it is extendable to two-dimensions.

CHAPTER 2

AN OVERVIEW OF FINITE ELEMENT MODELING CHARACTERISTICS

2.1 – Introduction

When a finite element model cannot represent the exact solution to a continuum problem, the result contains **discretization errors**. These errors are produced when the exact solution is more complex than the interpolation functions used to form the individual finite elements are capable of representing. The discretization errors can be removed or reduced to an acceptable level by improving the finite element model[1].

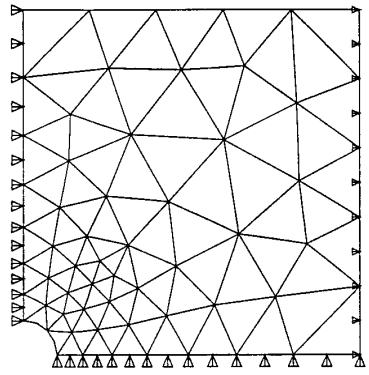

a) Initial Mesh

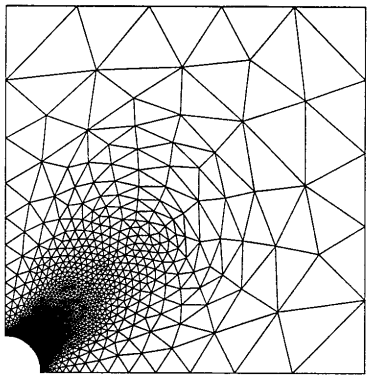

b) Adaptively Refined Mesh

Figure 2.1 – Adaptively Refined Stress Concentration

In theory, even an inexperienced analyst can produce accurate finite element results by repeatedly subdividing **every** element in the model until convergence is achieved. However, this procedure, known as **uniform refinement**, is impractical because it leads to unnecessarily large models. This inefficiency exists because elements are subdivided in regions of zero or acceptable error.

The practical alternative to uniform refinement is **adaptive refinement**, a procedure where the model is only improved in regions with unacceptably high errors. An example of adaptive refinement is illustrated in Fig. 2.1 for a shear panel with an internal circular hole. This

[1] The Weierstrass Approximation Theorem provides the theoretical basis for model refinement. The theorem says that any continuous function can be uniformly approximated on that interval by polynomials to any degree of accuracy. Note that this theorem does not say that the function can be represented exactly. The theorem says that the exact solution can be approximated as closely as desired [26, 27].

finite element model, an approximation of the Kirsch problem [25], contains a stress concentration at the upper-most point on the one-quarter circle in this doubly symmetric problem. The initial mesh of six-node triangles shown in Fig. 2.1a contains 430 degrees of freedom. This model is loaded with a uniform load on the right hand end of the panel.

When this problem is adaptively refined so that the estimated error in the strain energy content of each element is less than 5 percent, the final adaptively refined mesh contains 11,454 degrees-of-freedom as shown in Fig. 2.1b [23]. Note that the elements on the boundary are not subdivided. This means that these elements represent the exact solution with an adequate degree of accuracy.

For the sake of comparison, it is estimated that if the initial model is uniformly refined until the same level of error is achieved at the stress concentration that the model would contain over 10^6 degrees-of-freedom. This means that the nodal density for the uniformly refined mesh would be as dense everywhere as in the densest portion of the adaptively refined model, i.e., the final figure would be all black. This comparison highlights the fact that adaptive refinement is necessary if accurate approximate solutions are to be achieved with efficiency.

The adaptive refinement process consists of three distinct components: 1) an error estimator, 2) a termination criterion and 3) a refinement guide. The development and/or confident application of each of these components depends on an understanding of the source of the discretization errors, a recognition of the effect of these errors on the approximate solution and an understanding of how to improve the finite element model to reduce the errors.

The three objectives of this Chapter are designed to provide this understanding of the errors in finite element models. These objectives are the following:

1) To demonstrate the effect of discretization errors on finite element solutions.

2) To provide an intuitive understanding of the cause of discretization errors that exist in finite element solutions.

3) To demonstrate approaches for improving the finite element representation.

These objectives will be achieved with a series of demonstrations.

In the next Section, two examples of finite element models that produce exact results are presented. As can be seen these solutions are continuous. That is to say, these solutions contain no inter-element jumps in the strain representations, which is the signature of an exact solution.

Next examples are presented where the finite element models are incapable of representing the exact solutions. This inability to represent the exact solution can be seen by the presence of inter-element jumps in the strain representations. Furthermore, it will be seen that the inter-element jumps in the strains are reduced as the model is improved so that it better represents the exact solution. Then, it will be demonstrated that the discretization errors are produced when the strain model in the individual finite elements cannot exactly represent the actual strain distribution that exist on the domains of the individual elements.

2.2 - Characteristics of Exact Finite Element Results

The objective of this Section is to demonstrate the characteristics of a finite element solution when it is identical to the exact solution. As will be seen, an exact finite element solution exhibits no discontinuities in the strain representation.

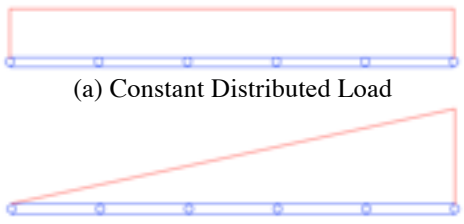

(a) Constant Distributed Load

(b) Linearly Varying Load

Figure 2.2 – Two Finite Element Models with Distributed Loads

The fact that an **exact** finite element solution produces a strain representation that is continuous is demonstrated with the two examples shown in Fig. 2.2. The finite element model consists of five, four-node bar elements of equal length fixed at both

ends. Only the inter-element nodes are shown in this figure. The model is loaded with the two distributed loads shown in Figs. 2.2a and 2.2b, respectively.

In Fig. 2.2a, the finite element model is loaded with a constant load distribution. In Fig. 2.2b, the model is loaded with a linearly varying load. It should be noted that the loads shown are actually in the horizontal direction so they produce tension and compression in the bar.

The strain distributions produced by the finite element model for these two loading conditions are shown in Fig. 2.3a and b, respectively. The inter-element nodes are shown as "o's" and the interior nodes are shown as "x's" in these figures. Both of the finite element strain distributions in Fig. 2.3 are continuous. If the finite element results were not continuous, jumps would exist in the strain representation at the inter-element nodes identified with the "o's." The fact that there are no discontinuities in the strain representations means that both finite element results shown in Fig. 2.3 are exact solutions.

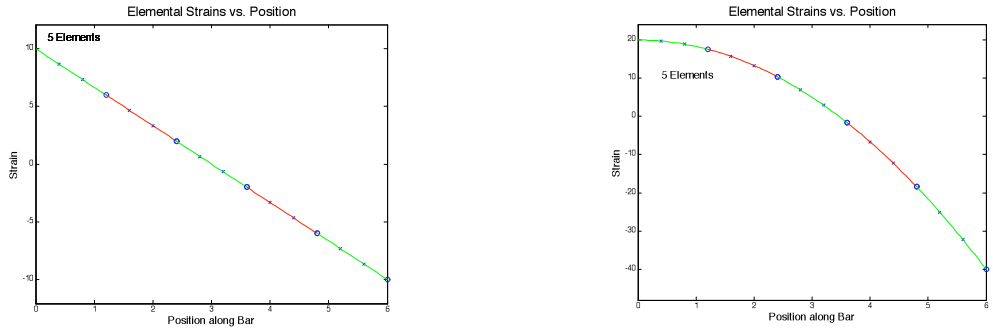

a) Constant Load Strain Distribution b) Linear Load Strain Distribution

Figure 2.3 – Exact Finite Element Strain Distributions

In Chapter 3, the modeling capabilities of the individual four-node elements are investigated. It will be seen that a four-node bar element is capable of representing strain distributions that are a linear combination of constant strain, linearly varying strain and quadratically varying strain. When the behavior of the individual elements in Fig. 2.3a is

examined, it is seen that each element is representing the same linear variation of strain and there are no inter-element jumps in the strain representation.

In Fig. 2.3b, the individual elements each represent a parabolic strain distribution and there are no inter-element jumps in the strain representation. Since each of the four-node elements is capable of representing the strain distribution of the exact result on its domain, there are no discretization errors and, hence, there are no inter-element jumps in the strains. This means that the finite element result is identical to the exact result.

The two foregoing examples identify the two primary characteristics of finite element representations that are at the heart of adaptive refinement:

1) A finite element solution contains no errors if the interpolation polynomial of each element is able to capture the exact strain distribution in the portion of the solution that it represents.
2) There are no inter-element jumps in the strains if the finite element exactly reproduces the actual solution.

Since an exact finite element result does not contain any inter-element jumps in its strain representations, **the goal of adaptive refinement** is to modify a finite element model so that the inter-element jumps are reduced to a level that produces acceptable stress and strain results. In some of the examples that follow, the magnitudes of the inter-element jumps are used as an error estimator and as a termination criterion.

2.3 - More Demanding Loading Conditions

The next objective of this Chapter is to demonstrate the existence of a direct connection between the errors in a finite element result and the size of the discontinuities in the inter-

element strains. This goal is accomplished by applying two loading conditions that produce strain distributions that are too complex for the four-node bar element to represent.

These two loading conditions are presented in this Section. It is shown in the next Section that these loading conditions produce complex strain distributions in the bar element. The initial five-element model will be seen to contain significant inter-element jumps in the strain. That is to say, the individual elements are incapable of representing the complexity of the exact strain distribution on their domain that is produced by these two loading conditions.

The first loading condition is centered on the bar as shown in Fig. 2.4a. It produces the exact strain distribution shown in Fig. 2.4b, which contains the following types of variation in the strains: 1) regions that are close to linearly varying, 2) regions that approximate parabolic variations, 3) a maximum extreme point, 4) a minimum extreme point, and 5) three inflection points that are indicated on the figure.

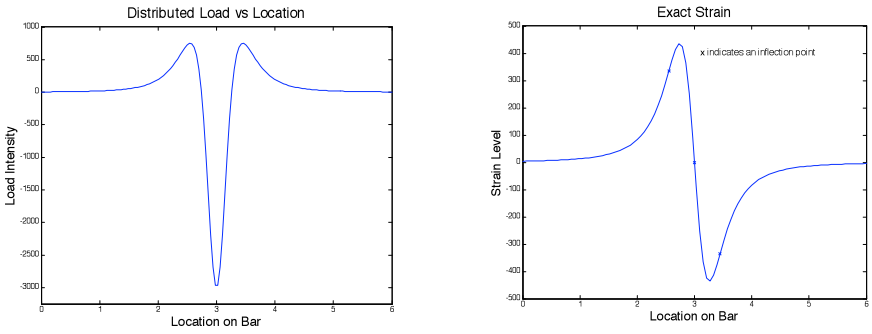

a) Centered Load b) Resulting Strain Distribution

Figure 2.4 – A "High-Demand" Loading Condition and Resulting Strain Distribution

The second loading condition is shown in Fig. 2.5a. It is similar to the loading condition in Fig. 2.4a, except that it is shifted slightly to left of center. This loading condition produces the exact strain distribution shown in Fig. 2.5b. This non-symmetric strain distribution is nearly identical to the one for the symmetric case. However, it is shown in later Sections that this non-symmetric loading condition surfaces modeling characteristics that are submerged in the symmetric case.

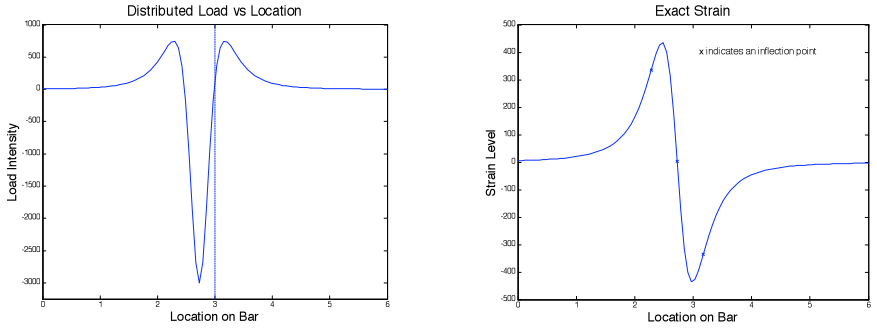

a) Load Shifted to the Left b) Resulting Strain Distribution

Figure 2.5 – A "High-Demand" Loading Condition and Resulting Strain Distribution

The two loading conditions shown in Figs. 2.4a and 2.5a are not random choices. They are used because they produce displacements in the continuous bar that are Runge functions. Runge functions are often used to test interpolation procedures because they are difficult for a polynomial interpolation function to reproduce [28]. The displacement of the bar produced by the symmetric loading condition is shown in Fig. 2.6.

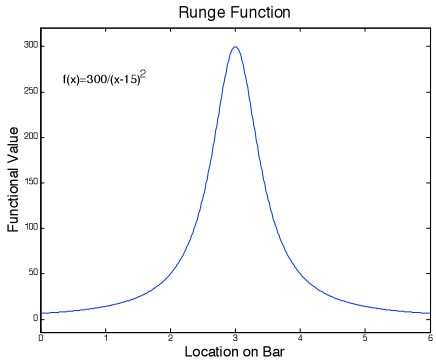

Figure 2.6 – A Runge Function

The Runge functions that represent the displacements can be integrated twice to produce the loading conditions. The loading condition shown in Fig. 2.4.a is derived from the following Runge function: $f(x) = 300/(x + 30.0 / 2.0)^2$. For completeness, the off-center distributed load shown in Fig. 2.5a is found by integrating the following displacement function twice, $f(x) = 300/(x + 30.0/2.2)^2$. It should be noted that the exact strains contained in the example problems shown in Figs. 2.4b and 2.5b are the first derivative of the displacement functions.

2.4 – Discretization Errors in an Initial Model

When the symmetric distributed load shown in Fig. 2.4a is applied to a bar problem that is modeled with five four-node elements and fixed ends, the strain distribution produced by the

finite element model is compared to the exact result in Fig. 2.7a. The difference between the two curves identifies the **actual error** in the finite element solution. In order to clearly identify the boundaries of the individual elements, the end nodes of the individual elements are designated with "o's."

In Fig. 2.7b, only the finite element approximation of the strain distribution is shown. The interior nodes of the individual elements are designated as "x's" in this figure. The finite element solution is shown separately in this figure because in later refinements it can be difficult to visually separate the exact and the approximate solutions.

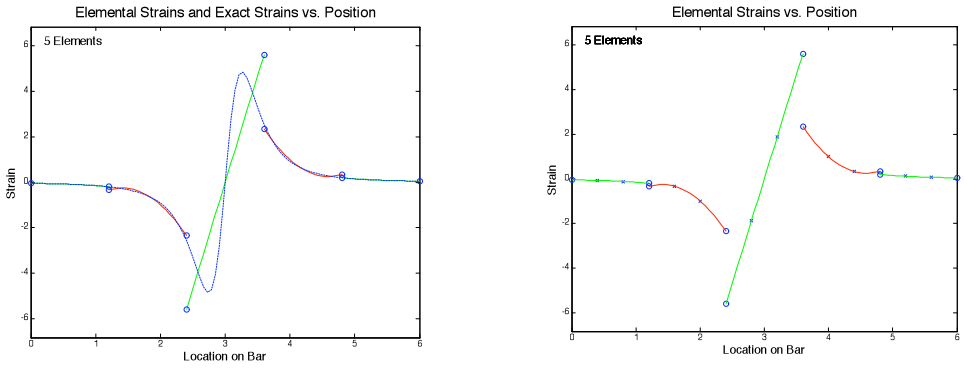

a) Compared to Exact Result b) Result with Inter-Element Jumps Emphasized

Figure 2.7 - An Unconverged Finite Element Result

As can be seen in Fig. 2.7a, the finite element solution differs markedly from the exact solution in the region containing the critical maximum and minimum points. However, the finite element solution is close to the exact solution in the portions of the bar that start from each of the fixed boundaries. This figure demonstrates the two primary objectives of this Chapter: 1) discretization errors are produced when the individual finite elements cannot represent the exact strain distribution and 2) the inter-element jumps in the strain identify the location and magnitude of the discretization errors.

When the modeling characteristics of the individual elements are studied, it is observed that the errors in the finite element result are inversely proportional to the ability of the

individual finite elements to represent the exact result. The nearly linear strains represented by the first and last elements in Fig. 2.7 are very close to the exact result. Similarly, the strains represented by the second and next to last element are nearly parabolic and are quite close to the exact result. As shown in the previous section, four-node finite elements can represent linear and quadratic distributions exactly. Since each of these elements is very close to representing the exact strain distribution, the contributions made by these elements to the inter-element jumps are small.

In contrast to this accurate representation of the exact strain distribution, the strain distribution produced by the center element is not even close to the exact result. The exact result has an "S" shape that contains two extreme points, the maximum and the minimum, and three inflection points. A single four-node element does not have the capacity to represent this complex strain distribution so the inter-element jumps contributed by this element are large.

Figure 2.7a has demonstrated the correlation between the failure of the finite element model to represent the exact strain and the inter-element jumps. The inter-element jumps in the finite element strain representation are small at the two end portions of the bar where the finite element result is close to the exact result. Conversely, the inter-element jumps are large in the center of the bar where the approximate solution and the exact result differ widely. Thus, it can be deduced that the discretization errors are quantified by the inter-element jumps. As mentioned earlier, this observation will be given a solid theoretical basis in later Chapters.

This section has demonstrated two important characteristics of finite element results. First, the inter-element jumps are correlated to the difference between the exact result and the finite element representation. Second, the differences between the exact solution and the exact

result depend on the ability of the interpolation function in the finite element to capture the exact strain distribution.

2.5 - Error Reduction and Uniform Refinement

The problem that was just solved will now be refined by subdividing each element into two equal length elements. The model is uniformly refined in order to: 1) examine the behavior of individual elements as the finite element model is improved and 2) identify the need for the adaptive refinement process. Two uniform refinements will be applied to the five-element model solved in the previous Section to produce models with ten and twenty elements, respectively. The result for the first application of uniform refinement is shown in Fig. 2.8.

When Figs. 2.8a and b are compared to Figs. 2.7a and b, it is seen that the ten-element approximation is significantly closer to the exact result than the five-element representation. Replacing the (over-driven) center element with two elements allows the finite element model to capture the general "S" shape of the exact result because of the ability of the individual elements to represent quadratic strain distributions. Since the individual finite elements provide a better representation of the exact solution everywhere in the bar than was the case for the five-element representation, the inter-element jumps are reduced. This reduction in the errors is expected as the increasing the number of elements in the model better represent the exact solution.

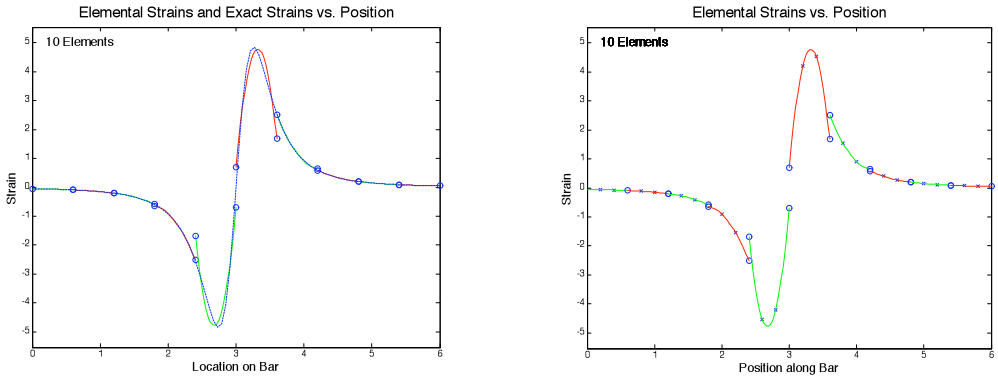

a) Compared to Exact Result b) Result with Inter-Element Jumps Emphasized

Figure 2.8 – A Uniformly Refined Finite Element Result

The inter-element jumps associated with the two elements in the center of the ten-element model are still relatively large compared to the errors in the remainder of the problem. These errors exist because the exact strain distribution in the region of these two elements is still too complex for the two four-node elements to capture. Specifically, the modeling capabilities of the two elements in the center of the bar are incapable of capturing the complex shape of the exact result that contains both the peak values and the inflection points identified in Fig. 2.4b.

The strain distribution produced by the second uniform refinement is shown in Fig. 2.9. As can be seen, the four elements representing the center portion of the bar are better able to capture the "S" shape than were the two elements in the previous model. Due to the improvement in the finite element strain model, the inter-element jumps are reduced, as would be expected.

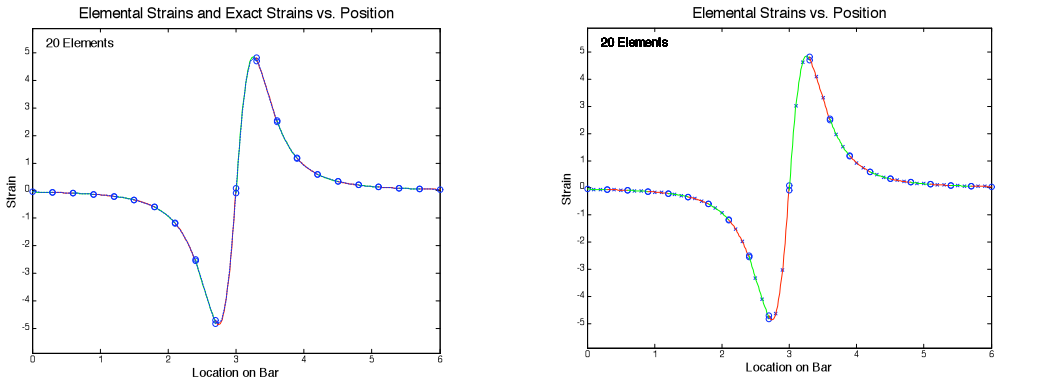

a) Compared to Exact Result b) Result with Inter-Element Jumps Emphasized

Figure 2.9 – A Uniformly Refined Finite Element Result

The primary flaw in uniform refinement can be seen in this sequence of refinements. These examples show that uniform refinement introduces too many elements into regions of the model with little or no error. This can be seen at the two ends of the bar. Little, if any, error exists in these regions after the first uniform refinement. Hence, little improvement is possible in these two regions as a result of a second uniform refinement. Thus, little, if any, improvement

occurs in the finite element representation at the two ends of the bar when the number of elements is doubled in these two regions. It can be concluded that this use of additional modeling capacity in regions of low error is wasted.

This section has identified the need for adaptive refinement by demonstrating that uniform refinement introduces unnecessary modeling capability in regions that are already well represented. Inversely, a comparison of Figs. 2.8 and 2.9 demonstrated that the finite element model was significantly improved when additional elements were introduced into regions of high error. This improvement is produced because the subdivision of the exact result simplifies the strain distribution that an individual element must represent.

2.6 - Error Reduction and Adaptive Refinement

In this section, the effectiveness of the adaptive refinement process will be demonstrated. This will be shown by subdividing only the elements with the highest levels of inter-element jumps and comparing the results to those produced by uniform refinement. It will be seen that the selective refinement of the finite element model produces a more efficient use of the modeling capabilities of a finite element model.

In this Section, the elements to be subdivided are identified by visual inspection. In later Chapters, refinement guides are developed that improve the model using a wide variety of criteria. In its simplest form, a refinement guide subdivides individual elements by quantifying the discretization errors using metrics (measures, quantities) that are computed with error estimators.

As can be seen in Fig. 2.7, the largest error in the five-element mesh is contained in the center element. In this first example of adaptive refinement, only the center element is

subdivided. The finite element solution for the resulting six-element model is presented in Fig. 2.10 side-by-side with the ten-element uniformly refined model.

When the result from the adaptively refined model is compared to the result for the ten-element uniformly refined model, the results are seen to be quite similar. The two extreme values are captured by both approximations, and the largest inter-element jumps are similar in size and location. Minor differences occur in the inter-element jumps at less critical points in the strain distribution. The differences between the two solutions are quantified in later Chapters after the error estimators are developed.

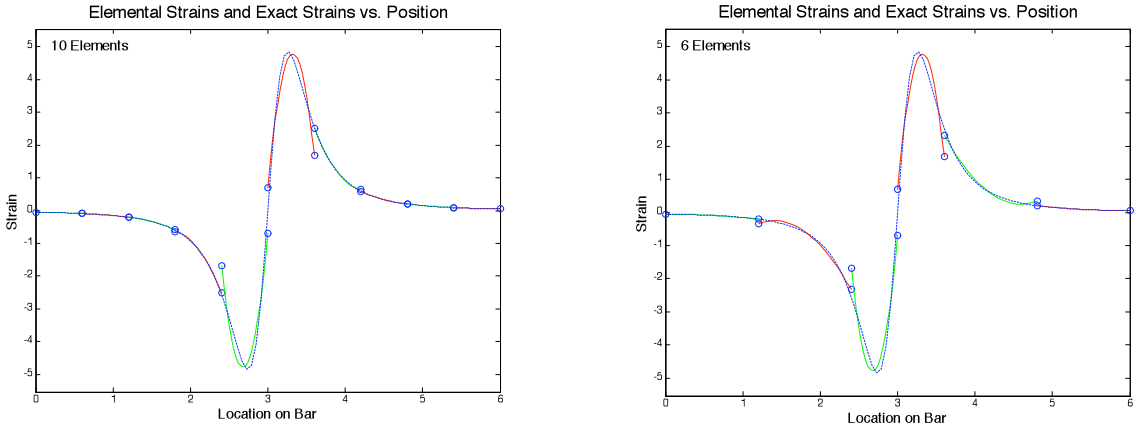

a) A Ten Element Uniformly Refined Result b) A Six Element Adaptively Refined Result

Figure 2.10 – A Uniformly Refined Result and An Adaptively Refined Finite Element Result

The two elements in the center of the model in Fig. 2.10b are easily identified as containing the highest level of errors because they are associated with the largest jumps in the inter-element strains. To further demonstrate the advantages of adaptive refinement, these two high-error elements will be subdivided.

When Fig. 2.10b is compared to Fig. 2.10a, it can be observed that slightly more error is present in the two elements flanking the center elements in the adaptively refined model than in the elements of the corresponding region of the ten-element uniformly refined model. Even though the strain is nearly zero in this region, i.e., this is not a region of critical strain, these two

elements will be adaptively refined because the error is slightly higher in this region than in the corresponding region of the uniformly refined model. When the six-element model is adaptively refined, the result is a ten-element model.

The strain distribution for the adaptively refined ten-element model is shown side-by-side with the result from the uniformly refined model with twenty elements in Fig. 2.11. When these two results are compared, it can be seen that the two approximations are nearly identical. This example further demonstrates the fact that the judicious refinement of a model produces an efficient use of modeling capacity.

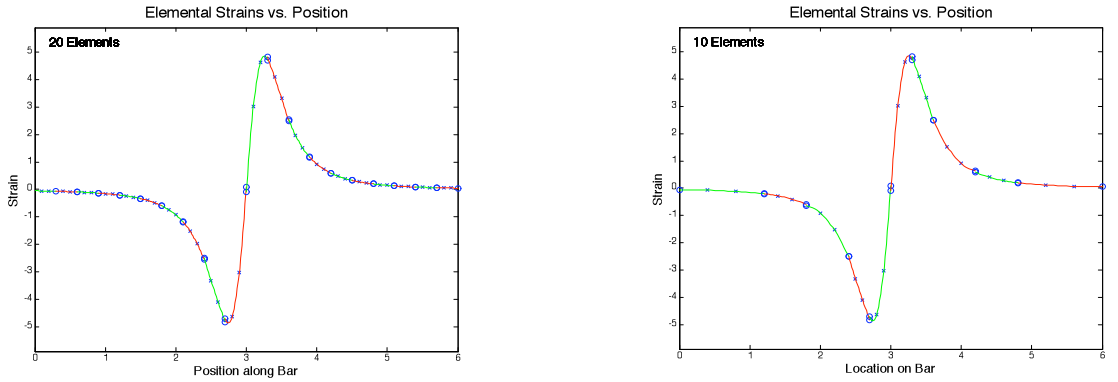

a) A Twenty Element Uniformly Refined Result b) An Eight Element Adaptively Refined Result

Figure 2.11 – A Uniformly Refined Result and An Adaptively Refined Finite Element Result

This section has shown the modeling efficiency that results from applying adaptive refinement. However, the visual identification of elements that can be profitably subdivided must be replaced with procedures that can be applied automatically. This will be accomplished in later Chapters.

2.7 – The Effect of Element Modeling Capability on Discretization Errors

The objective of this section is to further highlight the direct relationship between the discretization errors and the modeling characteristics of individual finite elements. This is accomplished by comparing and contrasting the results for a problem modeled using both four-node and three-node elements. The two models have different numbers of elements but they

contain the same number of degrees-of-freedom. An initial model of twenty-three degrees-of-freedom as well as a uniformly refined model of forty-seven degrees-of-freedom are solved. This problem is deformed with the non-symmetric loading condition shown in Fig. 2.5.

The exact solution and the approximate strain distributions for the two initial models are shown in Fig. 2.12. The primary purpose of this example is to compare and contrast the way the two different elements attempt to capture the extreme points in the stress distribution. Both models overshoot the maximum strain with a linear representation. Neither element can capture both extreme points because the exact strain distribution is more complex than either element can represent.

The most significant qualitative difference between the modeling capabilities of the four- and the three-node elements is seen in their attempts to represent the minimum peak. Because the strain representation of the four-node element is capable of representing a quadratic curve, it closely captures the actual shape near the minimum extreme point. The three-node model cannot capture the extreme point on the domain of an element because a three-node element can only represent linear strain.

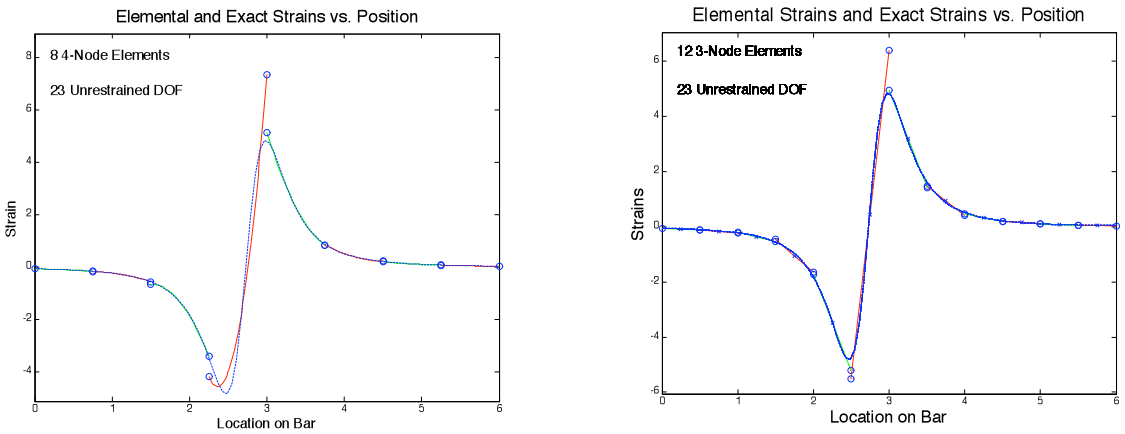

a) Four-Node Elements b) Three-Node Elements

Figure 2.12 – Twenty-Three Degree-of-Freedom Models

In the Figs. 2.12a and 2.12b, the magnitudes of the inter-element jumps for both of the finite element models are too large with respect to the absolute value of the maximum strains to be acceptable. The two models are uniformly refined in order to improve the representations of the strains. The results of these improvements to the models are presented in Fig. 2.13.

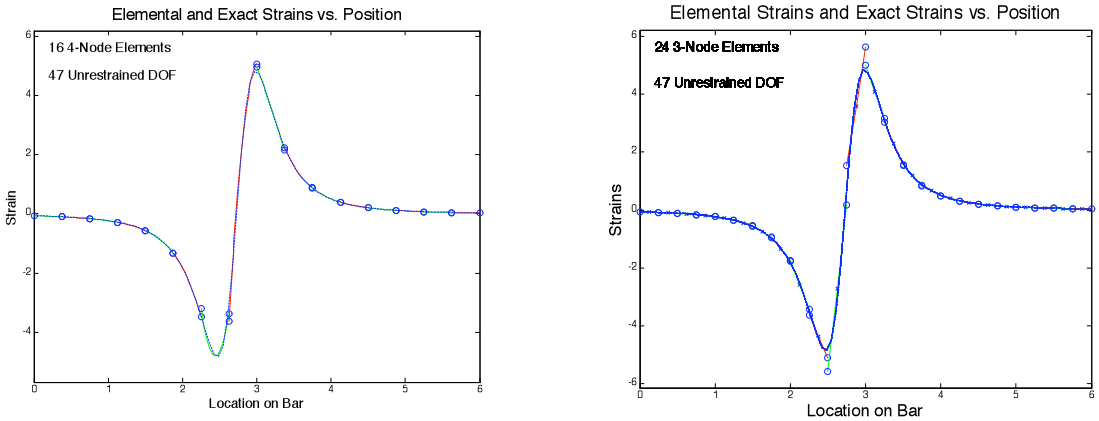

a) Compared to Exact Result b) Result with Inter-Element Jumps Emphasized

Figure 2.13 - An Unconverged Finite Element Result

As can be seen in Fig. 2.13a, the four-node model closely captures both extreme values of the strain distribution. In the case of the three-node-model shown in Fig. 2.13b, there are significant inter-element jumps in the regions of the extreme values.

The contrasting behavior of the two models at the minimum extreme point is highlighted in Fig. 2.14. In this figure, the regions containing the minimum extreme values for the two refinements of both the four-node and the three-node models are magnified as if examined under a microscope. In both four-node representations shown in Figs. 2.14a and c, the extreme value is captured on the domain of a single element. When these two figures are compared, it can be seen that the location and the magnitude of the representation of the minimum strain is improved in the second model so that it almost matches the exact result.

When the two representations produced by the two models formed with three-node elements shown in Figs. 2.14b and d are examined, it can be seen that further refinement is

needed if the three-node model is going to capture the location of the extreme value more closely.

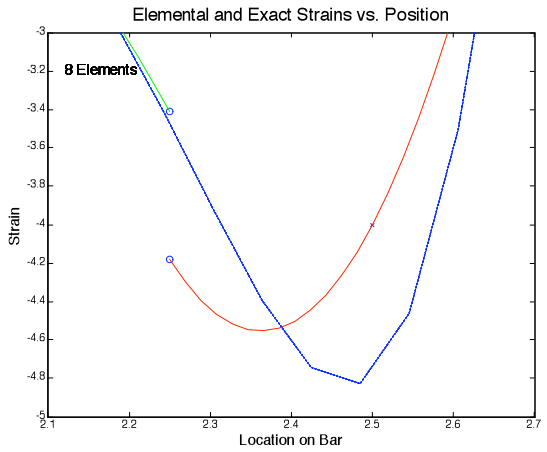

a) Initial Four-Node Model

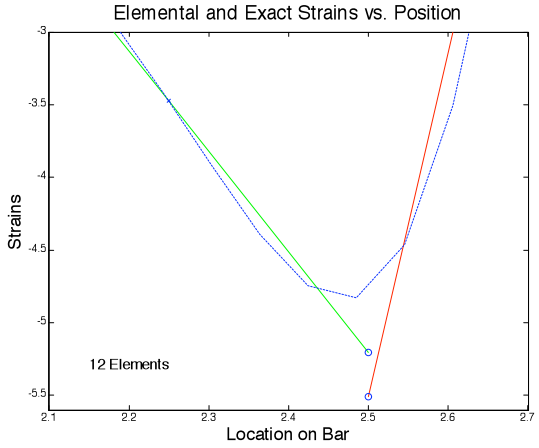

b) Initial Three-Node Model

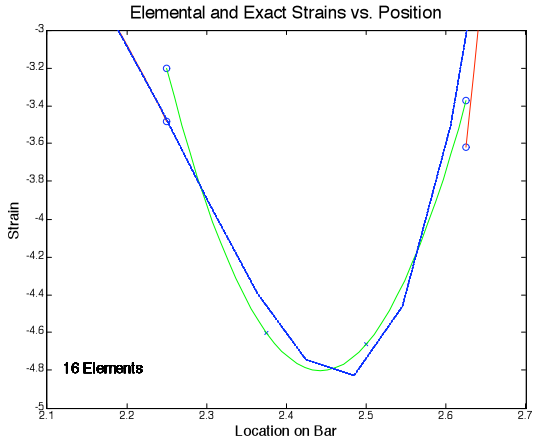

c) Uniformly Refined Four-Node Model

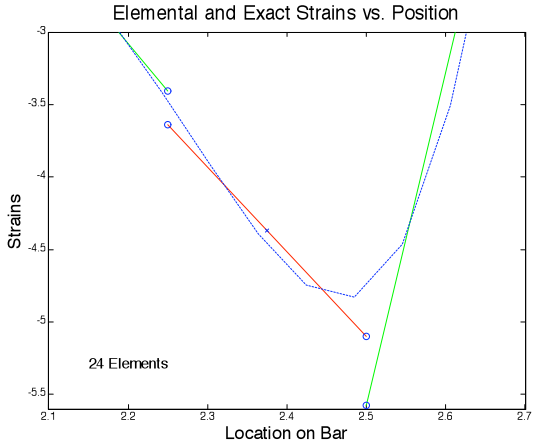

d) Uniformly Refined Three-Node Model

Figure 2.14 – Magnification of the Minimum Points

This section has shown that the modeling capabilities of the individual elements are related to the accuracy of the solution. In later Chapters, it is shown that higher-order elements are significantly more efficient than lower-order elements when the modeling capability of the elements is fully utilized.

It should be made clear that no one best element exists for every application. For example, if the maximum stress or strain concentration occurs on the boundary, an element

capable of representing linear strain distributions is adequate. This can be seen in Figs. 2.12 and 2.13 by the accuracy of the results as they approach the extreme points.

If the stress concentration takes the form of an extreme value, elements that are capable of representing a quadratic strain distribution have the advantage of being able to capture the extreme value on the domain of a single element. This advantage has been shown clearly in this Section.

2.8 - Summary and Conclusion

This Chapter has accomplished the three objectives identified in the Introduction of this Chapter, namely:

1) It has been shown that modeling errors appear in finite element models as inter-element jumps in the stresses or strains and that the size of the jump is proportional to the severity of the modeling error.
2) It has been shown that the modeling errors are directly connected to the ability of the individual elements to represent the complexity of the exact solution to the problem, i.e., the errors are related to the modeling characteristics of the individual finite elements.
3) It has been shown that models can be improved with uniform refinement, adaptive refinement and with the use of higher-order finite elements.

The applications of uniform and adaptive refinement have shown that the practical application of the finite element method requires the use of adaptive refinement. If uniform refinement is used instead of adaptive refinement, inefficient models with too many degrees of freedom are generated. The use of higher-order elements is studied in detail in later Chapters.

As described in this Chapter, the implementation of adaptive refinement requires the following three capabilities:

1) The ability to identify the location and to estimate the magnitude of discretization errors in the finite element model.
2) The ability to identify when to terminate the adaptive refinement process, i.e., the ability to identify when the solution is as accurate as is desired.
3) The ability to identify how to effectively refine the finite element model in regions of excessive error, i.e., develop refinement guides.

The knowledge gained in this Chapter is used as the basis for developing the three capabilities just identified for the implementation of the adaptive refinement process. That is to say, in later Chapters, the following is developed: 1) error estimators, 2) termination criteria, and 3) refinement guides.

CHAPTER 3

STRAIN MODELING CAPABILITIES OF INDIVIDUAL FINITE ELEMENTS

3.1 – Introduction

In the previous Chapter, it was shown that the errors in finite element results appear as jumps in the inter-element strains. It is demonstrated in the next Chapter that these jumps are produced when an individual finite element cannot capture the complexity of the exact solution that exists on its domain. These errors are called discretization errors because the discrete number of finite elements in the model cannot capture the shape of the exact solution. Examples of inter-element jumps in the strain that identify discretization errors are shown in Fig. 3.1.

The ability with which a finite element model can represent an exact solution depends on the modeling capabilities of the individual finite elements. This can be seen in Fig. 3.1 by comparing the four-node element representation of a minimum point with that of a three-node element representation.

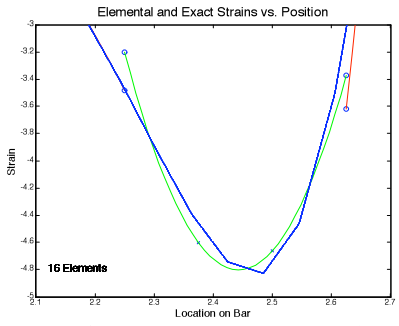

(a) A Four-Node Representation

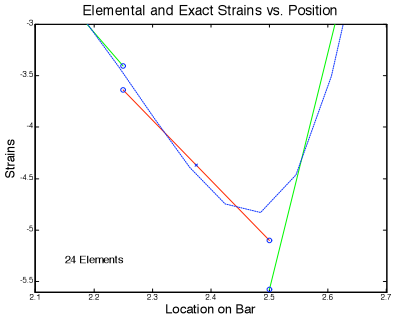

(b) A Three-Node Representation

Figure 3.1 – Finite Element Strain Representations vs. The Exact Result

As can be seen in Fig. 3.1a, a single four-node element captures the minimum point on its interior. In contrast, a three-node model cannot capture an extreme point on its interior as shown in Fig. 3.1b. This means that it is more efficient to represent an extreme point with the higher-order element because there are fewer constraints on the model, i.e., an inter-element node need not be located at or near the extreme point.

The goal of adaptive refinement is to efficiently identify regions with unacceptable levels of error and to improve the finite element model in these regions. The model is improved by modifying the discrete finite element representation in regions of unacceptable error so that it is better able to capture the exact solution. The model is improved by subdividing the existing elements or by introducing higher-order elements.

In later Chapters, procedures are developed for estimating the magnitude of the localized errors and identifying the level of refinement needed in these regions to produce an acceptable solution. The implementation of these procedures requires two capabilities: the ability to identify the modeling characteristics of individual elements and the ability to identify *in situ* the details of the strain representation that actually exist in the individual elements in a finite element solution.

The objective of this Chapter is to present and apply a procedure for evaluating the strain modeling capabilities of individual elements. This is accomplished by replacing the standard form of the displacement interpolation functions with polynomials that are physically interpretable. The replacement of the standard form of the displacement interpolation functions is accomplished by expressing the coefficients of the interpolation function in terms of quantities that cause displacements in the continuum, namely, rigid body displacements and strains. This form of the interpolation polynomial will be used in the development of error measures and refinement guides.

In the Sections that follow, a procedure is presented for representing the displacement interpolation polynomials in terms of physically interpretable quantities, namely, rigid body motions and strain quantities; identify the modeling capability of several elements during the formulation process; and determine the strain characteristics being represented by individual

elements in a loaded finite element model. Each of these topics is covered in more detail in Reference 1.

3.2 – Identification of the Modeling Capabilities of a Three-Node Bar Element

The strain modeling capabilities of a three-node element are introduced and discussed in this Section. The nodal displacements in a three-node bar are a combination of three linearly independent displacement patterns. Each of these displacement patterns can be formed so they represent a clearly defined strain state. The three physically interpretable strain states represent a rigid body displacement, a deformation due to a constant strain and a deformation due to a linearly varying strain. The procedure for forming these physically interpretable deformation patterns is outlined and developed in detail in the next two Sections.

(a) Displacement due to Rigid Body Motion

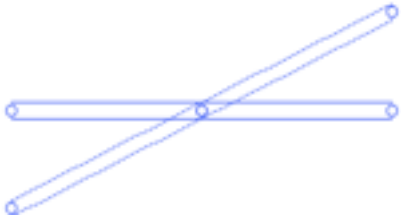

(b) Displacement due to Constant Strain

(c) Displacement due to Linearly Varying Strain

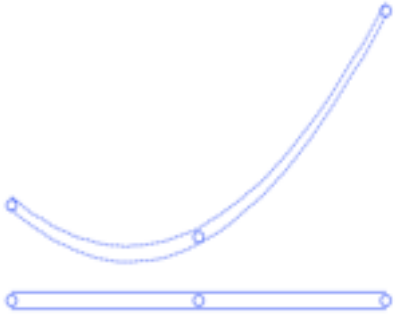

(d) Total Displacement; A Linear Combination of (a), (b), and (c)

Figure 3.2 – Linearly Independent Deformation Patterns for a Three-Node Bar and Their Sum

The displacement pattern for the three-node element that is due to a rigid body displacement is shown in Fig. 3.2a. As would be expected, the rigid body motion contributes the same displacement to each of the three nodes. The actual contribution of the rigid body displacement to the overall displacement depends on the participation level of this component.

It should be noted that, by definition, an element undergoing a rigid body displacement does not deform. Thus, the strain in an element undergoing a rigid body motion is equal to zero.

In order to make the discussion simpler in later sections, a rigid body motion is considered here as a "zero-th order" strain distribution.

When a three-node bar is deformed with a state of constant strain, the nodal displacements vary linearly in the element as shown in Fig. 3.2b. The actual displacements produced by this strain state depend on its level of participation in the overall solution. The center node is chosen as the local origin for the element so it does not displace.

The third physically interpretable displacement pattern that a three-node element can represent is shown in Fig. 3.2c. The displacement pattern for this contribution is parabolic. This displacement pattern is produced by a linearly varying strain distribution.

Every displacement of the three-node bar is a linear combination of these three linearly independent modeling capabilities. An example of such a linear combination is shown in Fig. 3.2d. This deformation is an example of the most complex shape that a three-node element can represent because it is composed of a linear combination of the three deformation patterns shown in Figs. 3.3a – 3.3c. It should be emphasized that the displacements in a bar are actually along the axis of the bar in the longitudinal direction. For visual clarity, these axial displacements appear as lateral representations in Fig. 3.2.

3.3 – An Overview of Self-Referential Notation for a Three-Node Bar Element

An overview of the motivation for and an outline of the derivation of the self-referential coefficients of the displacement interpolation polynomial are presented in this Section. This presentation gives an analytic perspective to the modeling capacities illustrated in the previous Section. The contents of this Section are condensed in Fig. 3.3. The detailed derivation presented in the next Section puts this physically interpretable notation on a solid theoretical foundation.

Before outlining the derivation, the limitations of the standard form of the displacement interpolation polynomial, shown in Fig. 3.3a, are identified. The arbitrary coefficients, the "a's", have no clearly identified physical meaning. This means that they have no direct connection to the physical phenomenon they represent, namely, the displacements in the continuum. As a result, the strain modeling capabilities of an individual element cannot be evaluated by inspecting the displacement interpolation polynomial.

This deficiency can be eliminated by forming an interpolation polynomial in which the coefficients are expressed directly in terms of strain quantities. This is desirable because the deformations in the continuum are produced by strains and the strains are quantities sought in the analysis. The ability to identify the strain modeling capability of individual elements by visual inspection is demonstrated in this and in later Sections.

This development forms the physically interpretable interpolation polynomial in a three-step process. In the first step of the derivation, shown in Fig. 3.3b, the standard form of the interpolation function is interpreted as a truncated Taylor series expansion of the displacements

(a) An Arbitrary Interpolation Function

$$u(x) = a_1 + a_2 x^1 + \cdots + a_n x^{n-1}$$

(b) A Taylor Series Representation of the Interpolation Function

$$u(x) = u_o + \left(\frac{du}{dx}\right)_o x + \left(\frac{d^2u}{dx^2}\right)_o \frac{x^2}{2!} + \cdots + \left(\frac{d^nu}{dx^n}\right)_o \frac{x^n}{n!}$$

(c) Define Taylor Series Coefficients in Terms of Strain Quantities

$$u_o = u_{\substack{\text{Rigid}\\ \text{Body}}} \quad ; \ 0^{\text{th}} \text{ Order Strain Quantity}$$

$$\left(\frac{du}{dx}\right) = (\varepsilon_x)_o \quad ; \ 1^{\text{st}} \text{ Order Strain Quantity}$$

$$\left(\frac{d^2u}{dx^2}\right)_o = \frac{d}{dx}\left(\frac{du}{dx}\right)_o = \left(\frac{d\varepsilon_x}{dx}\right)_o = (\varepsilon_{x,x})_o \quad ; \ 2^{\text{nd}} \text{ Order Strain Quantity}$$

(d) Transformed Interpolation Function

$$u(x) = u_{\substack{\text{Rigid}\\ \textit{Body}}} + (\varepsilon_x)_o x + (\varepsilon_{x,x})_o \frac{x^2}{2!} + \cdots + (\varepsilon_{x,xx\cdots})_o \frac{x^n}{n!}$$

Figure 3.3 - The Formulation of Self-Referential Interpolation Polynomials

with respect to a local origin. This step replaces the content-free "a's" with coefficients expressed in terms of the displacement and its derivatives. The constant term is interpreted as a rigid body displacement.

In the next step, shown in Fig. 3.3c, the derivatives of the displacements in the Taylor series expansion are expressed in terms of strain and the derivatives of strain. This is accomplished by introducing the strain-displacement relation, $\varepsilon_x = du/dx$. The coefficients of the displacement interpolation function are now expressed in terms of quantities that are directly related to the deformation of the continuum.

Two features of the notation need to be emphasized. The subscripts written after the comma indicate a derivative and the subscript zero indicates that the quantity is evaluated at the local origin of the finite element. As mentioned in the previous Section, a rigid body motion is identified as a zero-th order strain term since a rigid body motion does not cause the continuum to deform.

A simple substitution remains as the final step. The coefficients of the Taylor series presented in Fig. 3.3b are replaced with the coefficients expressed in terms of the strain quantities contained in Fig. 3.3c. The final form of an interpolation polynomial is shown in Fig. 3.3d. The displacement interpolation function is now expressed directly in terms of quantities that are important to solid mechanics problems, namely, the strains.

When Fig. 3.3d is examined, the modeling capabilities of an individual finite element can be identified by inspection. For example, a three-node element will have a displacement interpolation function that consists of the first three terms shown in Fig. 3.3d. When the three coefficients expressed in physically interpretable notation are extracted from Eq. 3.3d, they are the following:

$$u_{\text{Rigid Body}}$$
$$(\varepsilon_x)_o$$
$$(\varepsilon_{x,x})_o$$

These three coefficients indicate that a three-node bar element can represent a rigid body displacement, a constant strain and a linearly varying strain distribution. The physical meaning of these three terms is discussed in detail in Section 3.2 and illustrated in Fig. 3.2.

This result might, at first, seem somewhat simplistic. The one-dimensional case is used almost exclusively in this presentation in order to provide a straightforward, compact introduction to the physically interpretable, self-referential notation. In a later Section, the displacement interpolation polynomials for a four-node planar element are presented in this physically interpretable notation. The coefficients are expressed in terms of rigid body displacements, rigid body rotation, normal strains, and shear strain.

The analysis of a two-dimensional element is introduced solely to demonstrate another facet of the power and usefulness of this self-referential notation. The use of this physically interpretable notation allows modeling errors inherent in the four-node quadrilateral to be identified by inspection.

3.4 – Identification of the Physically Interpretable Coefficients

The previous Section discussed the significance of the self-referential notation for a three-node bar and outlined the procedure for forming the coefficients for this physically interpretable notation. In this Section, the procedure for forming these coefficients in detail is presented. This is done to show that this process is straightforward and easily implemented.

The standard interpolation polynomial for the three-node element is the following:

$$u(x) = a_1 + a_2 x + a_3 x^2 \qquad \text{(Eq. 3.1)}$$

In Eq. 3.1, the coefficients of the interpolation function do not have any obvious physical meaning. For example, the physical meaning of the coefficient a_3 was identified in the previous Section as being the derivative of the normal strain, i.e., $a_3 = \varepsilon_{x,x}$. The process for identifying the arbitrary 'a' coefficients in terms of strain quantities is presented next.

The first step toward embedding physical meaning into these arbitrary coefficients is to interpret Eq. 3.1 as a truncated Taylor series expansion. When Eq. 3.1 is written as a second-order Taylor series expansion, the following is obtained:

$$u(x) = u_0 + \left(\frac{du}{dx}\right)_0 x + \left(\frac{d^2u}{dx^2}\right)_0 \frac{x^2}{2} \qquad \text{(Eq. 3.2)}$$

where the subscript zero refers to the local origin, which is located at the center of the element in this analysis.

Equation 3.2 directly introduces physical meaning into the interpolation polynomial. This is the case because the dependent variable of Eq. 3.2 is chosen to be the displacement of the continuous bar being analyzed.

The constant term of Eq. 3.2 is interpreted as a rigid body displacement. It represents the displacement of the local origin, the point designated as "0." As mentioned in the previous Section, the rigid body displacement is considered as a zero-th order strain term because a rigid body motion does not cause a deformation. The coefficient of the constant term is expressed as:

$$u_0 = \left(u_{rb}\right)_0 \qquad \text{(Eq. 3.3)}$$

where "rb" designates a rigid body displacement in the x direction.

The coefficient of the linear term is interpreted as a constant normal strain since the strain-displacement relation from linear elasticity is $\varepsilon_x = du/dx$. In order to make it clear that the

coefficient of the linear term refers to the value of the constant strain at the local origin, the coefficient is written with a subscript zero as:

$$\left(\frac{du}{dx}\right)_0 = (\varepsilon_x)_o \qquad \text{(Eq. 3.4)}$$

The coefficient of the quadratic term is interpreted as the rate of change of the normal strain in the x direction. When this coefficient is expressed in terms of the derivatives of the normal strain, the following is obtained:

$$\left(\frac{\mathrm{d}^2 \mathrm{u}}{\mathrm{d}\,\mathrm{x}^2}\right)_0 = \frac{d}{dx}\left(\frac{du}{dx}\right)_0 = \frac{d}{dx}(\varepsilon_x)_o = \left(\frac{d\varepsilon_x}{dx}\right)_0 = (\varepsilon_{x,x})_0 \qquad \text{(Eq. 3.5)}$$

where a subscript after the comma, e.g., 'x,x' indicates a derivative with respect to x. This term is a gradient of the normal strain. As a result, this self-referential notation is designated as **strain gradient notation**.

When the coefficients of Eq. 3.2 are expressed in terms of the physically interpretable quantities as presented in Eqs. 3.3 – 3.5, the result is the following:

$$\mathrm{u(x)} = (\mathrm{u_{rb}})_0 + (\varepsilon_\mathrm{x})_0 \mathrm{x} + (\varepsilon_{\mathrm{x,x}})_0 \frac{\mathrm{x}^2}{2} \qquad \text{(Eq. 3.6)}$$

where the subscript 0 refers to the local origin and the subscript following the comma indicates differentiation with respect to x.

Equation 3.6 indicates that the displacements in a three-node element are produced by a rigid body displacement, a constant strain and a linearly varying strain. The displacements produced by these three independent components are illustrated in Fig. 3.2.

3.5 – The Decomposition of Element Displacements into Strain Components

One of the objectives of this Chapter is the development of the capacity to identify the details of the strain representation for an individual element in a finite element solution. This is accomplished by introducing the nodal displacements of an element into Eq. 3.6 to extract the level of participation of each of the strain states that the element can represent.

The participation factors for the individual strain states are found by treating the displacement at each of the nodes on an individual element as a boundary condition. To implement this idea, Eq. 3.6 is equated to the nodal displacement at each of the nodes in an element. The nodal locations for the example presented here are shown in Fig. 3.4.

When Eq. 3.6 is evaluated at node 1, the displacement is equal to the nodal displacement, u_1, and the nodal location is given as $x_1 = -L/2$. When these conditions are introduced into Eq. 3.6, the result is the following:

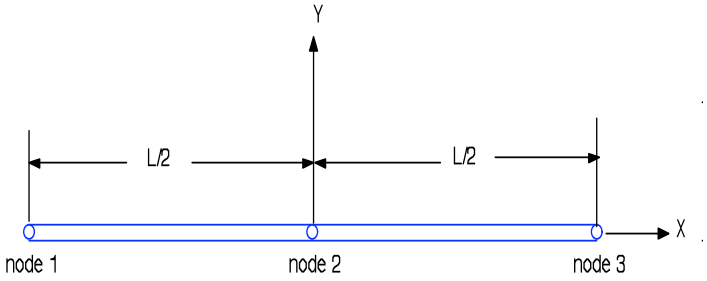

Figure 3.4 - A Three-Node Element with a Local Coordinate System

$$\begin{aligned} u_1 &= u(x = x_1) \\ &= (u_{rb})_0 + (\varepsilon_x)_0 x_1 + (\varepsilon_{x,x})_0 \frac{x_1^2}{2} \\ &= (u_{rb})_0 + (\varepsilon_x)_0 \left(\frac{-L}{2}\right) + (\varepsilon_{x,x})_0 \frac{1}{2}\left(\frac{-L}{2}\right)^2 \end{aligned} \qquad \text{(Eq. 3.7)}$$

When Eq. 3.6 is evaluated at the location of each of the three nodes of the finite element in the local coordinate system as shown in Fig. 3.2, the result is as follows:

$$\begin{Bmatrix} u_1 \\ u_2 \\ u_3 \end{Bmatrix}_i = \begin{bmatrix} 1 & x_1 & x_1^2/2 \\ 1 & x_2 & x_2^2/2 \\ 1 & x_3 & x_3^2/2 \end{bmatrix} \begin{Bmatrix} u_{rb} \\ \varepsilon_x \\ \varepsilon_{x,x} \end{Bmatrix}_0$$

$$\begin{Bmatrix} u_1 \\ u_2 \\ u_3 \end{Bmatrix}_i = \begin{bmatrix} 1 & -L/2 & (-L/2)^2/2 \\ 1 & 0 & 0 \\ 1 & +L/2 & (+L/2)^2/2 \end{bmatrix} \begin{Bmatrix} u_{rb} \\ \varepsilon_x \\ \varepsilon_{x,x} \end{Bmatrix}_0 \qquad \text{(Eq. 3.8)}$$

This equation relates the three nodal displacements of a three-node element to the three physically interpretable quantities that produce displacements in the element. The subscript '0' on the last term of Eq. 3.8 implies that those quantities are being evaluated at the local origin, which in this case is located at node 2. The subscript "i" indicates a reference to the i-th element.

Equation 3.8 presents an intermediate step in our development. The inverse of this equation contains the relationship being sought. This is the case because after a finite element problem is solved, the nodal displacements of each of the individual elements are known. As a result, the quantities on the left-hand side of Eq. 3.8 are known and the quantities on the right-hand side of Eq. 3.8 are sought.

When Eq. 3.8 is inverted, the following system of equations is obtained:

$$\begin{Bmatrix} u_{rb} \\ \varepsilon_x \\ \varepsilon_{x,x} \end{Bmatrix}_0 = \begin{bmatrix} 0 & 1 & 0 \\ -1/L & 0 & 1/L \\ 4/L^2 & -8/L^2 & 4/L^2 \end{bmatrix} \begin{Bmatrix} u_1 \\ u_2 \\ u_3 \end{Bmatrix}_i \qquad \text{(Eq. 3.9)}$$

Equation 3.9 allows the identification of the contributions of the independent strain states to the nodal displacements that exist in a three-node bar element. The quantities on the left hand side of Eq. 3.9 are referred to as participation factors.

3.6 – A Common Basis for the Finite Element and Finite Difference Methods

Equation 3.9 has a significance that extends far beyond that discussed in the previous Section. The finite difference approximations of the derivatives are implicitly contained in Eq.

3.9. This is demonstrated in this Section. In Ref. 1, it is shown that Eq. 3.9 can serve as the basis for forming finite element stiffness matrices. This means that the finite difference method and the finite element method have a common basis.

The existence of a common basis for the two methods means that the finite difference method can be rationally extended to represent practically any domain or boundary condition that can be modeled by the finite element method. In later Chapters, the common basis of the two methods is used to provide the theoretical and practical foundation for pointwise error measures.

Next, it is demonstrated that Eq. 3.9 implicitly contains the standard form of the finite difference approximations for the first and second derivatives. This is accomplished with a slight change of notation.

Figure 3.5 presents a one-dimensional, three-node finite difference template with even spacing. This figure is similar to Fig. 3.4 except that the notation is changed so that it matches the standard notation for a central difference template. In this notation, the nodal spacing is designated as h instead of as L/2. When Eq. 3.9 is rewritten with this notation, it becomes:

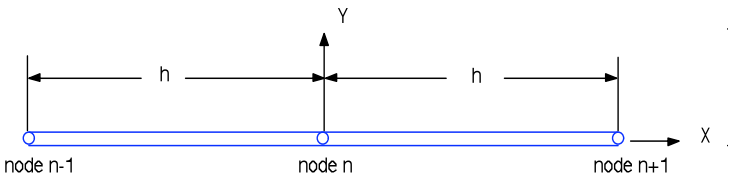

Figure 3.5 - A Three-Node Finite Difference Template

$$\begin{Bmatrix} u_{rb} \\ \varepsilon_x \\ \varepsilon_{x,x} \end{Bmatrix}_0 = \begin{bmatrix} 0 & 1 & 0 \\ -1/2h & 0 & 1/2h \\ 1/h^2 & -2/h^2 & 1/h^2 \end{bmatrix} \begin{Bmatrix} u_{n-1} \\ u_n \\ u_{n+1} \end{Bmatrix}_i \qquad \text{(Eq. 3.10)}$$

The first row indicates that every node has a rigid body displacement that corresponds to the displacement of the local origin. When the equations contained in the second and third rows are extracted from Eq. 3.10, the following is obtained:

$$\varepsilon_x = \frac{du}{dx} = \frac{u_{n+1} - u_{n-1}}{2h}$$
$$\varepsilon_{x,x} = \frac{d^2u}{dx^2} = \frac{u_{n+1} - 2u_n + u_{n-1}}{h^2} \qquad \text{(Eq. 3.11)}$$

The two components of Eq. 3.11 are identical to the standard form of the central difference template approximations of the first and second derivatives at the local origin.

The components of Eq. 3.11 are developed for evenly spaced nodes. The nodes can, in general, be unevenly spaced [24]. The use of unevenly spaced nodes reduces the order of the error in a finite difference template. However, it is not clear whether the idea of the order of error has much meaning in an adaptively refined problem where the introduction of smaller elements is the objective of the process.

It should be noted that Eq. 3.10 can be extended to multi-dimensions. The procedure for developing finite difference templates in two-dimensions for unevenly spaced nodes is presented and demonstrated in Ref. 1. This capability may provide another important contribution to computational mechanics by leading to a revival of the finite difference method in solving solid mechanics problems. In fact, adaptive refinement procedures for finite difference models have been demonstrated using an error measure that can be used with either finite element or finite difference representations [24, 29].

3.7 – Modeling Capabilities of the Four-Node Bar Element

In Fig. 3.1, the ability of a four-node bar element to better represent a minimum point than a three-node element was shown. In this Section, the modeling capability of a four-node element that makes this improved result possible is identified. Then, using this result, a relationship is formed that allows the identification of the *in situ* participation of the individual

strain components of individual four-node elements. In the next Section, the capability developed in this Section is used to identify the *in situ* performance of four-node bar elements.

When the displacement interpolation function for a four-node bar element is expressed in terms of the physically interpretable quantities, the result is the following:

$$u(x) = (u_{rb})_0 + (\varepsilon_x)_0 x + (\varepsilon_{x,x})_0 \frac{x^2}{2} + (\varepsilon_{x,xx})_0 \frac{x^3}{6} \qquad \text{(Eq. 3.12)}$$

where the subscript "0" refers to the local origin and the subscript following the comma indicates differentiation with respect to x.

This interpolation function is identical to the one for a three-node bar given by Eq. 3.6 with the addition of a cubic term. Equation 3.12 indicates that the displacements in a four-node element are produced by a rigid body displacement, a constant strain, a linearly varying strain and a quadratically varying strain. That is to say, this element can represent a strain distribution that is one-order higher than can be represented by a three-node element. The difference in the modeling capabilities produced by this additional term is shown graphically in Fig. 3.1.

An analogous relationship to Eq. 3.9 is developed here for a four-node element using Eq. 3.12. This process is demonstrated for the four-node bar shown with even spacing in Fig. 3.6. The local origin is located at the center of the bar.

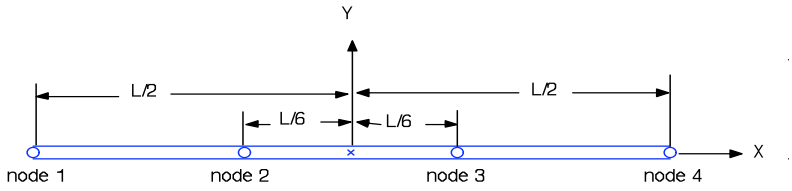

Figure 3.6 - A Four-Node Element with a Local Coordinate System

When Eq. 3.12 is evaluated at the four nodal locations of a four-node bar, the following system of equations is formed:

$$\begin{Bmatrix} u_1 \\ u_2 \\ u_3 \\ u_4 \end{Bmatrix}_i = \begin{bmatrix} 1 & x_1 & x_1^2/2 & x_1^3/6 \\ 1 & x_2 & x_2^2/2 & x_2^3/6 \\ 1 & x_3 & x_3^2/2 & x_3^3/6 \\ 1 & x_4 & x_4^2/2 & x_4^3/6 \end{bmatrix} \begin{Bmatrix} u_{rb} \\ \varepsilon_x \\ \varepsilon_{x,x} \\ \varepsilon_{x,xx} \end{Bmatrix} \qquad \text{(Eq. 3.13a)}$$

When Eq. 3.13a is evaluated at the four nodal locations shown in Fig. 3.6, the following is obtained:

$$\begin{Bmatrix} u_1 \\ u_2 \\ u_3 \\ u_4 \end{Bmatrix}_i = \begin{bmatrix} 1 & -L/2 & L^2/8 & -L^3/48 \\ 1 & -L/6 & L^2/72 & -L^3/1296 \\ 1 & L/6 & L^2/72 & L^3/1296 \\ 1 & L/2 & L^2/8 & L^3/48 \end{bmatrix} \begin{Bmatrix} u_{rb} \\ \varepsilon_x \\ \varepsilon_{x,x} \\ \varepsilon_{x,xx} \end{Bmatrix}_0 \qquad \text{(Eq. 3.13b)}$$

This equation relates the nodal displacements of a four-node element to the four physically interpretable strain components that exist at the local origin of the element being analyzed. The subscript "i" on the first term relates the nodal displacements to the i-th element. The subscript "0" on the last term relates these quantities to the local origin of the i-th element. The four nodal locations are identified in Fig. 3.6 as $x_1 = -L/2$, $x_2 = -L/6$, $x_3 = L/6$ and $x_4 = L/2$.

As was the case for Eq. 3.8, Eq. 3.13 is an intermediate step to the desired result. The level of participation of the individual strain states that exist for a given set of element displacements is sought. The participation factors are found by inverting Eq. 3.13b.

When Eq. 3.13 is inverted, the system of equations becomes the following:

$$\begin{Bmatrix} u_{rb} \\ \varepsilon_x \\ \varepsilon_{x,x} \\ \varepsilon_{x,xx} \end{Bmatrix}_0 = \begin{bmatrix} -1/16 & 9/16 & 9/16 & -1/16 \\ -11/2L & 9/L & -9/2L & 11/2L \\ 9/2L^2 & -9/2L^2 & -9/2L^2 & 9/2L^2 \\ -27/L^3 & 81/L^3 & -81/L^3 & 27/L^3 \end{bmatrix} \begin{Bmatrix} u_1 \\ u_2 \\ u_3 \\ u_4 \end{Bmatrix}_i \qquad \text{(Eq. 3.14)}$$

Equation 3.14 allows the identification of the contribution of the independent strain quantities that a four-node bar element is capable of representing to the known nodal displacements of the element.

3.8 – Identification and Evaluation of Element Behavior

In this Section, the usefulness of the physically interpretable notation is demonstrated further. This is accomplished by identifying the strain states that an individual element is actually representing in an existing finite element result. This result is obtained by using Eq. 3.14 to decompose the *in situ* displacements of individual elements into the contributions of the strain quantities that produce the nodal displacements. In later Chapters, this ability is used to evaluate element performance and to formulate refinement guides.

The *in situ* behavior of the individual elements is identified here for an example problem. The example is the fixed-fixed bar represented with five four-node elements that is loaded with the symmetric load shown in Fig. 2.4a. The finite element strain representation and the exact strain distribution for this problem were originally shown in Fig. 2.7 and are reproduced here for the convenience of the reader as Fig. 3.7.

The participation factors for the linearly independent strain states that produce the displacements of the individual elements contained in Fig. 3.7 are presented in Table 3.1. These values are found by using Eq. 3.14 to decompose the nodal displacements of each of the five elements.

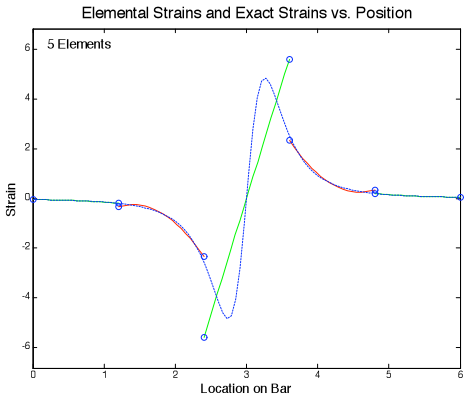

Figure 3.7 – A Five Element Finite Element Result Compared to the Exact Result

The quantities in the column labeled as $(u_{rb})_0$ identify the contribution of the rigid body displacement to the nodal displacements for the individual elements. These quantities designate the total displacements of the local origin of the individual bars. This meaning can be seen in Eq. 3.12 because this equation is the Taylor series representation of the displacement interpolation polynomial. The other terms in the expansion

do not contribute to the displacement of the local origin since they are multiplied by an x-term ($x, x^2, \ldots$), which is zero at the origin.

Table 3.1 – Physically Interpretable Components

Element No.	$(u_{rb})_0$	$(\varepsilon_x)_0$	$(\varepsilon_{x,x})_0$	$(\varepsilon_{x,xx})_0$
Element 1	-0.0390	-0.0897	-0.1204	-0.1903
Element 2	-0.3212	-0.5785	-1.6580	-4.2016
Element 3	-2.7992	0.0	9.3401	0.0
Element 4	-0.3212	0.5785	-1.6580	4.2016
Element 5	-0.0390	0.0897	-0.1204	0.1903

The column labeled as $(\varepsilon_x)_0$ contains the constant strain at the local origin of the individual elements. The meaning of this quantity can be correlated to Fig. 3.7 by comparing the strain at x = 3.0 in the figure to the value for $(\varepsilon_x)_0$ of Element 3 in Table 3.1. This comparison is possible because the point, x = 3.0, is also the local origin of Element 3. As can be seen, the strain at x = 3.0 is equal to zero in both the plot and in the table.

The quantities labeled as $(\varepsilon_{x,x})_0$ in Table 3.1 are the slopes of the strain at the center of the individual elements. These quantities measure the rate of change of ε_x in the x direction. The meaning of this quantity can be given substance by comparing the values in Table 3.1 to the slopes at the center of Elements 2 and 4 that are identified in Fig. 3.8.

The slopes, $(\varepsilon_{x,x})_0$, of Elements 1 and 5 are negative and small relative to the other three elements in the model. This can be seen either by consulting Table 3.1 or by inspecting Fig. 3.8. The slopes of Elements 2 and 4 are both negative and significantly larger in magnitude than the slopes of Elements 1 and 5. Both Fig. 3.8 and Table 3.1 show that the slope of the center element, Element 3, is large and positive.

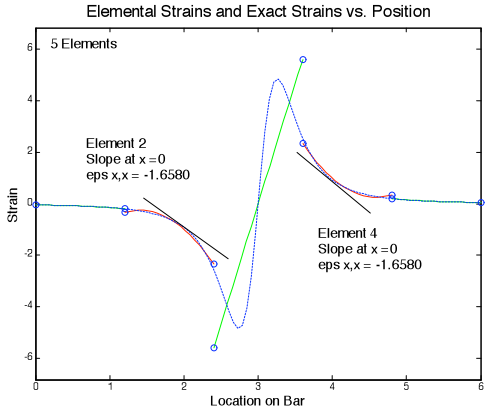

Figure 3.8 – Slope at x =0, $(\varepsilon_{x,x})_0$ for Elements 2 and 4

The quantities in the final column of Table 3.1 are the values of the second derivative of the strain at the local origin, $(\varepsilon_{x,xx})_o$. These quantities can be interpreted geometrically as the curvature of the strain representation at the center of the individual elements.

The meaning of curvature is illustrated in Fig. 3.9. In this Figure, the radii of curvature for Elements 2 and 4 are shown. The radius of curvature indicates the size of the circle that has the same curvature as the function being analyzed at the point of tangency. The curvature is equal to the reciprocal of the radius of curvature, curvature = 1/ (radius of curvature).

An inspection of Fig. 3.9 shows that Elements 1 and 5 are nearly straight lines, so they have a small curvature as is validated in Table 3.1. On the other hand, Fig. 3.9 and Table 3.1 show that Elements 2 and 4 have a significantly larger curvature than Elements 1 and 5. The curvature of Element 3 is given as 0.0 in Table 3.1. This means that the radius of curvature for this element approaches infinity. That is to say, the strain representation in Element 3 is a straight line, which can be seen in Fig. 3.9.

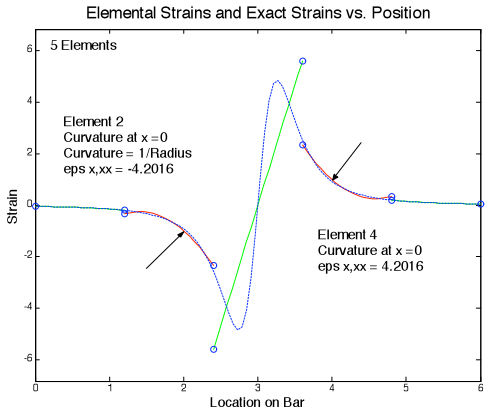

Figure 3.9 – Curvature at x =0, $(\varepsilon_{x,xx})_0$ for Elements 2 and 4

The ability of Eq. 3.14 to identify the *in situ* participation of the individual strain states for individual elements was demonstrated in this Section. This capability is used to decompose the nodal displacements of an element into the independent strain states in order to form refinement guides in later Chapters.

3.9 – Formulation of a Two-Dimensional Strain Model

The one-dimensional problems are presented as a way to introduce and extend the components that make up the adaptive refinement process. However, the focus on the one-

dimensional problem does not exhibit a major contribution resulting from the use of self-referential notation, namely, the identification of strain modeling errors in multi-dimensional finite elements.

The objective of this Section is to show that physically interpretable notation allows individual finite element strain modeling characteristics to be identified by inspection. This *a priori* evaluation of the modeling capability of an element is possible because the self-referential notation allows problem-specific knowledge to be brought to bear on the analysis. The value of this capability will be shown by identifying strain modeling errors in four-node quadrilateral finite elements that are submerged when the standard notation is used.

This Section and the one following demonstrate the power and usefulness of self-referential notation when it is applied to multi-dimensional solid mechanics problems. In this Section, the strain representations that are produced by the standard notation are compared to those produced by the physically interpretable notation for a four-node planar element, such as the one shown in Fig. 3.10.

In the following Section, the self-referential strain models that are formed in this Section are used to identify several strain modeling errors in the four-node planar element.

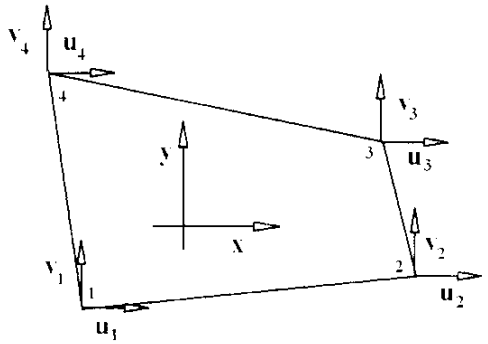

Figure 3.10 – A Four-Node Quadrilateral Element

The standard form of the displacement interpolation polynomials for a four-node element is the following [31, 32]:

$$u(x,y) = a_1 + a_2\,x + a_3\,y + a_4\,xy$$
$$v(x,y) = b_1 + b_2\,x + b_3\,y + b_4\,xy \qquad \text{(Eq. 3.15)}$$

As can be seen, these functions are augmented linear polynomials because an "xy" term augments the linear terms in the two equations. They are not complete quadratic polynomials

because they do not contain x^2 and y^2 terms. Note that the arbitrary coefficients – the "a's" and the "b's" – provide no direct information about the modeling capabilities of this finite element.

The displacement interpolation polynomials for the four-node quadrilateral expressed in physically interpretable notation are the following:

$$u(x,y) = (u_{rb})_0 + (\varepsilon_x)_0 x + (\gamma_{xy}/2 - r_{rb})_0 y + (\varepsilon_{x,y})_0 xy$$
$$v(x,y) = (v_{rb})_0 + (\gamma_{xy}/2 + r_{rb})_0 x + (\varepsilon_y)_0 y + (\varepsilon_{y,x})_0 xy \qquad \text{(Eq. 3.16)}$$

These displacement polynomials contain the following eight linearly independent coefficients: two rigid body displacements, $(u_{rb})_0$ and $(v_{rb})_0$; one rigid body rotation, r_{rb}; three constant strain terms, $(\varepsilon_x)_0$, $(\varepsilon_y)_0$ and $(\gamma_{xy})_0$; and two gradients of the normal strains, $(\varepsilon_{x,y})_0$ and $(\varepsilon_{y,x})_0$. That is to say, the four-node quadrilateral can represent the three rigid body motions, the three constant strain states and two other deformation patterns. For a complete development of Eq. 3.16, see Ref. 1.

The next step in identifying the advantages of the strain gradient notation is to form the strain models that are produced by the standard and the physically interpretable forms of the displacement interpolation polynomials given by Eqs. 3.15 and 3.16, respectively. When the definitions of the three strain components from linear elasticity are applied to the standard form of the displacement polynomial given by Eq. 3.15, the following strain models are obtained:

$$\varepsilon_x(x,y) = \frac{\partial u(x,y)}{\partial x} = a_2 + a_4 y \qquad \text{(Eq. 3.17)}$$

$$\varepsilon_y(x,y) = \frac{\partial v(x,y)}{\partial y} = b_3 + b_4 x \qquad \text{(Eq. 3.18)}$$

$$\gamma_{xy}(x,y) = \frac{\partial u}{\partial y} + \frac{\partial v}{\partial x} = (a_3 + b_2) + b_4 x + a_4 y \qquad \text{(Eq. 3.19)}$$

This result shows that the two normal strains contain a constant term and a linearly varying term. Neither of the normal strain representations are complete linear polynomials, i.e.,

they do not contain both an x and a y term. The shear strain component is a complete linear polynomial because it contains both an x and a y term. Nothing can be said about the detailed strain modeling capabilities of this element from visually inspecting Eqs. 3.17 – 3.19 because the coefficients of these equations have no intrinsic physical meaning.

The strain representations for the four-node quadrilateral element produced by the self-referential displacement polynomials given by Eq. 3.16 are the following:

$$\varepsilon_x(x,y) = \frac{\partial u(x,y)}{\partial x} = (\varepsilon_x)_0 + (\varepsilon_{x,y})_0\, y \qquad \text{(Eq. 3.20)}$$

$$\varepsilon_y(x,y) = \frac{\partial v(x,y)}{\partial y} = (\varepsilon_y)_0 + (\varepsilon_{y,x})_0\, x \qquad \text{(Eq. 3.21)}$$

$$\gamma_{xy}(x,y) = \frac{\partial u}{\partial y} + \frac{\partial v}{\partial x} = (\gamma_{xy})_0 + (\varepsilon_{x,y})_0\, x + (\varepsilon_{y,x})_0\, y \qquad \text{(Eq. 3.22)}$$

When Eqs. 3.20 – 3.22 are inspected, it is seen that the strain representations formed from the self-referential notation are expressed in terms of physically meaningful quantities. The three strain expressions given by Eqs. 3.20 – 3.22 contain five different quantities. The deformations produced by the three constant strain terms, $(\varepsilon_x)_0$, $(\varepsilon_y)_0$ and $(\gamma_{xy})_0$ are shown superimposed on the original shape of an element in Figs. 3.11a –3.11c, respectively.

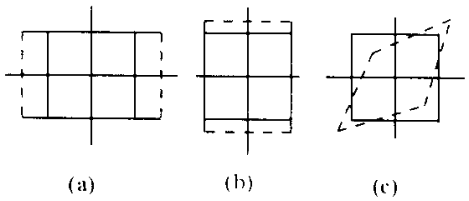

Figure 3.11 – Constant Strain States

The displacements produced by the two strain gradient terms $(\varepsilon_{x,y})_0$ and $(\varepsilon_{y,x})_0$ are shown superimposed over the original shape of the element in Fig. 3.12. The two strain states shown in Fig. 3.12 can be interpreted as flexure terms, since they have the form of the strain distribution contained in beam elements. As can be seen in Fig. 3.12, one side of the

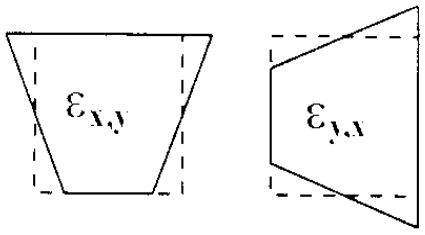

Figure 3.12 – Flexural Strain States

element is in tension and the other is in compression.

As these two figures show, the coefficients of the strain expressions can be directly related to the physical problem being represented. In the next Section, the strain models for the four-node planar element given by Eqs. 3.20 – 3.22 are evaluated by comparing them to the expected representation from continuum mechanics.

3.10 – Analysis by Inspection in Two Dimensions

In this Section, it is shown that the physically interpretable notation provides a transparency to the finite element method that does not exist with the standard notation. The value of this transparency is demonstrated by identifying several strain modeling errors that exist in the four-node quadrilateral by visually comparing the strain models given by Eqs. 3.20 – 3.22 to the strain representations from linear elasticity.

In order to simplify the comparison of the strain model in the four-node quadrilateral element to the expected result from continuum mechanics, both strain representations are expressed in a similar form so they can be compared visually. When the strain expressions from continuum mechanics are expanded as Taylor series and put in vector form, the following is obtained:

$$\begin{Bmatrix} \varepsilon_x \\ \varepsilon_y \\ \gamma_{xy} \end{Bmatrix} = \underbrace{\begin{Bmatrix} \varepsilon_x \\ \varepsilon_y \\ \gamma_{xy} \end{Bmatrix}_0}_{\text{Constant Term}} + \underbrace{x \begin{Bmatrix} \varepsilon_{x,x} \\ \varepsilon_{y,x} \\ \gamma_{xy,x} \end{Bmatrix}_0 + y \begin{Bmatrix} \varepsilon_{x,y} \\ \varepsilon_{y,y} \\ \gamma_{xy,y} \end{Bmatrix}_0}_{\text{Linear Term}} + \cdots \qquad \text{(Eq. 3.23)}$$

Only the constant and linear terms of this Taylor series expansion are explicitly presented. The higher-order terms are not presented in detail because the strain models for the four-node planar element do not contain any higher-order terms.

For completeness, it should be noted that the strain modeling errors in the four-node element result from the fact that the displacement interpolation polynomials for the element are not complete polynomials. As an aside, it should be noted that a six-node triangle, the linear strain triangle, is derived from complete displacement interpolation polynomials. The strain models for the six-node element match the complete linear representations presented in Eq. 3.23; hence, it contains no inherent strain modeling errors. Since the six-node element contains no inherent strain modeling errors, it is to be preferred to the four-node element in practically any application.

In order to more easily evaluate the strain modeling capabilities of the four-node element, Eqs. 3.20 – 3.22 are presented in the following vector form:

$$\begin{Bmatrix} \varepsilon_x \\ \varepsilon_y \\ \gamma_{xy} \end{Bmatrix} = \underbrace{\begin{Bmatrix} \varepsilon_x \\ \varepsilon_y \\ \gamma_{xy} \end{Bmatrix}_0}_{\uparrow} + \underbrace{\left[x \begin{Bmatrix} 0 \\ \varepsilon_{y,x} \\ 0 \end{Bmatrix}_0 + y \begin{Bmatrix} \varepsilon_{x,y} \\ 0 \\ 0 \end{Bmatrix}_0 \right]}_{\uparrow} + \underbrace{\left[x \begin{Bmatrix} 0 \\ 0 \\ \varepsilon_{x,y} \end{Bmatrix}_0 + y \begin{Bmatrix} 0 \\ 0 \\ \varepsilon_{y,x} \end{Bmatrix}_0 \right]}_{\uparrow} \qquad \text{(Eq. 3.24)}$$

Constant Term First Linear Term Second Linear Term

This form of the strain representation for the four-node element contains a constant term and two separate linear terms, both of which contain an x and a y component. This demonstration will show that the quantity labeled as the First Linear Term contains errors of omission and the quantity labeled as the Second Linear Term contains errors of commission.

The errors of omission are seen when the First Linear Term of Eq. 3.24 is compared to the Linear Term in Eq. 3.23. The First Linear Term of Eq. 3.24 contains four zeros. When this term is compared to the Linear Term of Eq. 3.23, no similar zeros exist in the continuum representation. The four strain quantities missing from Eq. 3.24 are the following: $(\varepsilon_{x,x})_0$ x , $(\gamma_{xy,x})_0$ x , $(\varepsilon_{y,y})_0$ y and $(\gamma_{xy,y})_0$ y. The absence of these terms can be viewed as imposing physical

constraints on the individual four-node elements, which has the tendency to make the individual elements overly stiff.

The errors of commission are seen when the Second Linear Term of Eq. 3.24 is compared to the Linear Term in Eq. 3.23. If the shear strain representation is extracted, which is contained in Eq. 3.24 for the convenience of the reader, the following equation that is identical to Eq. 3.22 is obtained:

$$\gamma_{xy}(x,y) = (\gamma_{xy})_0 + (\varepsilon_{x,y})_0\, x + (\varepsilon_{y,x})_0\, y \qquad \text{(Eq. 3.25)}$$

When Eq. 3.25 is compared to the third row of Eq. 3.23, it is seen that they do not match each other. The constant terms are the same, but the linear terms are different. The coefficients of the two linear terms x and y in Eq. 3.25 are the normal strain quantities $(\varepsilon_{x,y})_0$ and $(\varepsilon_{y,x})_0$, instead of the expected shear strain quantities $(\gamma_{xy,x})_0$ and $(\gamma_{xy,y})_0$. The existence of these differences in the shear strain model in the four-node element represents errors in the modeling capabilities of this element.

The fact that the two normal strain terms contained in Eq. 3.25 are in error can also be demonstrated with a physical argument. The two normal strain terms contained in the shear strain expression are incorrect because they violate the constitutive relationship for solid mechanics. There is no connection between the shear strains and the normal strains in linear elasticity. Thus, this element incorrectly engages a shear strain when the element is experiencing any linearly varying normal strain. This error is well known in finite element analysis and is identified as parasitic shear.

Planar eight- and nine-node elements also possess errors of the type identified for four-node elements. If the standard approach of using reduced-order Gauss quadrature integration is used in an attempt to eliminate parasitic shear from these elements, other errors are likely to be

introduced. The errors in these elements can be minimized by identifying these errors and improving the strain model during the formulation process using self-referential notation [24]. Because these higher-order elements still contain errors even after they are improved, these elements are less effective than the six-node linear strain triangle. Thus, it is recommended that the six-node element be used exclusively in place of eight- and nine-node elements.

This discussion of the modeling characteristics of the four-node element is intended to demonstrate the direct connection between the approximate solution technique and the solid mechanics problem provided by the self-referential notation. This brief analysis has shown that the four-node quadrilateral element contains several strain modeling errors. Since the four-node quadrilateral element contains modeling errors in all three strain components, the four-node element is less capable of representing the continuum than is a three-node element except possibly in certain special problems. In a converged result, the effect of the existing linear terms would be eliminated because the four-node element cannot capture the Poisson effect [24]. In a non-converged result, the four-node element is overly stiff because of the strain modeling errors[2].

3.11 – Summary and Conclusion

This Chapter introduced the physically interpretable notation that provides a direct connection between the formulation of finite elements and the equations of continuum mechanics that are being represented by the finite element method. This notation expresses the interpolation polynomials that are used to form the finite element method in terms of strain quantities, the quantities that produce the displacements in the continuum. That is to say, this physically based notation provides a transparency to the finite element method that is not

[2] At the element level, the new ability to analyze the element formulation process eliminates the need to use the isoparametric formulation process [30], eliminates the need to consider spurious zero energy modes, provides a way to eliminate shear locking, and explains aspect ratio stiffening. These ideas and others for improving element development are presented in detail in Reference 1.

available with the standard notation. This self-referential notation was related to the arbitrary coefficients of the standard interpolation polynomials in Section 3.3.

It was shown that this notation allows the improvement of every facet of the finite element method. In Sections 3.4, 3.8, 3.9 and 3.10, this self-referential notation was used to evaluate the strain modeling capabilities of individual finite elements during the formulation process. In Sections 3.5, 3.7 and 3.8, the ability to evaluate the in-situ performance of individual elements was developed and applied.

In Section 3.6, it was shown that there is a direct relationship between the finite element and the finite difference methods. As is seen in later Chapters, the identification of this relationship provides the theoretical foundation and practical basis for pointwise error measures, termination and refinement guides.

This paragraph contains a disclaimer concerning the self-referential notation presented in this Chapter. It should be noted that an understanding of the self-referential notation is only mandatory for researchers and practitioners who seek to understand the finite element method in depth. Once the insights provided by the physically based notation are embedded in the code used in application programs, the casual user never need know what errors have been eliminated from the analysis procedure as a result of using the techniques introduced here and developed in depth in Ref. 1. However, the understanding and appreciation of this notation opens the door for research in the application of the **finite difference** method to solid mechanics problems, in the development of mesh refinement strategies and in the development of error estimators.

CHAPTER 4

THE SOURCE AND QUANTIFICATION OF DISCRETIZATION ERRORS

4.1 – Introduction

When a finite element model cannot capture the exact solution, inter-element jumps or discontinuities exist in the approximate strain representation. As shown in Fig. 4.1, the inter-element jumps are reduced as the finite element model is improved and approaches the exact solution. In this figure, the uniformly refined results are contrasted to the exact solution.

The results shown in Fig. 4.1 imply that differences between the exact solution and the finite element result are correlated to the inter-element jumps in the strains. These differences between the exact solution and the finite element result are called **discretization errors.**

These errors get their name from the fact that differences between the exact and the finite element solution are produced when the polynomial approximations in the discrete number of finite elements cannot capture the exact result.

The objective of this Chapter is to show that the

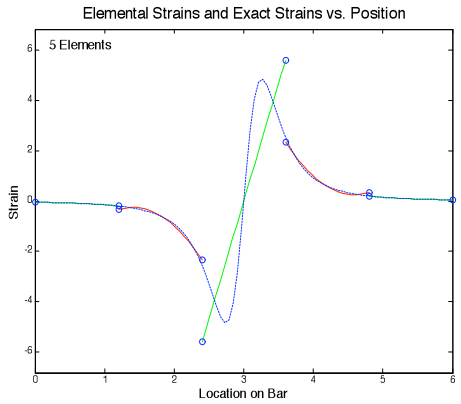

(a) Five Element Model

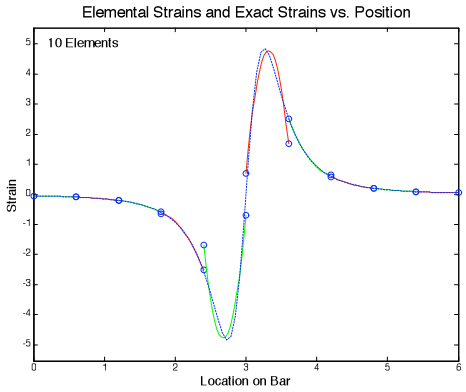

(b) Ten Element Model

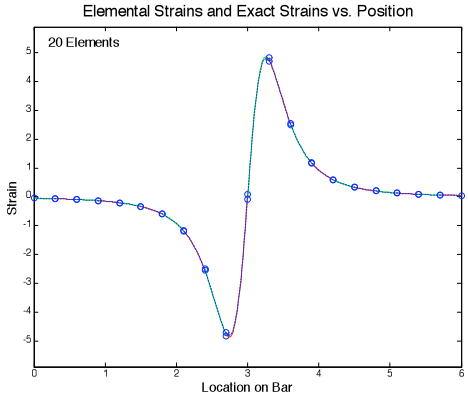

(c) Twenty Element Model

Figure 4.1 – A Uniformly Refined Model vs. The Exact Solution

inter-element jumps in the strain are directly related to the inability of the finite element model to capture the exact solution.

This objective will be accomplished by showing that the inter-element jumps in the strains are directly related to the differences between the exact solution and the finite element result for four-node bar elements. The result is extendible to higher-dimension elements.

The errors in the finite element result are produced by the failure of the finite element solution to satisfy the governing differential equation at every point on the domain of an individual element, i.e., equilibrium is not satisfied.

When these failures to satisfy equilibrium are treated as fictitious distributed loads on the individual elements, it can be shown that the inter-element jumps are, indeed, a quantification of the discretization errors.

In a later Chapter, the inter-element jumps are used as an *a posteriori* error estimator to introduce the adaptive refinement process. After the introduction to adaptive refinement, it is shown that more efficient and practical error estimators exist for identifying discretization errors. However, the results developed in this Chapter provide the theoretical basis and/or intuition for the more efficient and practical error estimators.

4.2 – Background Concepts

This Section contains an overview of an approach to error analysis that was developed by Kelly et al. [3]. Kelly's work provides a point of view for identifying the source of discretization errors and shows that the inter-element jumps in the stresses and/or strains quantify the discretization errors. The objective of this Section is to outline this point of view so the individual steps that are presented in later Sections to demonstrate Kelly's contention can be seen in context.

It is clearly understood that discrete finite element models cannot represent the exact solutions for each of the infinite number of loading conditions that can be applied to a given continuous physical system. The innovation in Kelly's work consists of turning this point of view on its head. Kelly postulates that an approximate finite element solution with its inter-element jumps is the exact solution to an auxiliary problem that is closely related to the original problem. The auxiliary problem is identified as the original problem with the addition of a set of applied loads that are introduced on the boundaries between the elements. Furthermore, these additional loads are directly related to the inter-element jumps in the stresses or strains in the original finite element result.

This idea is demonstrated with an example. The auxiliary problem for the finite element model shown in Fig. 4.2a is formed. The problem consists of the five-element bar model with the symmetric load that was discussed in Chapter 2. The strain distribution produced by this finite element model is shown in Fig. 4.2b along with the exact solution.

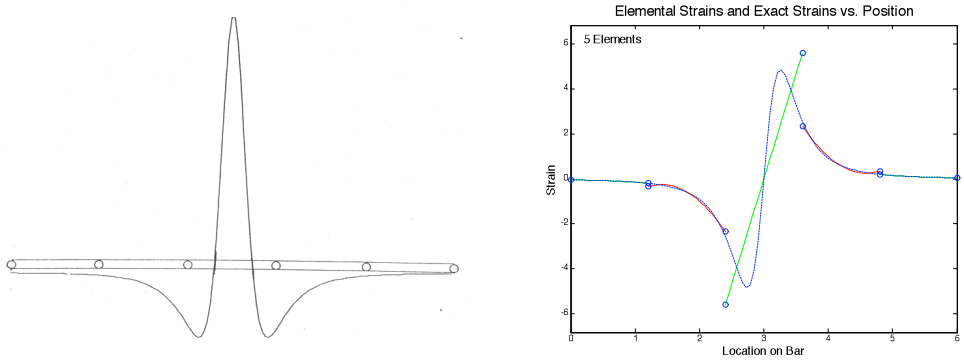

(a) Applied Load (b) Finite Element and Exact Strain Distributions

Figure 4.2 – A Finite Element Model and Its Strain Result

As can be seen, this finite element solution contains jumps in the strains between elements. It is important to note that the jumps are larger in the regions of high error. The errors are, of course, quantified by the differences between the approximate finite element result and the exact solution.

Figure 4.3 shows the auxiliary problem for which the finite element result shown in Fig. 4.2b is the exact solution. It consists of the original problem presented in Fig. 4.2a to which a set of auxiliary nodal forces has been added.

The additional forces are derived from the jumps in the strains that exist in the example problem. The auxiliary forces are equal to $F_{added} = AE\Delta_{strain}$. In this case, the forces are equal to the following: -12.9414, -294.7040, -294.7040 and -12.9414, respectively. As is apparent in Fig. 4.2b, the jumps in the strains are proportional to the errors in the approximate solution.

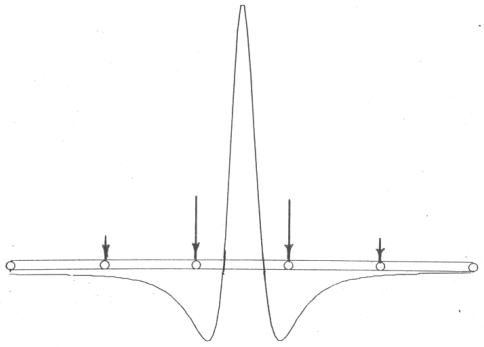

Figure 4.3 – Finite Element Model with the Augmented Load

In the next Section, it is shown that these inter-element point loads result from the failure of the individual elements to satisfy pointwise equilibrium on the individual elements. The inter-element forces are required to produce equilibrium at the nodes in the finite element model because of the modeling failure of the individual elements. As a result, the inter-element jumps decrease as the model is refined and the individual elements better represent the exact solution. Thus, the inter-element jumps can serve as *a posteriori* (after the fact) error measures. It should be noted that the inter-element jumps in strains for two-dimensional problems consists of three components on the boundaries between the elements and not just at the nodes.

In addition to identifying the magnitudes and locations of the discretization errors, the inter-element jumps in the strains can serve as termination criteria. This is the case because of the physical nature of the error measure. The jumps measure quantities that are directly related to the failure of the material in the continuum being modeled, e.g., steel or aluminum. That is to say, if the jumps are relatively small with respect to the stresses on the interface or small with

respect to the failure criterion, the model need not be refined further because the approximate results can be considered as accurate representations of the exact result.

4.3 – Quantifying the Failure to Satisfy Pointwise Equilibrium

In this Section, it is demonstrated that the inter-element jumps in the finite element solutions are due to the failure of the approximate solution to satisfy pointwise equilibrium over the domains of the individual finite elements. This is accomplished with the following three steps:

a) Form a residual function that quantifies the pointwise failure of the finite element solution to satisfy the governing differential equation over the domain of the individual elements.

b) Form equivalent elemental nodal residuals by treating the elemental residual functions as fictitious or auxiliary distributed loads.

c) Form a global nodal residual vector by assembling the elemental nodal residuals into an auxiliary global load vector and compare it to the fictitious loads that are produced by the jumps in the inter-element strains.

It is shown in this demonstration that the equivalent nodal loads formed from the residual quantities are identical to the loads formed from the jumps in the inter-element strains. This allows the conclusion to be made that the inter-element jumps are produced by the failure of the finite element solution to satisfy pointwise equilibrium over the domain of the problem.

This process is now demonstrated for the problem shown in Fig. 4.2a by computing the auxiliary loads shown in Fig. 4.3 using the step-by-step process just presented.

Step 1 – Residual Function Formulation: The failure of an approximate solution to satisfy pointwise equilibrium will be quantified as a residual quantity. The residual computes the

amount by which the finite element solution fails to satisfy the governing differential equation. The governing differential equation for a uniform bar is the following:

$$E\,A\frac{d^2\,u(x)}{dx^2} = f(x) \qquad \text{(Eq. 4.1)}$$

where u is the displacement along the bar and f(x) is the applied load.

If the approximate solution produced by the finite element model, $\tilde{u}(x)$, is substituted into Eq. 4.1, the equation may not be satisfied identically because the finite element result is not necessarily the exact solution. The amount by which the approximate solution fails to satisfy pointwise equilibrium is quantified with the following relationship:

$$r(x) = E\,A\frac{d^2\,\tilde{u}(x)}{dx^2} - f(x) \qquad \text{(Eq. 4.2)}$$

where r(x) is called the residual. The computation of the residual can be extended to higher dimensions.

Note that the residual has units that are identical to the applied force. Because of this similarity in units, the residual will be treated as a distributed force. That is to say, the residual is considered as an auxiliary or a fictitious force in the remainder of this Section.

An example of a residual formed with Eq. 4.2 for the problem shown in Fig. 4.2a is shown in Fig. 4.4. The residual, which is shown as the solid (blue) line, is discontinuous on the full domain of the problem, but continuous over the

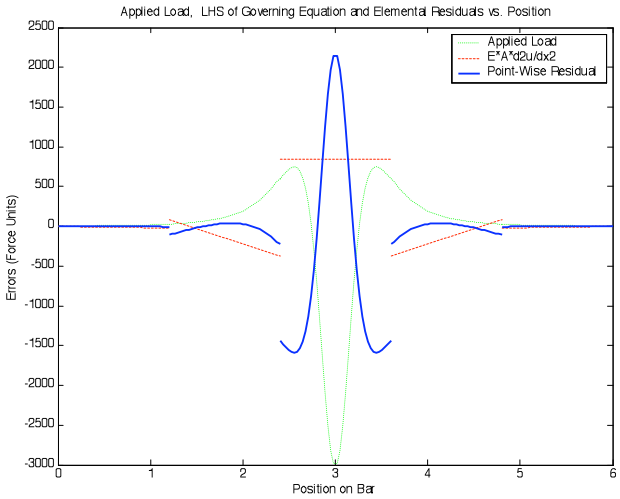

Figure 4.4 – The Elemental Pointwise Residuals and Their Components

individual elements. This is to be expected when the two components of Eq. 4.2 are considered. These two components are also shown in Fig. 4.4. Both components are continuous over the individual elements, but the contributions of the individual finite elements are discontinuous at the inter-element nodes.

Step 2 – Elemental Nodal Residual Formulation: In this step, the residual functions for the individual elements are transformed into equivalent nodal quantities for the separate elements. The equivalent nodal residuals are formed by using the standard finite element approach for including distributed loads into a finite element model. This procedure is applied because, as was noted in the previous step, the residual function has the same units as a distributed load.

The formulation of these nodal quantities proceeds as follows. First, a function is formed that is equivalent to the work function that is part of the potential energy expression for a bar element. That is to say, an integrand is formed that consists of the residual function for a bar that is multiplied by the displacement interpolation function for the bar. Then, this result is integrated over the domain of the element. Finally, the derivatives are taken that are required in the application of the principle of minimum potential energy to form the equivalent nodal residuals. The formulation of these elemental nodal residuals for this example is presented next.

The fictitious work done by the residual identified in Eq. 4.2 is produced when it is moved by the displacement along the domain of the bar. The fictitious work function for the i-th element is given as follows:

$$W_i = \int_{L_i} (r_i(x) * u_i(x))\, dx \qquad \text{(Eq. 4.3)}$$

When Eq. 4.2 and the displacement interpolation polynomial for a four-node bar are introduced into Eq. 4.3, the following is obtained:

$$W_i = \int_{L_i} (r_i(x) * \tilde{u}_i(x))\,dx$$

$$= \int_{L_i} \left(E\,A \frac{d^2\,\tilde{u}(x)}{dx^2} - f(x) \right)_i * \tilde{u}_i(x)\,dx \qquad \text{(Eq. 4.4)}$$

$$= \int_{L_i} \left(E\,A \frac{d^2\,\tilde{u}(x)}{dx^2} - f(x) \right)_i * (N_1\ N_2\ N_3\ N_4) \begin{Bmatrix} u_1 \\ u_2 \\ u_3 \\ u_4 \end{Bmatrix}_i dx$$

When the necessary derivatives are taken to form the equivalent nodal loads, the following is obtained:

$$\begin{pmatrix} F_1 & F_2 & F_3 & F_4 \end{pmatrix}_i = \begin{pmatrix} \frac{\partial W}{\partial u_1} & \frac{\partial W}{\partial u_2} & \frac{\partial W}{\partial u_3} & \frac{\partial W}{\partial u_4} \end{pmatrix}_i \qquad \text{(Eq.4.5)}$$

The components of this row vector are the equivalent nodal residuals for the i-th element.

When this operation is performed for the five elements contained in the problem shown in Fig. 4.2a using the residuals shown in Fig. 4.4, the results are presented in Tables 4.1 – 4.3.

Table 4.1 contains the contribution of the first term of Eq. 4.2 or Eq. 4.4 to the equivalent nodal loads, namely, the portion of the residual due to the internal loads in the finite element solution for the five individual elements of the model. Table 4.2 contains the contribution of the second term of Eq. 4.2 or Eq. 4.4 to the equivalent nodal loads for the five individual elements of the model. Note that the quantities in Table 4.2 are equal to the negative of the distributed loads applied to the original problem.

Table 4.1 – Internal Load Component of the Nodal Residuals, $EAd^2\tilde{u}/dx^2$

El. No.	F_1	F_2	F_3	F_4
1	-0.4951	-2.1016	-7.6494	-2.7553
2	2.5747	-5.8890	-128.4081	-47.3405
3	126.0909	378.2728	378.2728	126.0909
4	-47.3405	-128.4081	-5.8890	2.5747
5	-2.7553	-7.6494	-2.1016	-0.4951

Table 4.2 – Applied Load Component of the Nodal Residuals (-1*Applied Load)

El. No.	F_1	F_2	F_3	F_4
1	0.8959	2.1016	7.6494	3.3529
2	9.7690	5.8890	128.4081	67.2726
3	148.6809	-378.2728	-378.2728	148.6809
4	67.2726	128.4081	5.8890	9.7690
5	3.3529	7.6494	2.1016	0.8959

Table 4.3 contains the sum of Tables 4.1 and 4.2. These quantities are the equivalent nodal residuals for the individual elements produced by Eqs. 4.3 – 4.5. These residual quantities will be treated as auxiliary forces in the analysis that follows.

Table 4.3 – Elemental Equivalent Nodal Residuals

El. No.	F_1	F_2	F_3	F_4
1	-0.4008	0.0	0.0	-0.5976
2	-12.3438	0.0	0.0	-19.9321
3	-274.7718	0.0	0.0	-274.7718
4	-19.9321	0.0	0.0	2.5747
5	-0.5976	0.0	0.0	-0.4951

When Table 4.3 is examined, it is seen that the residuals associated with the interior nodes of the individual elements are equal to zero. This result is consistent with the fact that that there are no discontinuities in the finite element strains on the interior of the element. As a result of this continuity, there is no mechanism available for correcting any failure of the element to satisfy pointwise equilibrium except at the inter-element nodes.

Step 3 – Global Nodal Residual Formulation and Comparison: In this step, the elemental nodal residuals contained in Table 4.3 are assembled into the vector of global residual nodal loads that are applicable to the bar problem with two fixed ends. This is accomplished by assembling the global vector using the standard finite element procedure. Next, the two end loads are eliminated because of the fixed boundary conditions. These results are shown in Table 4.4. The zero loads on the interior of the bar are eliminated in order to highlight the non-zero

elements. The columns labeled F_{Left} and F_{Right} are the two elemental components that are summed to give the global result contained in the final column of Table 4.4.

Table 4.4 – Global Nodal Residuals

	F_{Left}	F_{Right}	F_{Total}
Load 1	-0.5976	-12.3438	-12.9414
Load 2	-19.9321	-274.7718	-294.7040
Load 3	-274.7718	-19.9321	-294.7040
Load 4	-12.3438	-0.5976	-12.9414

When the quantities in the last column of Table 4.4 are compared to the equivalent loads computed in Section 3.2 and shown in Fig. 4.3, they are found to be identical. This means that the jumps in the inter-element strains do, indeed, quantify the failure of the individual finite element models to satisfy pointwise equilibrium.

In Chapter 2, it was shown that as the finite element model is refined, either by uniform or adaptive refinement, two changes occurred in the approximate solutions. The finite element representation better approximates the exact solution and the inter-element jumps in the strain are reduced.

This combination of results is consistent with Kelly's contention that the inter-element jumps quantify the discretization errors in finite element models. The demonstration just presented shows that the inter-element jumps are equivalent to the failure of the finite element model to satisfy pointwise equilibrium. This example explains Kelly's contention and gives it a solid theoretical foundation.

Since the residual quantities are related to quantities of interest in continuum mechanics, such as strains, the residuals can serve as both an error measure and as a termination criterion. For example, if the residuals everywhere in the model are small with respect to the critical strain level, the approximate solution can be considered sufficiently accurate, and the analysis can be

terminated. This is the case because the addition of a sufficiently small change in the strain level will not be responsible for the failure of material.

4.4 – Every Finite Element Solution is an Exact Solution to Some Problem

Although it has been demonstrated that the inter-element jumps are equivalent to the failure of the finite element model to satisfy pointwise equilibrium, Kelly's interpretation that every finite element solution is the exact solution to some problem has not been explicitly demonstrated. The validity of this idea is demonstrated here by inverting Kelly's point of view. That is to say, the loads applied to a finite element model that has a result that contains inter-element jumps are modified so that the solution of the modified finite element model contains no inter-element jumps. The result can be considered an exact result at the inter-element nodes of the model. The new model is formed by adding a set of concentrated loads that are the negative of the "fictitious" loads shown in Fig 4.3. This situation is shown in Fig. 4.5.

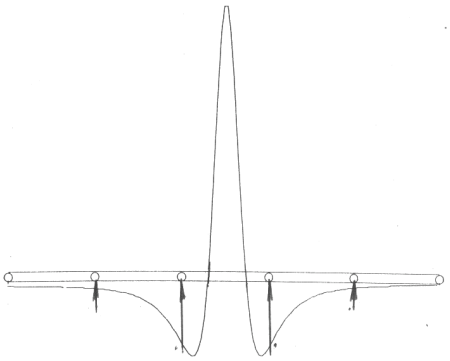

Figure 4.5 – Finite Element Model with "Strain Smooth" Loads

The rationale for this approach is the following. If the fictitious loads in Fig. 4.3 produce the inter-element jumps shown in Fig. 4.2b, then the opposite set of loads should eliminate these inter-element jumps in the strains. When this modified problem is solved, the finite element strain representation is shown in Fig. 4.6 along with the exact solution. As can be seen, the additional loads

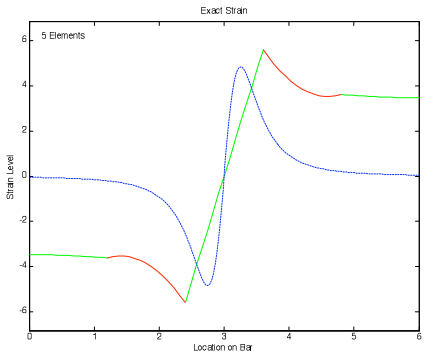

Figure 4.6 – A Smoothed Strain Result Compared to the Exact Result

have eliminated the inter-element jumps in the strain representation for this modified problem.

The elimination of the inter-element jumps by the introduction of these fictitious point loads shows that the inter-element jumps are caused by the failure of the finite element solution to satisfy the governing differential equations on a pointwise basis. This is demonstrated by the results shown in Fig. 4.6 because the added point loads are exactly equal to this failure to satisfy the pointwise equilibrium and they are applied in a direction that compensates for this deficiency.

4.5 - Summary and Conclusion

This Chapter has introduced and validated Kelly's approach for identifying the errors in finite element solutions. It was shown that the inter-element jumps quantify the discretization errors in the finite element result and that the discretization errors are due to the inability of the individual finite elements to satisfy pointwise equilibrium.

In Chapter 5, the inter-element jumps are used as an error measure to drive an adaptive refinement process. It is demonstrated there that it works well. However, the approach that uses the inter-element jumps as an error measure and a termination criterion has two deficiencies.

The primary deficiency is one of computational efficiency in the higher dimensions. Other approaches exist that are easier to compute that give equal or better results. The second deficiency is the fact that the errors are aggregated in this process. That is to say, positive pointwise errors can cancel negative pointwise errors in the integration used to compute the nodal residuals. This idea is discussed in detail in Chapter 6, which develops and applies energy-based error estimators.

However, the demonstration that the discretization errors are due to the failure to satisfy pointwise equilibrium and the fact that this failure is responsible for the inter-element jumps in

the strains provides the insight for guiding the development of other error estimators and termination criterion. Pointwise error measures that are easy to compute, have a higher resolution than the aggregated measures, such as those based on strain energy, and have a solid theoretical foundation are presented in later Chapters.

CHAPTER 5

INTRODUCTION TO ADAPTIVE REFINEMENT

5.1 - Introduction

The initial finite element model for a problem rarely provides a solution that is accurate enough for use in the design process. The obvious strategy for improving the model is to repeatedly subdivide every element in the model until the change in two successive results is acceptably small. However, this brute force approach for reaching a converged solution leads to finite element models that are unmanageably large because elements are needlessly introduced into regions containing little or no error.

The excessive growth produced by uniformly refining a finite element model can be eliminated by selectively improving the model only in regions containing high levels of error. A procedure for identifying regions of unacceptable error and improving the model in these regions is shown schematically in Fig. 5.1.

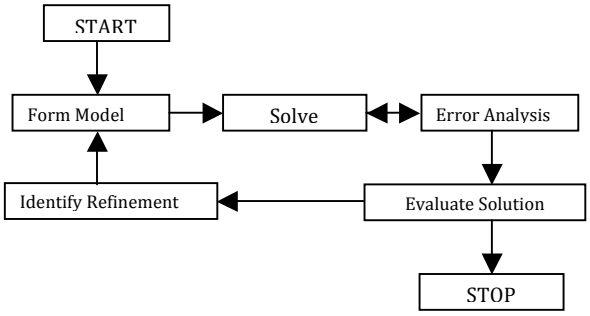

Figure 5.1 – Adaptive Refinement Schematic

This procedure, known as adaptive refinement, begins by forming an initial finite element model. The errors in the solution of the initial finite model are then estimated. If the specified level of accuracy is not achieved, the model is improved by refining the mesh in regions of unacceptable error. The process is repeated, starting with the improved model, until an acceptable solution is obtained.

The primary objective of this Chapter is to demonstrate the effectiveness of the adaptive refinement process. The secondary objective is to show that error estimators can be designed to produce finite element results with specified characteristics.

These objectives are achieved by developing error estimators based on physically interpretable quantities, namely, the inter-element jumps in the strain. Since strains are quantities of direct interest to the analyst, error estimators can be given a specialized, strain dependent focus. For example, the error estimators can be based on a specific failure criterion, such as introducing a bias on shear strains for a brittle material.

In the first demonstration, an error estimator that focuses the refinements of the finite element model on regions containing stress concentrations guides the adaptive refinement process. The second demonstration produces a final result with a uniform level of error over the domain of the finite element problem.

5.2 – Physically Interpretable Error Estimators

This Chapter demonstrates that error estimators can be designed to produce finite element results with given characteristics. The ability to specialize the error estimators is possible because they are based on physically interpretable quantities that are sought in the analysis [24]. In this case, the errors are based on the jumps in the inter-element strains, i.e., metrics that quantify the failure of the finite element result to satisfy the governing differential equation(s).

Two error estimators are applied to problems modeled with three-node bar elements to demonstrate that error estimators can be designed to produce results with specified characteristics. The first error estimator focuses on improving the model in regions of high strain and the second is designed to produce a uniform level of error everywhere in the problem.

The two error estimators demonstrated here have the following general form:

$$\eta_i = \left| \frac{(\Delta\varepsilon)_i}{(\varepsilon)_{\text{Normalizing}}} \right| \times 100 \qquad \text{(Eq. 5.1)}$$

where η_i = percent of estimated error at the i-th node.

$(\Delta\varepsilon)_i = (\varepsilon_{\text{Right Hand Element}} - \varepsilon_{\text{Left Hand Element}})_i$

$(\varepsilon)_{Normalizing}$ = the normalizing factor that focuses the model refinement.

The error estimator defined by Eq. 5.1 estimates the error given by the inter-element jumps in the strain at the i-th node as a percentage of the normalizing factor.

The numerator of Eq. 5.1, $(\Delta\varepsilon)_i$, is equal to the jump in the inter-element strain at the i-th inter-element node. This jump is directly related to the errors in the two elements adjacent to the node. The choice of the normalizing factor, $(\varepsilon)_{\text{Normalizing}}$, defines the focus of the error estimator and, ultimately, the characteristics of the final finite element model.

The first error estimator demonstrated here is designed to focus on regions containing stress concentrations. This focus is provided by choosing a normalizing factor, the denominator of Eq. 5.1, that has a constant value. As a result, regions of high error are highlighted.

This globally normalized error estimator focuses on stress concentrations for the following two reasons: **1)** stress concentrations are characterized by rapidly changing strain distributions and **2)** finite element models based on low-order polynomials contain large errors when they are attempting to represent complex functions unless they are highly refined. This version of the error estimator is demonstrated in Section 5.5.

On the other hand, if a normalizing factor is chosen that is closely related to the strain levels in the elements adjacent to i-th node, the errors in the final model are equally distributed over the domain of the problem regardless of the variations in the strain levels. That is to say, this locally normalized error estimator produces results in which the errors in regions of

low strains and in regions of high strain are nearly equal. This version of the error estimator is demonstrated in Section 5.6.

5.3 – A Model Refinement Strategy

With the development of an error estimator, a strategy must be implemented for improving the finite element model based on these error estimates. In the demonstrations of adaptive refinement presented in Sections 5.5 and 5.6, the decision on whether to subdivide an element is based on the average of the error estimates at the two ends of the finite element. If this average value for an element exceeds some threshold value, the element is divided into two equal sized elements.

This simple strategy is chosen because the purpose of these demonstrations is to present the efficacy of the adaptive refinement process, not to optimize the process. The issue of refinement strategies is revisited in later Chapters. It is shown in later discussions that the possibilities of refinement strategies are limited only by our imaginations.

5.4 – A Demonstration of Uniform Refinement

In preparation for demonstrating the adaptive refinement process, a sequence of uniform refinements is applied to a sample problem in this Section. The models that result from these uniform refinements serve two purposes: **1)** they show the explosive growth in the number of elements in a uniformly refined model that necessitates the use of adaptive refinement and **2)** the approximate strain distributions produced by these models provide a baseline against which to compare the results of the adaptive refinement process.

The finite element strain approximations and the associated error estimates associated with the initial five-element model are shown in Fig. 5.2. Figure 5.2a compares the strains in the finite element model to the exact solution. Figure 5.2b contains the error estimates at the nodes

of this model. The error estimate at each node is normalized with the magnitude of the largest strain in the finite element model. The error estimates at the nodes are connected by straight lines for visual convenience. The lines have no significance.

The error estimates at the two fixed ends of the finite element model are taken to be zero. These estimates are close to the actual error for this problem. The treatment of the boundary errors is postponed until Chapter 8 because the estimation of the errors on the boundaries is closely related to the pointwise error measures presented in Chapter 8.

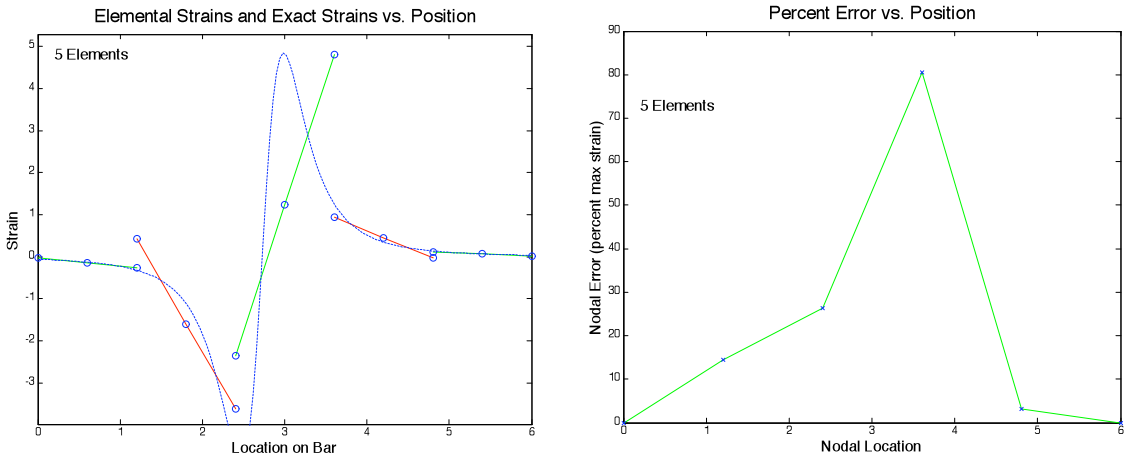

(a) Five Element Strain Results (b) Relative Nodal Errors

Figure 5.2 – Initial Mesh for Both Uniform Refinement and Adaptive Refinement

When the error estimates shown in Fig. 5.2b are compared to the actual errors that can be seen in Fig. 5.2a, that the error estimates are shown to correlate well with and the actual errors in the finite element strain distribution. The large errors exist where an attempt is being made to represent a complex strain distribution with a small number of elements that are, at most, capable of representing linear strain.

The finite element representation of the exact result will be improved by adding elements to the regions showing high error. This means that the error estimator given by Eq. 5.1 will successfully guide the adaptive refinement process. This contention is validated in the next Section.

The results of the first uniform refinement of the initial model are shown in Fig. 5.3. As can be seen in Fig. 5.3a, the strain distribution for the uniformly refined finite element model more closely resembles the exact solution than does the result shown in Fig. 5.2a. The finite element approximation is smoother and the strain representations in the regions of the stress concentrations, while still discontinuous, are located near the points of maximum absolute magnitudes in the exact solution.

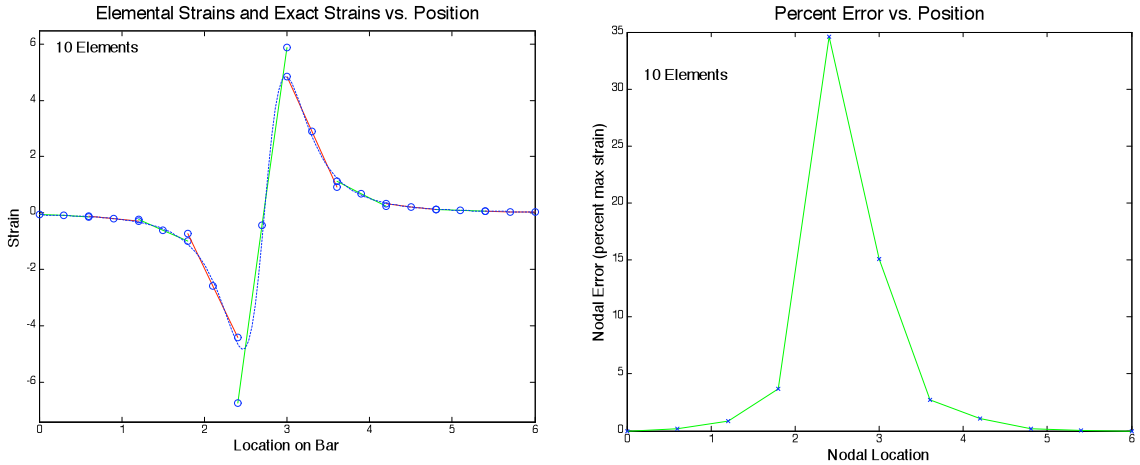

(a) Ten Element Strain Results (b) Relative Nodal Errors

Figure 5.3– First Uniformly Refined Finite Element Model

The error estimator captures these improvements in the finite element representation, as shown in Fig. 5.3b. When Fig. 5.3b is compared to Fig. 5.2b, it is seen that the error estimates over the whole model are reduced. The maximum error estimate has been reduced to approximately 35 percent from the previous estimate of approximately 80 percent. Again, the highest levels of error exist in regions of the exact strain distribution that are too complex to be captured by the linear strain representation of a single finite element.

The results of the second uniform refinement are shown in Fig. 5.4. The resulting error estimates contains an interesting result. The maximum error estimate has not changed much from the maximum estimate in the previous refinement. It is approximately 33 percent versus the approximate value of 35 percent in the previous refinement. However, the nature of the

strain in the location of the maximum error estimate has changed markedly. Instead of being associated with a maximum point in the strain distribution, the maximum error estimate occurs at an inflection point in a region with a very small strain value in the exact solution. That is to say, the maximum error exists in a region of a stress concentration with a rapidly changing strain distribution. Again, the error estimator has identified a region in a strain distribution that cannot be easily represented by a linear strain representation.

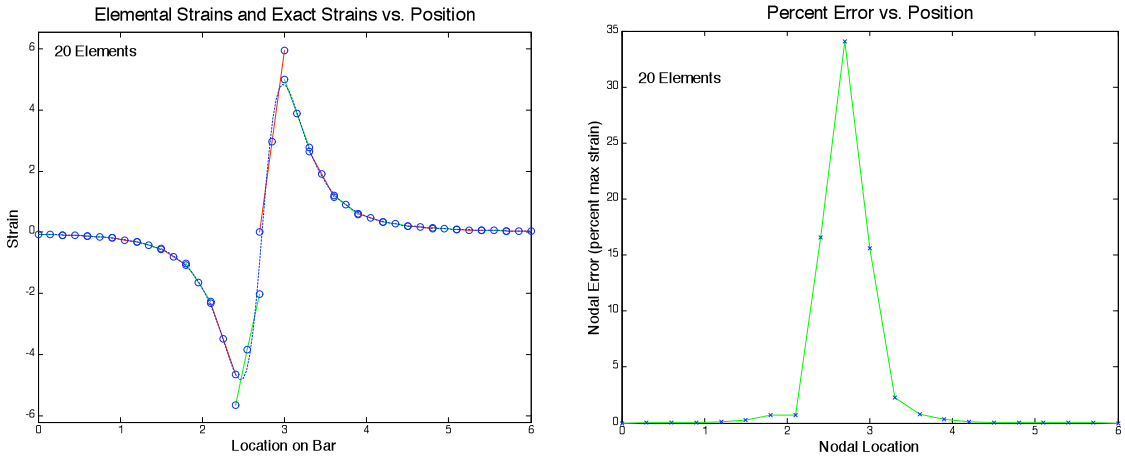

(a) Twenty Element Strain Results (b) Relative Nodal Errors

Figure 5.4– Second Uniformly Refined Finite Element Model

Figure 5.5 presents the result of the third uniform refinement. In this refinement, the maximum error estimate has been significantly reduced from approximately 33 percent to approximately seven percent. However, the error estimate in the region of the inflection point still exceeds the estimated error at the stress concentration.

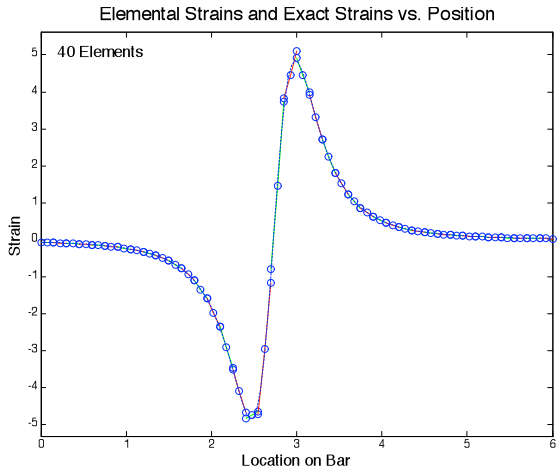

(a) Forty Element Strain Results

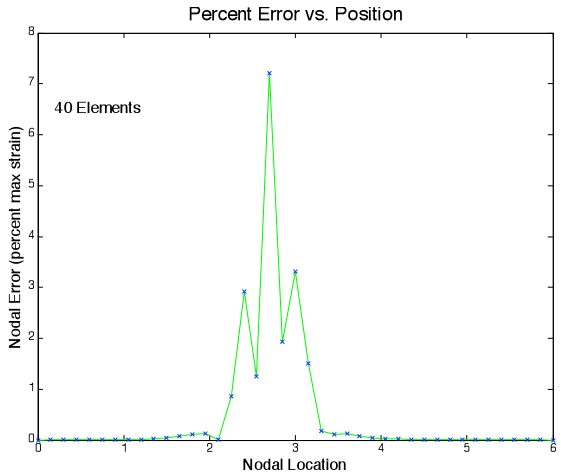

(b) Relative Nodal Errors

Figure 5.5 – Third Uniformly Refined Finite Element Model

The primary deficiency with uniform refinement is seen when Figs. 5.4 and 5.5 are compared. In Fig. 5.4b, it is seen that the error estimates are close to zero on the two outside portions of the model. In the uniform refinement shown in Fig. 5.5, the majority of the new elements are introduced into these regions of low error. That is to say, most of the new elements are introduced into regions where they are not needed.

The introduction of these unneeded elements characterizes the inefficiency found in the process of uniform refinement. It should be noted that the inefficiency seen in this one-dimensional case is minor when compared to the unneeded elements that can be introduced into two- and three-dimensional problems.

Figure 5.6 presents the results of the fourth uniform refinement of the model.

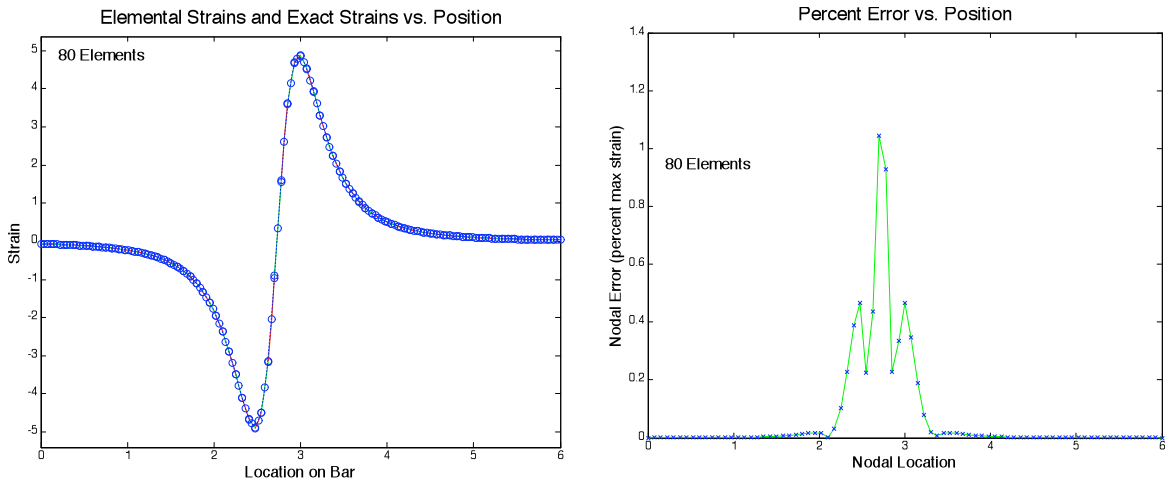

Eighty Element Strain Results (b) Relative Nodal Errors

Figure 5.6 – Fourth Uniformly Refined Finite Element Model

In this refinement, the errors have the same general distribution as that seen in the previous refinement shown in Fig. 5.5b. However, the magnitudes of the errors have been significantly reduced. In fact, they are reduced to a level that would be considered accurate enough for practically any design process. The inefficiency of the uniform refinement process is demonstrated again. Most of the new elements are introduced in regions of low error where no refinement is needed.

5.5 – A Demonstration of Adaptive Refinement

In this Section, the effectiveness of the adaptive refinement process is demonstrated. The initial finite element model used in Fig. 5.2 is adaptively refined under the guidance of the error estimator defined in Eq. 5.1. This error estimator is normalized with respect to the maximum strain in the finite element model. This is the same error estimator that was used in the previous Section to evaluate the results of the uniformly refined models. This choice for the normalizing factor means that the error estimator will focus on the stress concentrations.

The elemental error threshold for dividing an element in half is chosen as four percent. The demonstration will show that there are significantly fewer elements needed in the adaptively refined model to satisfy the termination criterion of four percent error or less at each node.

The adaptive refinement process achieved the desired level of accuracy after four iterations. The nodal error estimates for these five models are superimposed in Fig. 5.7. The most significant result shown in Fig. 5.7 is that the termination criterion was satisfied with only nineteen elements. This compares to the eighty elements that were contained in the uniformly refined model that was required to achieve the same level of accuracy.

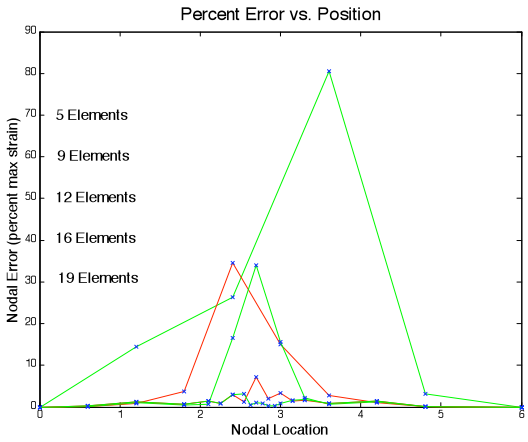

Figure 5.7 – Nodal Errors for Four Iterations of Adaptive Refinement

In order to better see how the finite element model formed by the adaptive refinement process compares to the final model produced by uniform refinement, the result of the final iteration of adaptive refinement is shown in Fig. 5.8.

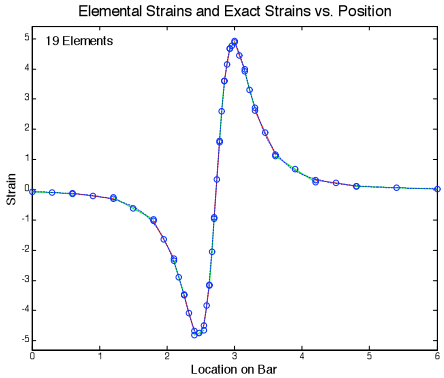

(a) Nineteen Element Strain Result

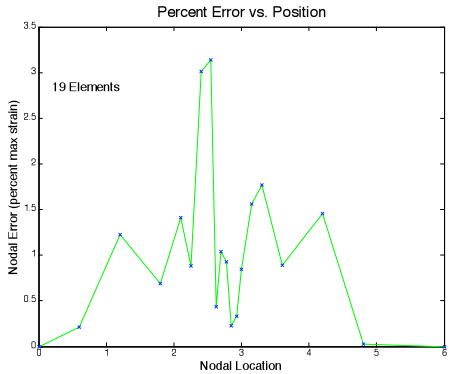

(b) Relative Nodal Errors

Figure 5.8 – Fourth Adaptively Refined Finite Element Model

As can be seen, there are fewer elements in the regions of low error at either end of the model when Fig. 5.8a is compared to Fig. 5.6a. This is as would be expected. The elements added by the adaptive refinement process are located where they do the most good, namely, in the regions of high error. In other words, the adaptive refinement process adds elements to the

region where the actual strain distribution is complex until there are enough elements to capture this complex strain distribution with linear strain representations.

Just to see what it takes in the way of adaptive refinement to reduce the estimated errors in the problem to a level below those in the final uniformly refined model, the problem is adaptively refined with a lowered value for the criteria for subdividing an element and for the termination of the adaptive refinement process. The result for a threshold value of 1.5 percent is shown in Fig. 5.9.

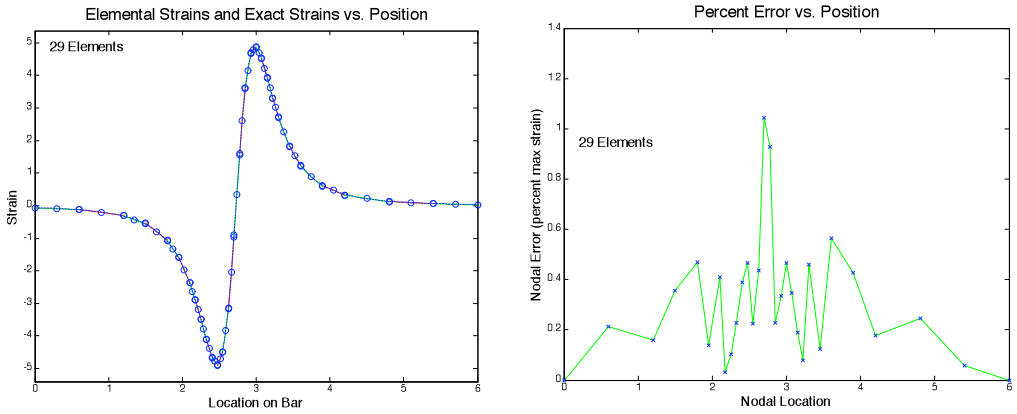

(a) Twenty-Nine Element Strain Result (b) Relative Nodal Errors

Figure 5.9 – Adaptively Refined Finite Element Model – 1.5% Threshold

When Fig. 5.9b is compared to Fig. 5.6b, it is seen that the error estimates in the central portion of the two figures are nearly identical. This result shows definitively that adaptive refinement produces finite element models that represent problems as well as a uniformly refined model with significantly fewer elements.

5.6 – An Application of an Absolute Error Estimator

In this Section, the example problem is adaptively refined under the guidance of an error estimator that estimates the "absolute" error at an inter-element node. That is to say, the error estimator defined by Eq. 5.1 is normalized with respect to a local value of the strain instead of with a large constant value of strain. The use of a local normalization of the error estimator is

designed to distribute the absolute errors more uniformly over the domain of the problem. Specifically, the normalizing factor used in Eq. 5.1 is the following:

$$(\varepsilon)_{Normalizing} = \left| \varepsilon_{\text{Local Average}} \right|_i = \frac{(\varepsilon_{\text{Right Hand Element}} + \varepsilon_{\text{Left Hand Element}})_i}{2} \qquad \text{(Eq. 5.2)}$$

This normalizing factor is the local average of the strains at the i-th node.

When the normalizing factor given by Eq. 5.2 is used, care must be taken that the average strain is not close to zero. If this is the case, division by zero can cause computational difficulties. In order to avoid this problem, a small value of strain is added to the denominator if the average of the two strains is close to zero. In the demonstration presented here, a small percentage of the maximum strain in the overall problem is added to the denominator if the existing average is close to zero.

The progression of the nodal error estimates is presented in Figs. 5.10 – 5.12. A sequence of figures is used to present the error estimates because the nodal errors do not decrease monotonically so it would be difficult to identify the progression of error estimates if they were all presented at once. In Fig. 5.10, the nodal error estimates for the initial finite element model and the first adaptively refined model are shown.

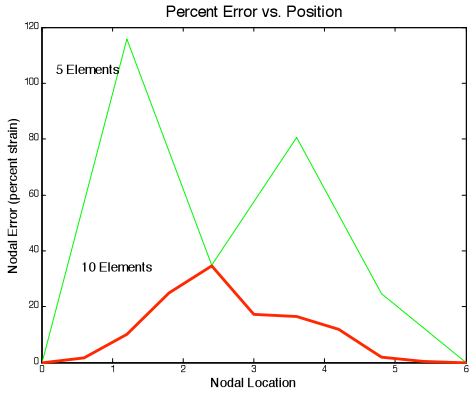

Figure 5.10 - Nodal Error Estimate for the First Two Models

As can be seen, the first application of adaptive refinement produces a model with ten elements. This is equivalent to a uniform refinement. Each element in the initial five-element model had an estimated error that was larger than the threshold value of four percent. As a result, every element was subdivided.

In Fig. 5.11, the nodal error estimate for the second adaptively refined model is superimposed on the error estimates for the previous two models. The primary significance of this figure is that it clearly shows that the error estimates based on the locally normalized inter-element jumps are not monotonic. In general, the error estimates for this third model are reduced, but the nodal error estimate for one point exceeds the maximum error estimate contained in the previous refinement.

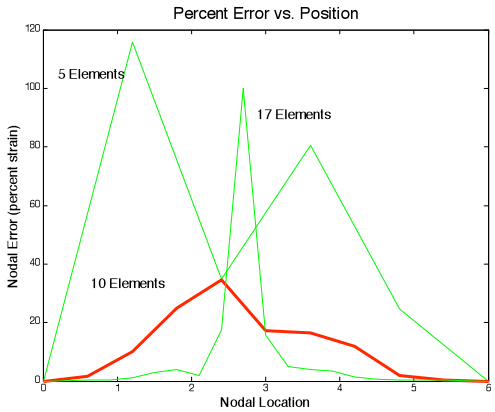

Fig. 5.11 – Nodal Error Estimate for the First Three Models

The nodal error estimates for three more iterations of the adaptive refinement process are introduced in Fig. 5.12. As can be seen, thirty-two elements are required to satisfy the termination criterion of four percent used in this analysis. This contrasts to the nineteen elements required with the error measure normalized with the maximum strain in the finite element model. This implies that the absolute error is equalized over the domain of the problems.

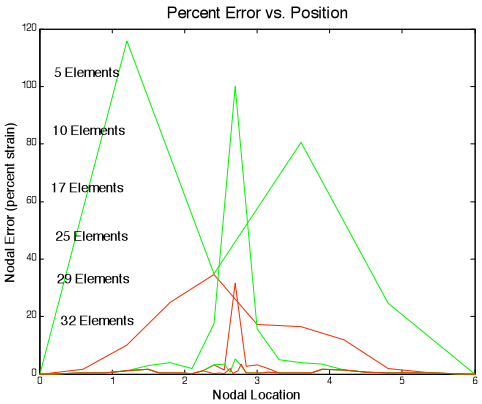

Fig. 5.12 – A Sequence of Nodal Error Estimates

More detailed results for the final adaptively refined model are shown in Fig. 5.13.

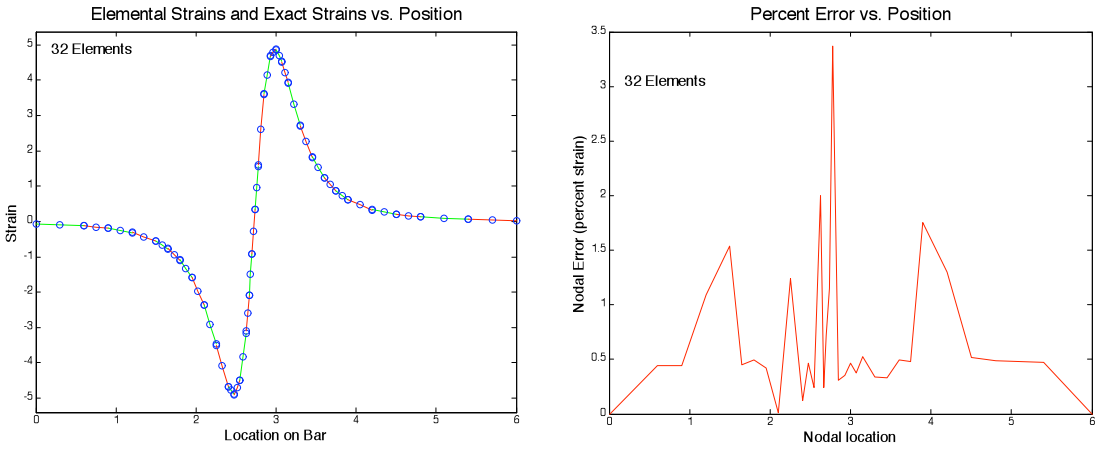

(a) Thirty-Two Element Strain Result (b) Absolute Nodal Errors

Figure 5.13 – Sixth Adaptively Refined Finite Element Model

The finite element approximation is superimposed on the exact solution in Fig. 5.13a. As can be seen, the strain representation is a good match. This conclusion is confirmed in Fig. 5.13b where the nodal errors are significantly below the threshold of the termination criterion.

When Fig. 5.13a is compared to Fig. 5.8a, it is observed that the number of elements in the region of the stress concentration is equal for both cases. However, in Fig. 5.13a, it is seen that the finite element representation is smoother and there are more elements in the regions of low strain. In other words, the error estimator normalized with a local strain value did the job it is designed to do. It distributed the "absolute" errors more uniformly over the domain of the problem being solved.

5.7 – Summary and Conclusion

The idea of the adaptive refinement process has been introduced and its effectiveness has been demonstrated. It has been shown that by refining a finite element model in regions of high error that the adaptive refinement process creates models that produce accurate representations of the exact result more efficiently than does uniform refinement.

In addition, it has been shown that the adaptive refinement process can be designed to produce a result with given characteristics. In one demonstration, the adaptive refinement

process focused on regions of critical strain. In another demonstration, the model was refined so the errors where more uniformly distributed over the domain of the problem.

The use of the inter-element jumps as the basis to the error estimates allows the errors to be interpreted in terms of quantities of interest to an analyst. Specifically, the errors are related to strain quantities so the termination criterion can be specified in terms of critical strain levels for the material being used.

Although, the error estimators based on the inter-element jumps are effective, they have the following deficiencies:

1. The inter-element jumps disguise the level of errors in individual elements when negative and positive errors exist in an element they cancel each other in the integration process.
2. The inter-element jumps aggregate the errors in adjacent elements so the errors in critical elements are diluted, i.e., the error resolution is reduced.
3. The inter-element jumps submerge the severity of the errors at critical points because the jumps depend on the sum of integrated quantities.
4. The inter-element jumps do not exist naturally on fixed boundaries so errors on these boundaries must be assessed differently.

In the following Chapters, error estimators are developed based on different theoretical bases that correct the deficiencies identified for the error estimators presented in this Chapter.

CHAPTER 6

STRAIN ENERGY BASED ERROR ESTIMATORS – THE ZZ ERROR ESTIMATOR

6.1 – Introduction

In the previous Chapter, the adaptive refinement procedure was introduced. As can be seen in the schematic diagram of the process shown in Fig.6.1, the critical component is the **error estimator**. After the initial and subsequent models are formed, the errors in the finite element solution are quantified with an error estimator. Then, on the basis of the error analysis, the finite element solution is found acceptable or the model is refined and the process is repeated.

Zienkiewicz and Zhu (ZZ) developed the first practical error estimator [2, 33]. This error estimator computes the strain energy in the difference between the discontinuous finite element strain distribution and a smoothed strain distribution formed using an average of the inter-element nodal strains. The ZZ approach does not have the resolution or the computational efficiency of the pointwise approaches that are the focus of this work, such as the error estimator developed in the previous Chapter.

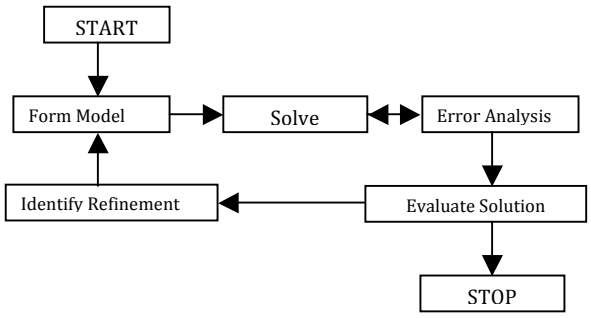

Figure 6.1 – Adaptive Refinement Schematic

The primary objectives of this Chapter are to present the development of the ZZ error estimator and to demonstrate the behavior of this error estimator in the adaptive refinement process.

The key step in the ZZ approach is the assumption that a smoothed strain distribution formed from the finite element result is closer to the exact solution than the discontinuous finite

element solution. This assumption is justified from an intuitive point of view by recognizing that the smoothed solution is continuous instead of discontinuous. However, this assumption is given a solid theoretical foundation by the results presented in Chapter 4 – The Source and Quantification of Discretization Errors.

In Chapter 4, it is shown that the inter-element jumps in the strains in a finite element result are due to the failure of the finite element solution to satisfy the governing differential equation being solved. In the smoothing process, a portion of the inter-element jump is added to the discontinuous finite element solution on the domain of the individual elements. As a consequence, the resulting strain representation is closer to the exact solution than the discontinuous finite element solution. The understanding that the inter-element jumps in the strain quantifies the discretization errors and the understanding of the role of the inter-element jumps in the smoothing process is exploited in Chapter 8 to propose a rational approach for forming refinement guides.

Figure 6.2 illustrates how the smoothed strain distribution is formed. The discontinuous finite element strains at the inter-element nodes are averaged. The smoothed strain representation is formed by fitting a polynomial to the resulting nodal strains and to the strains at any internal nodes.

Figure 6.2 – Smoothed vs. Finite Element Strain

The error in the finite element strain representation is taken as the difference between the smoothed strain and the discontinuous finite element representation. Then, the estimated error in the strain energy is computed by integrating a function of the estimated error over the domain of the element. Since the integrand for this strain energy quantity contains the square of the

difference between the two strain distributions, the pointwise magnitude of the integrand is always positive regardless of the sign of the estimated error in the strain.

The evolution of the procedure for forming the smoothed solution is presented in the next Section. Then the procedure for estimating the error in the strain energy is presented. In the next two Sections, versions of metrics used as error estimators are presented. The characteristics of an error estimator and its use in the adaptive refinement process are presented in the following Sections.

6.2 – The Basis of the ZZ Error Estimator – The Smoothed Strain Representation

At the heart of the ZZ approach to error estimation is the use of a smoothed solution formed from the finite element result that is a better approximation of the exact solution than is the discontinuous finite element solution. The inability of an individual element to represent the exact solution is taken as the difference between the smoothed strain representation and the finite element strain distribution. As shown in the next section, this estimated error is quantified as being the strain energy contained in the difference between these two strain representations.

In the original version of the ZZ approach, a smoothed solution was constructed for the total problem being evaluated. The smoothed solution was formed using a least squares approach with the following two constraints: **1)** the smoothed solution was forced of have the same amount of strain energy as the finite element result and **2)** the errors in the finite element result were distributed so the total error was minimized.

The computational effort for this process is of the same magnitude as the solution of the finite element model. In later developments, the smoothed solution was formed on an **element-by-element basis** that reduced this effort and did not compromise the results.

An overview of the first version of the ZZ error estimator that formed a smoothed solution on an **element-by-element basis** is shown in Fig. 6.3. In Fig. 6.3a, the strain distribution over a representative patch of three-node bar elements is shown along with the average of the inter-element nodal strains.

In Fig. 6.3b, the smoothed strain distribution formed by interpolating between the average of the inter-element jumps is overlaid on the strain contained in Element (n). In Fig. 6.3c, the estimated pointwise error in the finite element strain distribution is shown as the difference between the finite element and the smoothed strain representations.

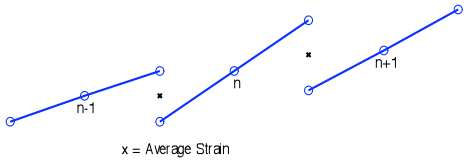

(a) Average Strains at Inter-Element Nodes

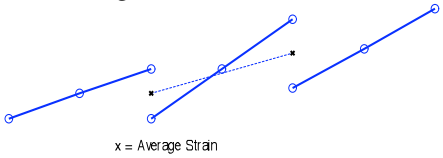

(b) Smoothed Strain for a Representative Element

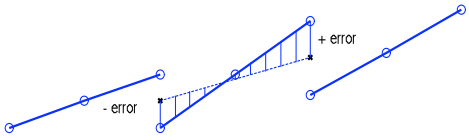

(c) Pointwise Error Distribution in a Representative Element

Figure 6.3 – The Basis of the ZZ Error Measure

As can be seen in Fig. 6.3c, the estimated errors can be either positive or negative depending on whether the finite element strain is larger or smaller than the smoothed strain. In order to eliminate the possibility of underestimating the error in the finite element strain representation by having positive differences cancel negative differences, the error measure is computed as the strain energy contained in the difference between these two strain representations. Since strain energy is a function of the square of the strain, the magnitude of the error estimator is unaffected by the sign of the differences in the strains.

Procedures for forming the locally smoothed strain representations were refined in later versions of the ZZ approach. These changes produced incremental improvements to the error estimates without changing the overall concept.

One modification developed the locally smoothed solution from the strains at the Gauss points of the element being evaluated and a patch of surrounding elements. This change was made because the finite element strains at the Gauss points may be closer to the actual strains than at other points on the domain of an element. However, when adaptive refinement is being used, it is not clear if this subtlety needs to be considered.

6.3 – The ZZ Elemental Strain Energy Error Estimator

As shown in Fig. 6.3c, the pointwise error in the finite element strain result for Element(n) is assumed to be the difference between the finite element and the "smoothed" strain representations. This idea is given in equation form as:

$$\Delta\varepsilon_n(x) = \left(\varepsilon_n(x)\right)_{\text{Finite Element}} - \left(\varepsilon_n(x)\right)_{\text{Smoothed}} \qquad \text{(Eq. 6.1)}$$

where

$\Delta\varepsilon_n(x)$ = the estimated pointwise strain error in Element (n).

$\left(\varepsilon_n(x)\right)_{\text{Finite Element}}$ = the finite element strain distribution.

$\left(\varepsilon_n(x)\right)_{\text{Smoothed}}$ = the improved or smoothed strain distribution over Element (n).

The estimated error in the strain energy of Element (n), ΔSE_n, with a constant cross section is given as:

$$\Delta SE_n = EA/2\int_0^L \left(\Delta\varepsilon_n(x)\right)^2 dx \qquad \text{(Eq. 6.2)}$$

where ΔSE_n = the estimated strain energy error in Element n.

In mathematical terms, the error measure given by Eq. 6.2 is called a weighted L_2 norm.

6.4 – The ZZ Error Estimator

The ZZ error estimator is formed by normalizing the error measure given by Eq. 6.2 as follows:

$$\eta_n = \left[\frac{(\Delta SE_n)^{1/2}}{(SE)^{1/2}_{Normalizing}} \right] \text{x } 100 \qquad \text{(Eq. 6.3)}$$

where η_n = the ZZ elemental error measure as a percentage.

ΔSE_n = the estimated strain energy error in Element (n).

$(SE)_{Normalizing}$ = the normalizing factor that focuses the error estimator.

The numerator of the elemental error estimator is the square root of the estimate of the error in the strain energy of an individual element given by Eq. 6.2. The denominator can be chosen to make the error estimator perform in different ways.

In the first form of the ZZ approach, the normalizing factor was identified as being equal to the total strain energy in the problem. Since the total strain energy depended on the size of the particular problem and the level of loading, this error estimator provided little, if any, physical insight into the accuracy of the result.

In order to provide some physical insight into the meaning of the error estimator, a normalizing factor based on the strain energy content of the element being analyzed can be used. The most obvious candidate for a localized normalizing factor is an estimate of the total strain energy in the element. This estimate is taken as the sum of the actual strain energy in the element plus the estimated error in the strain energy content of the element. This quantity is given as:

$$(SE)_{Normalizing} = (SE_n + \Delta SE_n) \qquad \text{(Eq. 6.4)}$$

where SE_n = the strain energy content of Element (n).

ΔSE_n = the estimated strain energy error in Element (n).

When the error estimator is normalized with Eq. 6.4, the result can be interpreted as a percentage of the total error in the Element (n).

However, this normalizing factor **can** cause the adaptive refinement process to diverge. The divergent behavior can occur because the numerator and the denominator of Eq. 6.3 have a different nature. The numerator of Eq. 6.3 contains contributions from the errors in the adjacent elements as well as from the element being analyzed. However, the denominator contains only contributions from the element being analyzed.

As a result of these different characteristics, a low error strain element adjacent to a high error element will have an error estimate that is excessive. This in turn may cause the unneeded refinement of this low error element. The refinement of this low error element exacerbates the problem and the refinement can diverge.

6.5 – A Modified Locally Normalized ZZ Error Estimator

The divergent behavior identified in the previous Section is eliminated by modifying the denominator of Eq. 6.3 so that it has the same characteristics as the numerator. This change is accomplished by including strain energy contributions from the elements adjacent to the element being evaluated into the denominator of the error estimator. When this is done, the modified version of the locally normalized ZZ error estimator becomes:

$$\eta_n = \left[\frac{(\Delta SE_n)^{1/2}}{(SE)^{1/2}_{Normalizing}} \right] \text{x } 100 \qquad \text{(Eq. 6.5)}$$

where η_n = the ZZ elemental error measure as a percentage.

ΔSE_n = the estimated strain energy error in Element (n).

$(SE)_{Normalizing} = SE_n + \Delta SE_n + C(SE_{n-1} + SE_{n+1})$.

C = A participation factor for the elements adjacent to Element (n).

When the denominator of Eq. 6.5 is compared to the denominator given by Eq. 6.4, it can be seen that it contains a contribution due to the strain energy content from the elements adjacent

to the element being evaluated. The amount of strain energy added to the denominator is controlled by the participation factor, C. The participation factor for these strain energy quantities is arbitrarily chosen as 0.5 for the examples presented in Sections 6.6 and 6.7.

6.6 – A Demonstration of the ZZ Error Estimator

In this Section, the ZZ error estimator defined by Eq. 6.5 is applied to a sequence of uniform refinements beginning with the five-element control problem. The result of analyzing the same problem with the residual approach developed in Chapter 4 is also presented. This is done to show that the two approaches have the same characteristics.

The results for the initial five-element model are shown in Fig. 6.4. Figure 6.4a compares the strains in the finite element model to the exact solution. Figure 6.4b contains the ZZ error estimates for the individual elements. Figure 6.4c contains the nodal error estimates produced by the residual approach.

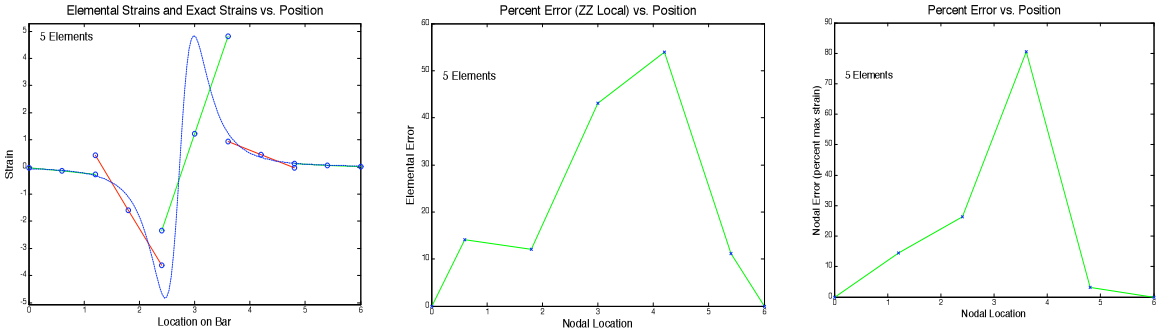

(a) Five Element Strain Result (b) ZZ Error Estimator (c) Residual Error Estimator

Figure 6.4 – A Five-Element Model

In the plots of the ZZ elemental error estimates, the estimates are arbitrarily presented as if they apply at the center points of the elements. The errors are presented in a continuous curve by connecting the error values with straight lines and by taking the errors at the ends of the bar to be zero. For this problem the errors are close to zero at the end points. The lines have no real meaning. They are presented for visual convenience.

The error estimates produced by the residual approach in Fig. 6.4c are nodal quantities. Since the ZZ error estimates are elemental quantities, the two error estimates do not have an exact one-to-one correspondence. However, when Fig. 6.4b and Fig. 6.4c are compared, it can be seen that the two error estimators identify the same regions as having large values of error. However, the residual result has a higher maximum value for the error estimator. This difference in magnitude is not significant for this discussion because the objective of this Chapter is to demonstrate the characteristics of the ZZ approach and to, ultimately, show that it successfully guides the adaptive refinement process.

When the five-element model is modified with two uniform refinements, the results for the ten- and twenty- element models are shown in Figs. 6.5 and 6.6, respectively.

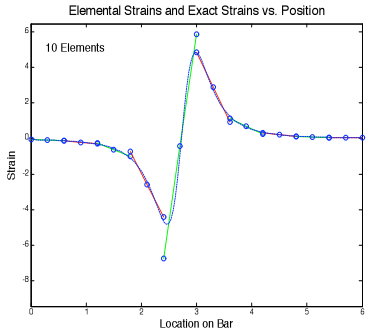

(a) Ten-Element Strain Result

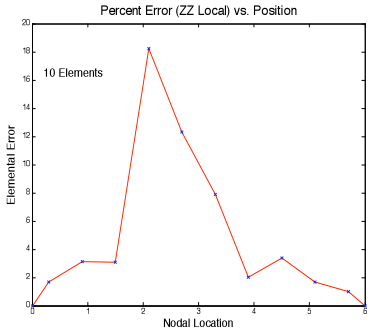

(b) ZZ Error Estimator

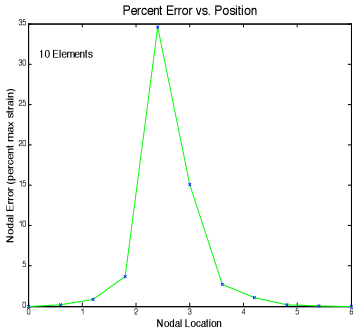

(c) Residual Error Estimator

Figure 6.5 – A Ten-Element Model

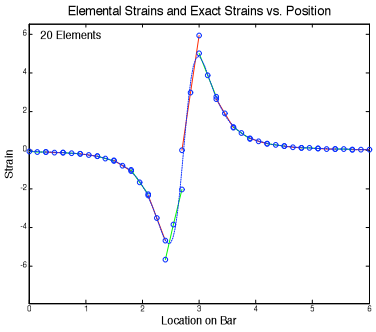

(a) Twenty-Element Strain Result

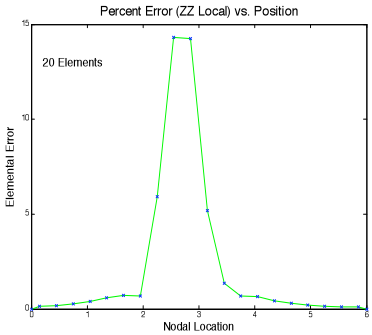

(b) ZZ Error Estimator

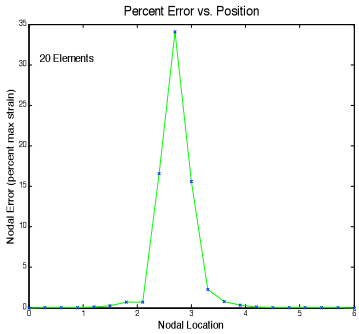

(c) Residual Error Estimator

Figure 6.6 – A Twenty-Element Model

As can be seen in Figs. 6.5 and 6.6, the qualitative characteristics of the two error estimators are similar. That is to say, both error estimators identified the same region as having

the maximum error in the first refinement. In the second refinement shown in Fig. 6.6, both approaches identified the same new location as having the maximum error. Furthermore, the regions identified with the highest level of error correspond to the regions actually containing the maximum error.

When the magnitudes of the error estimates are compared, both of the error estimates are reduced in a similar manner by the uniform refinements. In addition, the differences between the maximum and the minimum estimated errors were similar in the two error estimators. That is to say, they had approximately the same resolution between high and low errors. These results indicate that both approaches will successfully identify regions in the finite element model where the model must be refined in order to improve the results.

The results for uniformly refining the model two more times are shown in Figs. 6.7 and 6.8, respectively. As can be seen, both of these uniform refinements significantly reduce the maximum error for both approaches to error analysis. Furthermore, the shapes of the plots representing the error estimates for both approaches correlate well with the errors seen as the difference between the finite element results and the exact solution, which are shown in Fig. 6.7a and 6.8a, respectively.

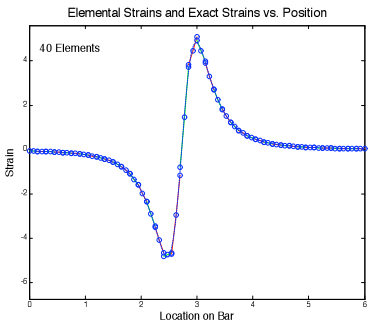

(a) Forty-Element Strain Result

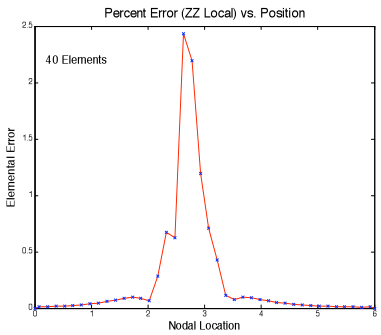

(b) ZZ Error Estimator

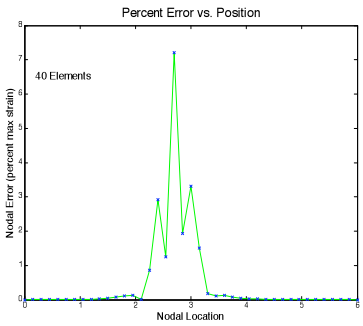

(c) Residual Error Estimator

Figure 6.7 – A Forty-Element Model

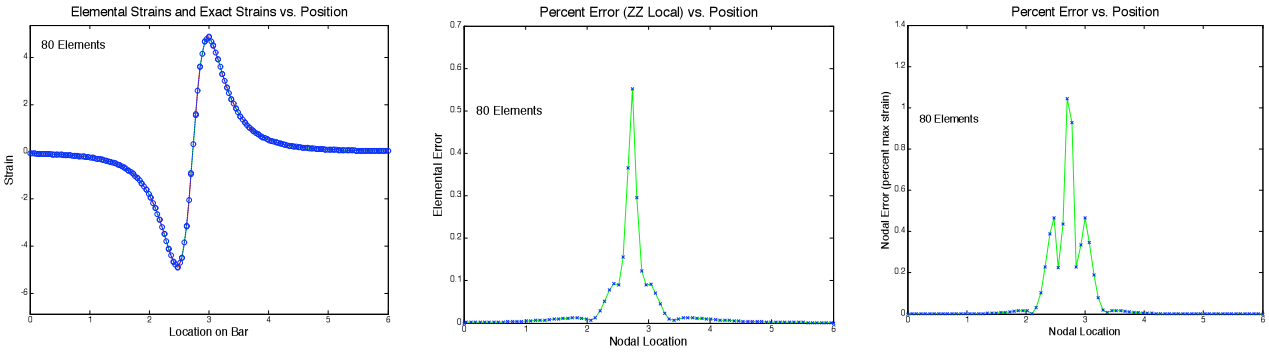

(a) Eighty-Element Strain Result (b) ZZ Error Estimator (c) Residual Error Estimator

Figure 6.8 – An Eighty-Element Model

Furthermore, this result validates the desirability of using adaptive refinement to improve finite element models instead of uniform refinement. That is to say, in uniform refinement, a majority of the elements added to the model are introduced in regions of low error.

6.7 – A Demonstration of Adaptive Refinement

The ZZ error estimator defined by Eq. 6.5 is used to guide the adaptive refinement of the five-element demonstration problem in this Section. In this demonstration, an element is subdivided into two equal length elements if the refinement guide given by Eq. 6.5 is greater than or equal to a value of four percent.

Figure 6.9 presents the results of solving the five-element model and its corresponding error analysis. As can be seen in Fig. 6.9a, the three lightly strained elements, Elements (1), (4) and (5), represent the exact solution reasonably well. In contrast, the two elements with the highest rates of change in strain (high strain gradients) and relatively high magnitudes of strains that are attempting to represent the regions of rapidly changing strains do not closely represent the exact solution.

The approximate error estimates presented in Fig. 6.9b do not totally agree with the observations just made about the accuracy of the strain representations of the individual elements. The element with the highest estimated error represents the exact solution reasonably

well. The error estimate for this element does not coincide with the actual error for two reasons: **1)** it is next to an element that is incapable of capturing the shape of the exact result with any accuracy so the inter-element jump between the two elements is large and **2)** this element and the element to its right are low strain elements.

As a result, the numerator of the error estimator is overly large and the denominator is relatively small. This leads to an error estimate that is not a good match with the actual error in the element. However, it does not affect the refinement of the model because the error estimates exceed the threshold value for refinement.

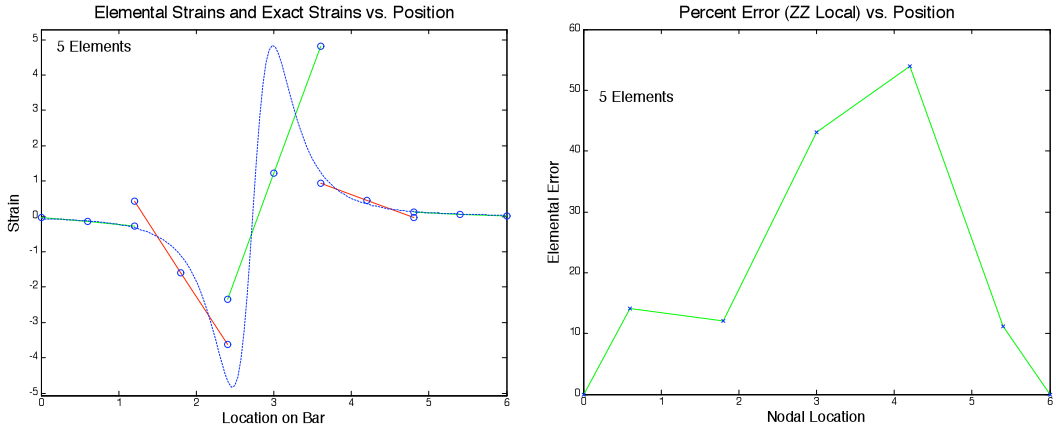

(a) Five-Element Strain Result (b) ZZ Error Estimates

Figure 6.9 – The Initial Five-Element Mesh

Since the error estimate for every element in this model exceeds the refinement threshold of four percent, every element in the model will be subdivided to form the new model. As a result, the initial refinement is equivalent to a uniform refinement. It is worth noting that the error estimate for every element is also larger than ten percent. This means that if the refinement threshold is relaxed, the refined model would not possess fewer elements.

The results of the first refinement are shown in Fig. 6.10. As can be seen, the maximum error has been reduced from approximately 55 percent to approximately 19 percent and the error estimates have been significantly reduced for every element. The error estimates for three of the

ten elements exceed the threshold level of four percent. All three of these elements either encompass the region of actual maximum error or are adjacent to this region. That is to say, this set of error estimates will refine the model where it needs refining.

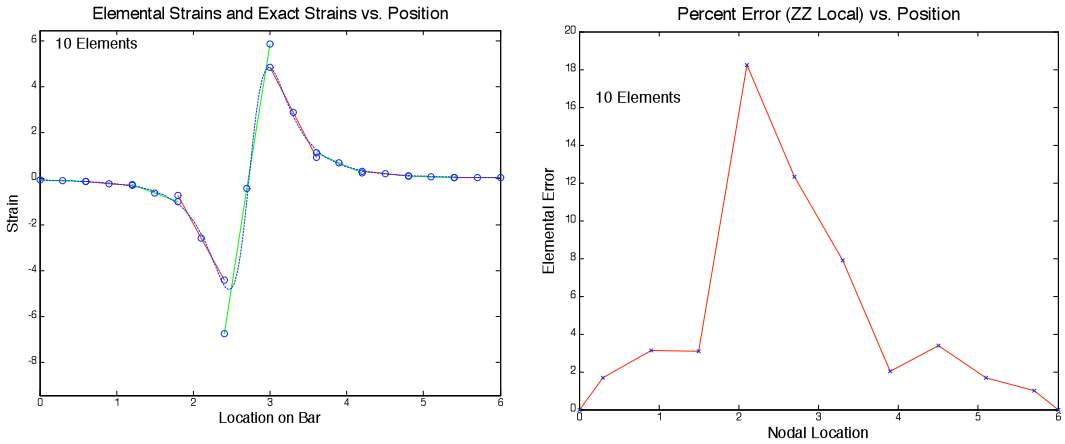

(a) Ten-Element Strain Model (b) ZZ Error Estimates

Figure 6.10 – The First Adaptively Refined Mesh of Ten Elements

Figures 6.11 - 6.13 contain the subsequent three adaptive refinements that are required to satisfy the termination criterion of four percent. The only feature of these refinements that might be unexpected is the fact that the maximum error increased in the second refinement as shown in Fig. 6.11b. The maximum error increased from approximately 18 percent in the first refinement to approximately 21 percent in the second refinement.

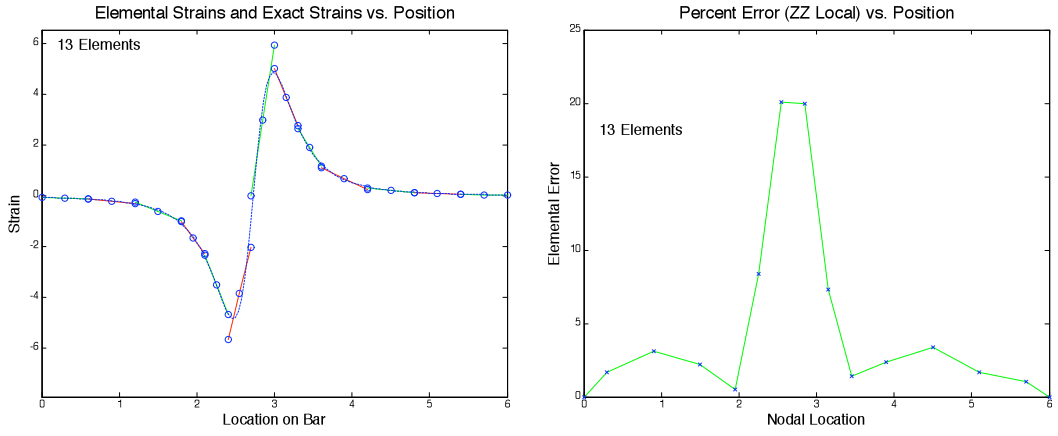

(a) Thirteen-Element Strain Model (b) ZZ Error Estimates

Figure 6.11 – The Second Adaptively Refined Mesh of Thirteen Elements

The reason for this increase can be seen by comparing Figs. 6.10a and 6.11a. The single element that is attempting to represent the two critical stresses and the inflection point between the positive and negative stress concentrations in Fig. 6.10a has been subdivided in the second refinement. As can be seen in Fig. 6.11a, there has been a significant inter-element jump introduced by subdividing the element in the region of the inflection point. That is to say, a modeling deficiency that was submerged on the interior of a single element has been made explicit on the boundary between two elements.

The refinements shown in Fig. 6.12a and 6.13a introduce elements into the regions where the error estimates exceed the refinement threshold and the finite element model fails to represent the exact solution with accuracy. Thus, it can be concluded that the locally normalized ZZ error estimator given by Eq. 6.5 produces a convergent result as it is designed to do.

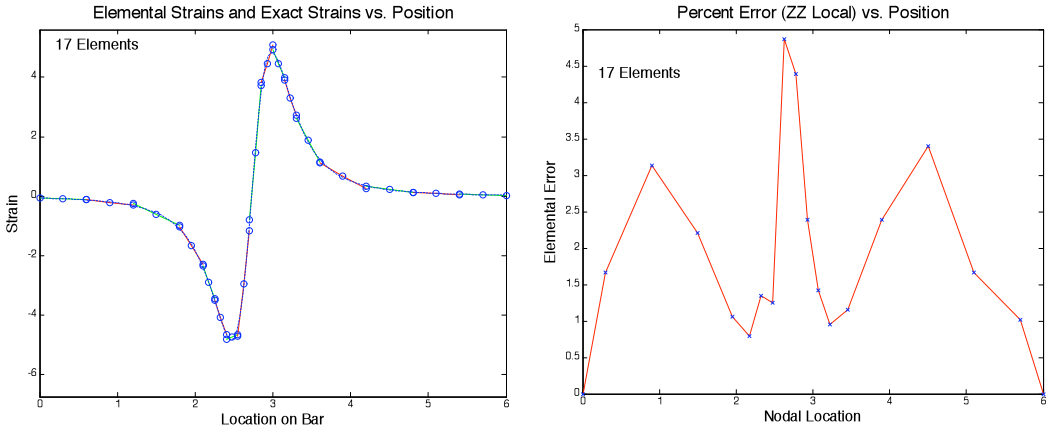

(a) Seventeen-Element Strain Model (b) ZZ Error Estimates

Figure 6.12 – The Third Adaptively Refined Mesh of Seventeen Elements

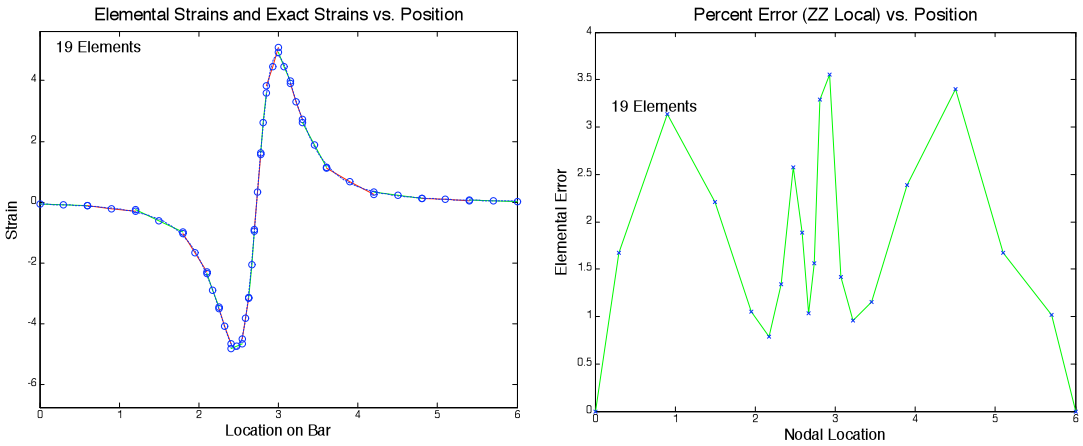

(a) Nineteen-Element Strain Model (b) ZZ Error Estimates

Figure 6.13 – The Fourth Adaptively Refined Mesh of Nineteen Elements

6.8 – Summary and Conclusion

This Chapter has presented and demonstrated the ZZ approach to error estimation. This intuitive approach estimates the error in the strain energy content of an individual element by comparing the discontinuous finite element strain results to a smoothed solution over the domain of an individual element.

The rationale behind this error estimator when it was originally developed was the assumption that the smoothed solution is closer to the exact result than the discontinuous finite element result because it is continuous. As discussed in the introduction of this Chapter, this assumption is given a solid theoretical foundation in Chapter 4 – The Source and Quantification of Discretization Errors, where it is shown that the inter-element jumps in the strains in a finite element result are due to the failure of the finite element solution to satisfy the governing differential equation being solved. In the smoothing process, a portion of the inter-element jump is added to the discontinuous finite element solution on the domain of the individual elements. As a consequence, the resulting strain representation is closer to the exact solution than the discontinuous finite element solution.

The smoothed solution used in this presentation is formed by interpolating the average of the inter-element strains over the element. This approach is shown to be effective in guiding the adaptive refinement process to convergent results starting with a five-element demonstration problem.

CHAPTER 7

CONVERGENCE OF INTER-ELEMENT JUMPS IN TWO-DIMENSIONAL FINITE ELEMENT MODELS

7.1 - Introduction

In the previous Chapters, it has been shown for the case of a one-dimensional bar element that the inter-element jumps are a direct measure of the inability of a finite element model to satisfy the governing differential equation being solved. As a result of this characteristic, the inter-element jump in the strain can serve as a direct measure of the discretization errors in a finite element model.

The objective of this Chapter is to extend the demonstration of the ability of the inter-element jumps in the strain components to serve as an error estimator to two-dimensional finite element models. This objective is accomplished by demonstrating that as the finite element result approaches the exact solution the inter-element jumps in the three strain components diminish.

The following two-dimensional physical system is used in this demonstration. A 6x6 unit in-plane shear panel, or membrane, with fixed boundaries is analyzed. The initial finite element model consists of 64 elements with 226 active degrees-of-freedom, i.e., degrees-of-freedom not associated with the fixed nodes on the boundaries. The initial model is shown in Fig. 7.1a.

The model is uniformly refined twice to produce the second and third models used in this demonstration. The first refinement contains 256 elements and 962 active degrees-of-freedom. The second uniform refinement contains 1024 elements and 3970 active degrees-of-freedom. These two models are shown in Fig. 7.1b and 7.1c, respectively.

Two different loading conditions are applied to the physical system for this demonstration. The first loading condition is a constant distributed load. This load is chosen because the resulting strain distribution is simple and, therefore, easy for the finite element model to represent. As a result, the third model will produce a nearly exact solution. The associated inter-element jumps will be seen to approach zero.

The second loading condition is designed to produce displacements and an associated strain distribution that are Runge functions [26, 27, 28]. The loading condition is shown in Fig. 7.2. It is the second integration of a displacement that is a Runge function. This load is a planar version of the load used in the one-dimensional demonstrations presented earlier. This loading condition is chosen because a Runge function is difficult for a polynomial representation to capture. This difficulty exists because a Runge function is a rational polynomial. This means that it can only be approximated as an infinite polynomial. Therefore, a

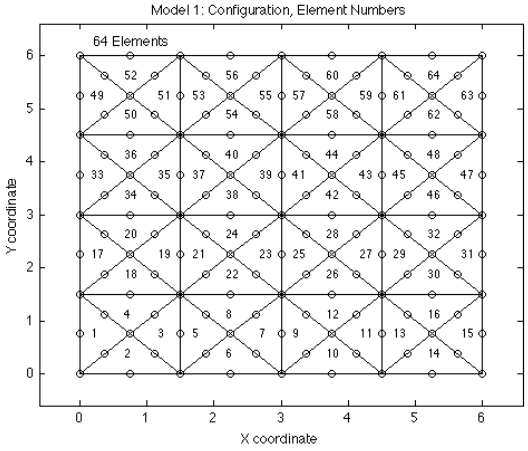

(a) Initial model

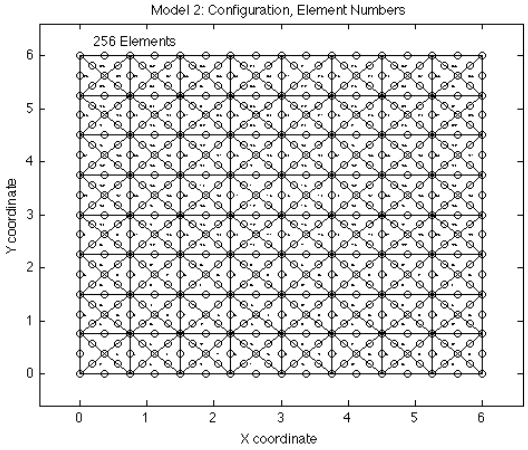

(b) Second model

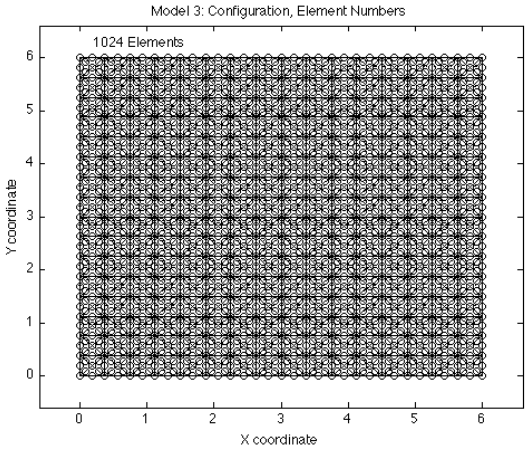

(c) Third model

Figure 7.1 – Three Models of the Physical System

finite element model cannot capture the strain distribution exactly. As a result, this loading condition is a severe test for the finite element model and, consequently, for the error estimator.

The inter-element jumps used in the error estimator demonstrated here are taken as the maximum absolute difference between the finite element nodal strains and the average of these strains at the node. The error estimator demonstrated here for the three strain components are the inter-element jumps divided by the maximum absolute strain in the finite element model. This normalization is performed so the error estimator has units of percent of the maximum strain. In problems solved in practice, the normalizing factor could be associated, for example, with some failure criteria or allowable strain.

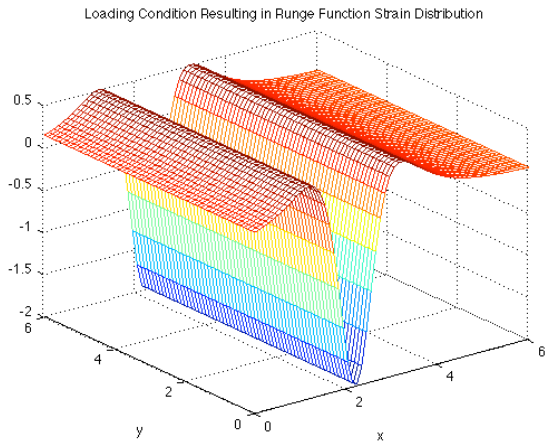

Figure 7.2 - The Second Loading Condition Applied to the Physical System

The smoothed strain representation is used as the baseline for the error estimator because it is an improvement on the discontinuous finite element strain distribution. The smoothed strain is an improvement because the inter-element jumps are a direct measure of the inability of the individual finite elements to satisfy the governing differential equation. Thus, the smoothed solution consists of the finite element result plus a component of the error. Therefore, it is an improvement on the finite element solution.

The reduction of the inter-element jumps as the model is improved is demonstrated through uniform refinement. The improvement of the model occurs, by definition, because the uniform refinements produce child meshes. That is to say, a child mesh can represent any strain distribution that the parent mesh can represent because it contains the same nodes as the parent

mesh as a subset. The solution is improved because the basis set of the child mesh is an augmentation of the parent mesh basis set.

The improvement to the model can also be seen by tracking the strain energy content of the overall model because of the Rayleigh-Ritz criterion. The Rayleigh-Ritz criterion states that the model with the most strain energy is the better model. The Rayleigh-Ritz criterion can be interpreted to mean that the model with the most energy has fewer constraints than the model with lower energy. In other words, the model is allowed to deform in more complex shapes. The increase in the strain energy is not a guarantee that the strain representation is better in the higher energy model, but it is implicit when uniform refinement is used.

In this demonstration, the relative capabilities of the models are quantified by comparing the magnitude of the strain energy and the maximum percent error in each model to demonstrate convergence and improved modeling capacity. The strain energy comparison is a gross measure of the modeling improvement. The nodal error estimates are a local measure of model improvement.

The results of these analyses are presented as follows. The discontinuous finite element strain distribution and a measure of the inter-element jumps are presented for each model along two lines of nodes. The location of the first line of nodes presented is off of center, at y=1.5. The line of nodes across the center of the model, at y=3, is the second line that will be considered. The strain energy content for each of the models is presented.

In the next two Sections, the inter-element jumps in the strain at interior nodes are seen to be zero in some cases. This is observed only at interior nodes along lines of nodes composed of both interior nodes and corner nodes. This result occurs when the finite element strain at the interior node is observed to be the same in the two elements of the model associated with that

node. Thus, the smoothed strain, found by averaging the finite element strains at the node, is also the same as the finite element strain at the node. Therefore, the resulting inter-element jump at the node is zero.

7.2 - Model with Constant Distributed Load

In this demonstration, a constant distributed load is applied over the entire domain of the physical system. For this example, the distributed load is applied in the x direction. The equivalent nodal loads are found for this loading condition and the model is analyzed. The nodal loads for a uniform load on a six-node linear strain triangle occur only at the interior node on each side of the individual elements. Conversely, this means that the equivalent nodal loads on the corner nodes are zero.

The following subsections demonstrate the reduction of the error estimator as the finite element model is improved. The three strain components will be examined sequentially.

Modeling the x-direction strain component, ε_x

In this subsection, the ability of the three successive models of the physical system to better represent the strain distribution in the x direction is examined. It is noted that the load is applied in this direction, thus the strains are larger in this direction. The capability of each model to represent this strain is observed by comparing the maximum and minimum strains that occur at the nodes from the finite element solution of the model to the smoothed strain representation. In the case of the inter-element jumps at the interior nodes of the six-node element, there are only two finite element strain values at the node. At the corner nodes, there are eight different finite element strain values.

The analysis of the initial model of the physical system at the off-center line of nodes is shown in Fig. 7.3. The first model captures a maximum strain of 0.1583 units. This value of

maximum strain does not appear in the figures presented for either line of nodes, as it occurs at a node elsewhere in the model. This model has an overall strain energy content of 7.9262 units.

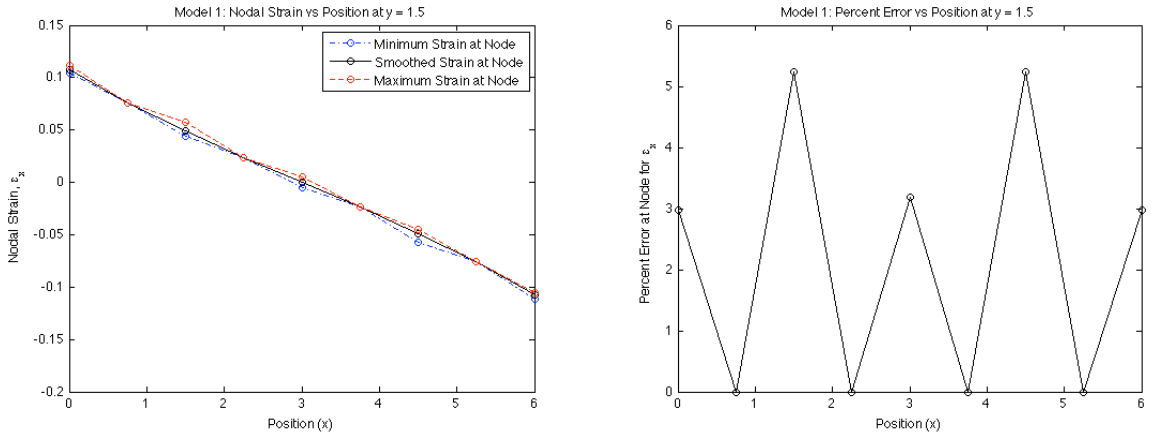

(a) Strain representation (b) Percent error

Figure 7.3 – Simple Load Case: Analysis of ε_x at Off-Center Line in Model 1

Figure 7.3a shows the strain representation at the off-center line of nodes for the first model. The minimum and maximum strains at each node are plotted against the smoothed strain result. The difference observed shows the modeling errors in the current model as inter-element jumps that occur at the nodes. The maximum absolute percent error at each of the nodes is shown in Fig. 7.3b. The maximum percent error along this line of nodes is approximately 5.2 percent in this model.

The analysis at the center line of nodes for the model is shown in Fig. 7.4.

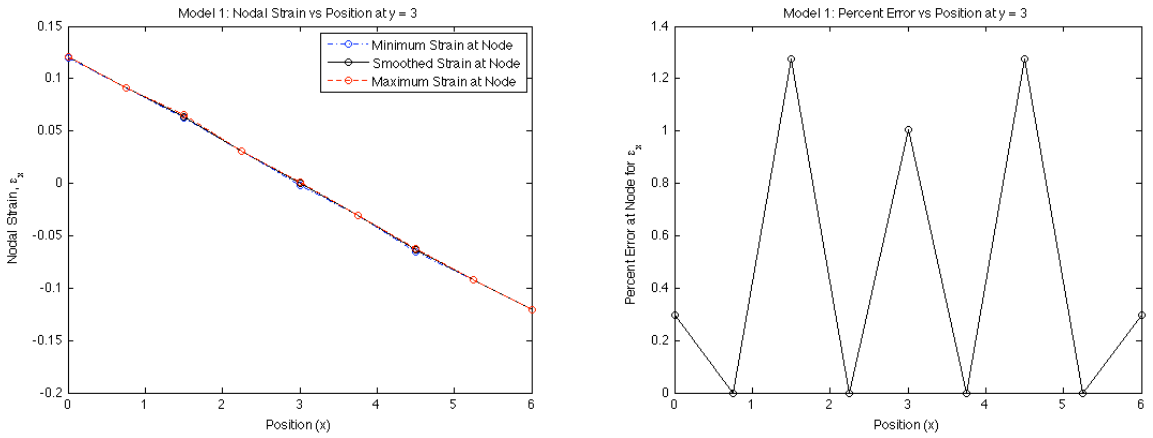

(a) Strain representation (b) Percent error

Figure 7.4 – Simple Load Case: Analysis of ε_x at Center Line in Model 1

As the center line of nodes is farther from the boundaries, the effects of the boundaries are reduced. Thus, the capability of the finite element solution to satisfy the governing differential equation at every point on the domain of an individual element, i.e., satisfy pointwise equilibrium, is more accurately represented. The finite element solution is closer to the smoothed strain representation for this line of nodes in the model, as shown in Fig. 7.4a, than for the off-center line of nodes. This is verified by observing that there is a reduction in the magnitude of the inter-element jumps along this line of nodes. The corresponding percent error has a maximum value of approximately 1.3 percent, as shown in Fig. 7.4b.

The analysis of the second model of the physical system at the off-center line of nodes is shown in Figure 7.5. This model captures a maximum absolute strain of 0.1594 units. Again, this maximum strain is not represented in the associated figures as it occurs elsewhere in the model. This model contains an overall strain energy content of 7.9381 units. This satisfies the Rayleigh-Ritz criterion because the total strain energy for the model is larger than for the initial model.

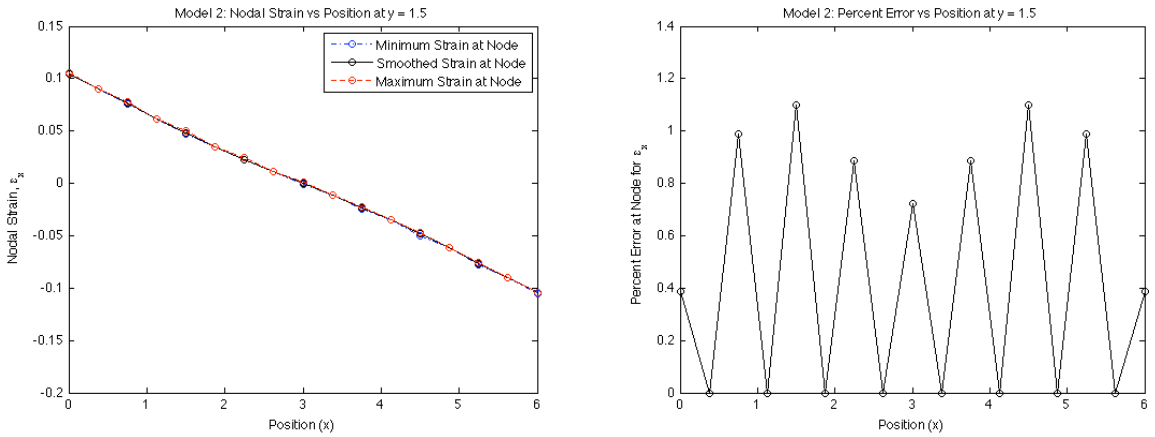

(a) Strain representation (b) Percent error

Figure 7.5 – Simple Load Case: Analysis of ε_x at Off-Center Line in Model 2

Figure 7.5a shows the strain representation at the off-center line of nodes for the second model. The finite element solution and the smoothed strain representation of this strain

component are closer along the off-center line of nodes in the current model than in the initial model of this loading condition. This is verified by observing that the magnitudes of the inter-element jumps in this line of nodes are reduced in the current model. The maximum absolute percent error is decreased to approximately 1.1 percent along this line of nodes, as shown in Fig. 7.5b.

Figure 7.6 shows the analysis of the second model at the center line of nodes.

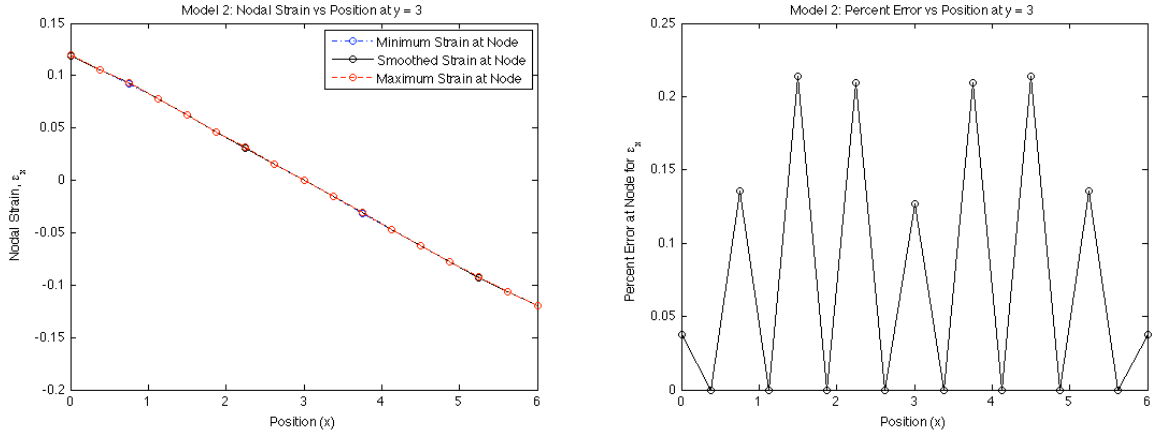

(a) Strain representation (b) Percent error

Figure 7.6 – Simple Load Case: Analysis of ε_x at Center Line in Model 2

Figure 7.6a shows the strain representation at the center line of nodes for the second model. The finite element solution and the smoothed strain representation of this strain component are closer along the center line of nodes in the current model than in the initial model of this loading condition. This is verified by observing that the magnitude of the inter-element jumps in this line of nodes is reduced in this model. The corresponding percent error has a maximum of approximately 0.22 percent in this model, as shown in Fig. 7.6b.

The analysis of the third model of the physical system at the off-center line of nodes is shown in Fig. 7.7. The third model applied to the physical system captures a maximum strain of 0.1596 units. This maximum strain is not represented in the associated figures as it occurs elsewhere in the model. This model contains an overall strain energy content of 7.9396 units.

Again, the Rayleigh-Ritz criterion is satisfied because the total strain energy has increased for this refined model.

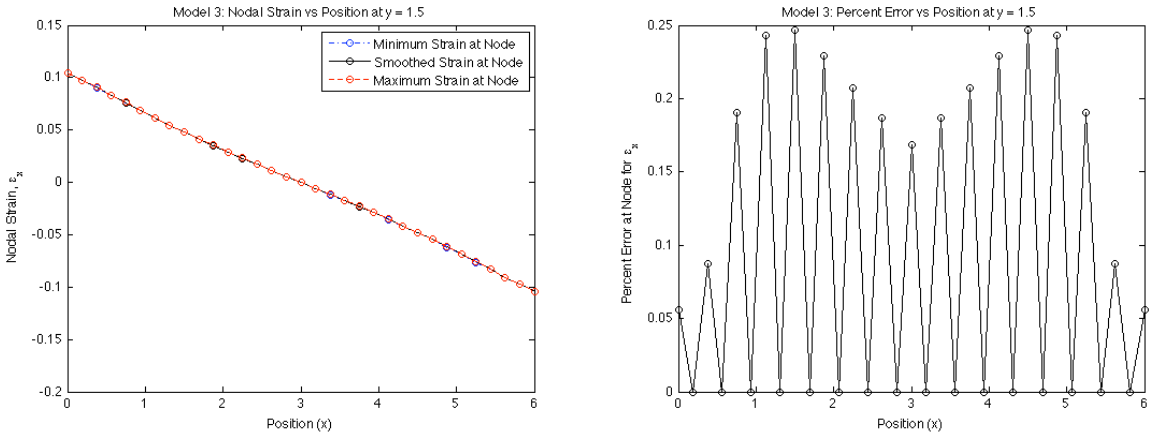

(a) Strain representation (b) Percent error

Figure 7.7 – Simple Load Case: Analysis of ε_x at Off-Center Line in Model 3

Figure 7.7a shows the strain representation at the off-center line of nodes for the third model. The finite element solution and the smoothed strain representation of this strain component are closer along the off-center line of nodes in the current model than in the two previous models of this loading condition. This is verified by observing that the magnitude of the inter-element jumps in this line of nodes is reduced in this model. The maximum absolute percent error is reduced to approximately 0.25 percent along this line of nodes, as shown in Fig. 7.7b.

Figure 7.8 shows the analysis of the third model at the center line of nodes.

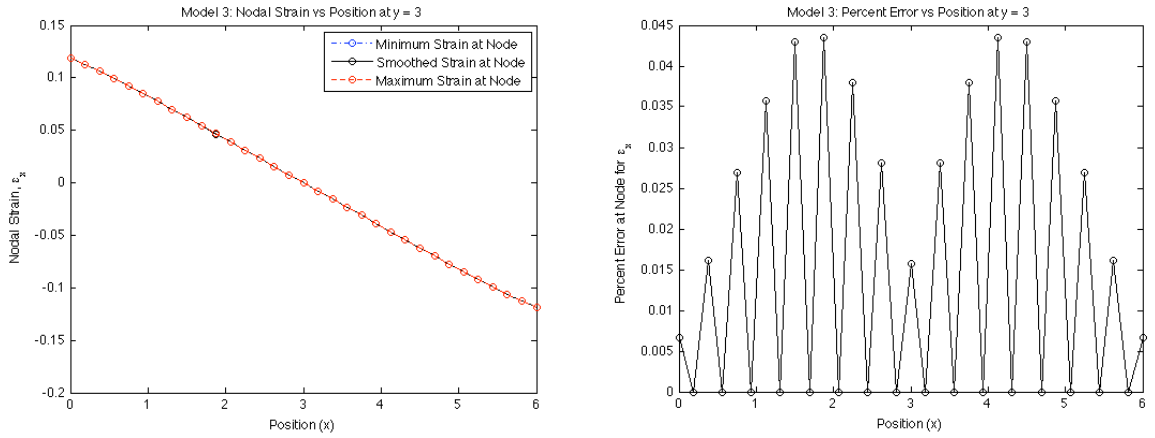

(a) Strain representation (b) Percent error

Figure 7.8 – Simple Load Case: Analysis of ε_x at Center Line in Model 3

Figure 7.8a shows the strain representation at the center line of nodes for the third model. The finite element solution and the smoothed strain representation of this strain component are closer along the center line of nodes in the current model than in the two previous models of this loading condition. This is verified by observing that the magnitude of the inter-element jumps in this line of nodes is reduced in this model and is approaching zero. The corresponding percent error has a maximum of approximately 0.044 percent in this model, as shown in Fig. 7.8b.

It is shown in this Section that the inter-element jumps decrease in magnitude as the model is improved for the strain in the x direction, ε_x. This result shows convergence in the strain representation for this strain component. In the next subsection, the capability of the three models to represent the behavior of the strain component in the y direction, ε_y, is presented.

Modeling the y-direction strain component, ε_y

In this subsection, the ability of the three successive models of the physical system to better represent the strain distribution in the y direction is examined. The capability of each model to capture this strain is observed by comparing the maximum and minimum strains that occur at the nodes from the finite element solution of the model to the smoothed strain representation. The maximum absolute strain in each model is restated, since this quantity is the

normalizing factor of the error estimator used in this work. The overall strain energy content in each model of this loading condition is not restated, as the model improvement is shown by the Rayleigh-Ritz criterion in the ε_x subsection.

The analysis of the first model of the physical system at the off-center line of nodes is shown in Fig. 7.9. The first model captures a maximum absolute strain of 0.1583 units. This value of maximum strain does not appear in the figures presented for either line of nodes, as it occurs at a node located elsewhere in the model.

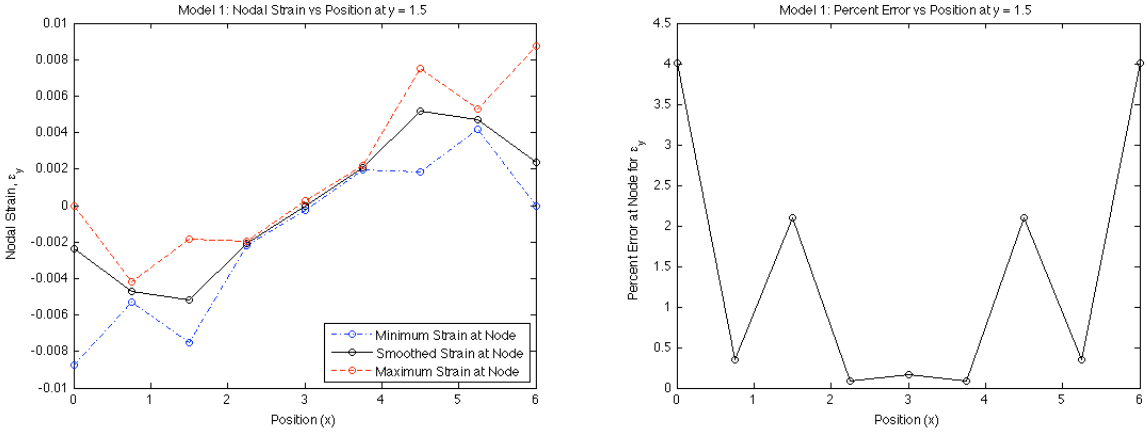

(a) Strain representation (b) Percent error

Figure 7.9 – Simple Load Case: Analysis of ε_y at Off-Center Line in Model 1

Figure 7.9a shows the strain representation at the off-center line of nodes for the first model. The minimum and maximum strains at each node are plotted against the smoothed strain result. The difference observed shows the modeling errors in the current model as inter-element jumps that occur at the nodes. The maximum absolute percent error at the nodes is shown in Fig. 7.9b. The maximum percent error along this line of nodes is approximately 4.0 percent in this model.

The analysis at the center line of nodes is shown in Fig. 7.10.

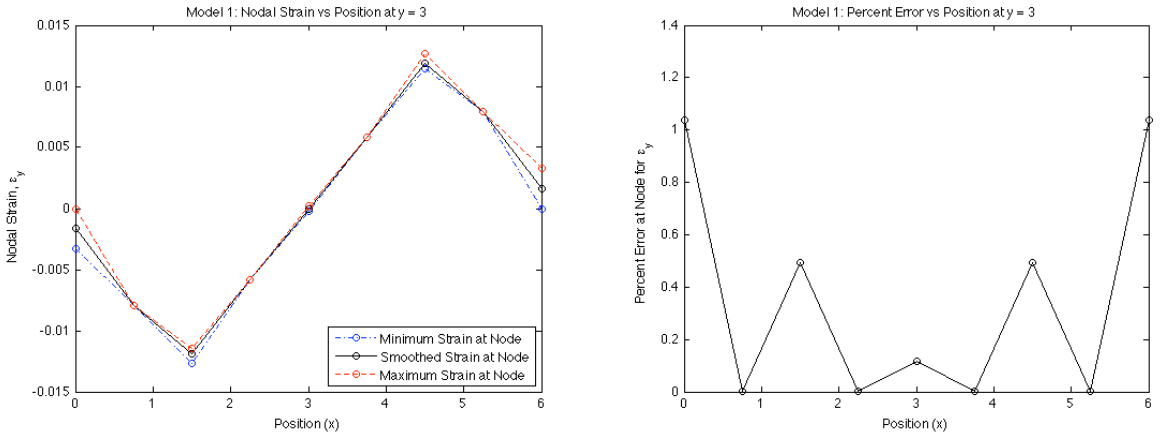

(a) Strain representation (b) Percent error

Figure 7.10 – Simple Load Case: Analysis of ε_y at Center Line in Model 1

As the center line of nodes is farther from the boundaries, the effects of the boundaries are reduced. Thus, the capability of the finite element solution to satisfy the governing differential equation at every point on the domain of an individual element, i.e., satisfy pointwise equilibrium, is more accurately represented. The finite element solution is closer to the smoothed strain representation for this line of nodes in the model, as shown in Fig. 7.10a, than for the off-center line of nodes. This is verified by observing that there is a reduction in the magnitude of the inter-element jumps along this line of nodes. The corresponding percent error has a maximum absolute value of approximately 1.04 percent, as shown in Fig. 7.10b.

The analysis of the second model of the physical system at the off-center line of nodes is shown in Figure 7.11. This model captures a maximum strain of 0.1594 units. Again, this maximum strain is not represented in the associated figures as it occurs at a node located elsewhere in the model.

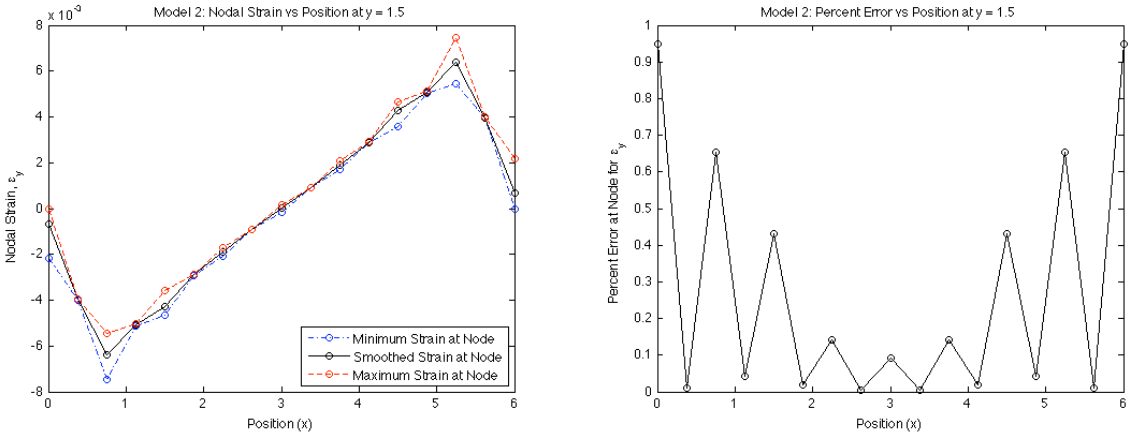

(a) Strain representation (b) Percent error

Figure 7.11 – Simple Load Case: Analysis of ε_y at Off-Center Line in Model 2

Figure 7.11a shows the strain representation at the off-center line of nodes for the second model. The finite element solution and the smoothed strain representation of this strain component are closer along the off-center line of nodes in the current model than in the initial model of this loading condition. This is verified through observing that the magnitudes of the inter-element jumps in this line of nodes are reduced in the current model. The corresponding percent error is reduced to approximately 0.96 percent along this line of nodes, as shown in Fig. 7.11b.

Figure 7.12 shows the analysis of the second model at the center line of nodes.

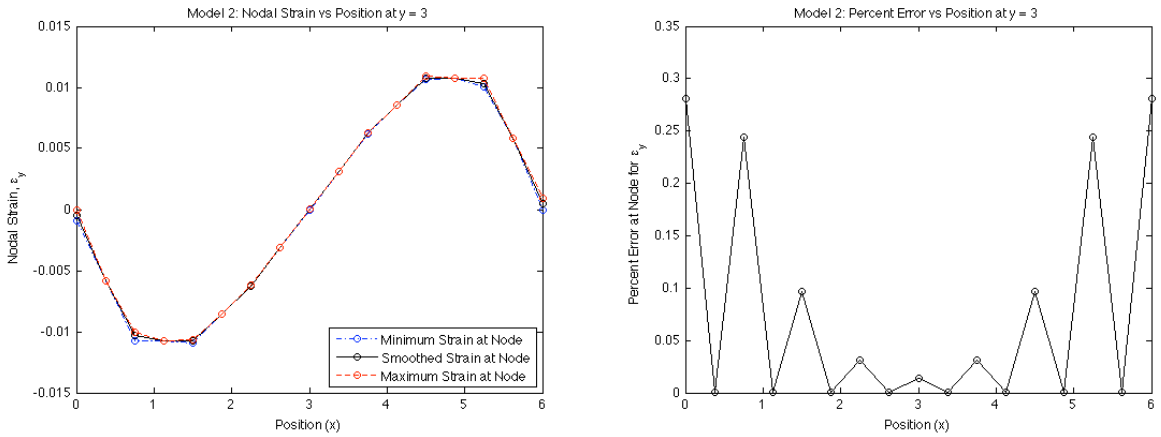

(a) Strain representation (b) Percent error

Figure 7.12 – Simple Load Case: Analysis of ε_y at Center Line in Model 2

Figure 7.12a shows the strain representation at the center line of nodes for the second model. The finite element solution and the smoothed strain representation of this strain component are closer along the center line of nodes in the current model than in the initial model of this loading condition. This is verified by observing that the magnitude of the inter-element jumps in this line of nodes is reduced in this model. The maximum absolute percent error has decreased to approximately 0.28 percent in this model, as shown in Fig. 7.12b.

The analysis of the third model of the physical system at the off-center line of nodes is shown in Fig. 7.13. The third model applied to the physical system captures a maximum strain of 0.1596 units. Again, this maximum strain is not represented in the associated figures as it occurs at a node located elsewhere in the model.

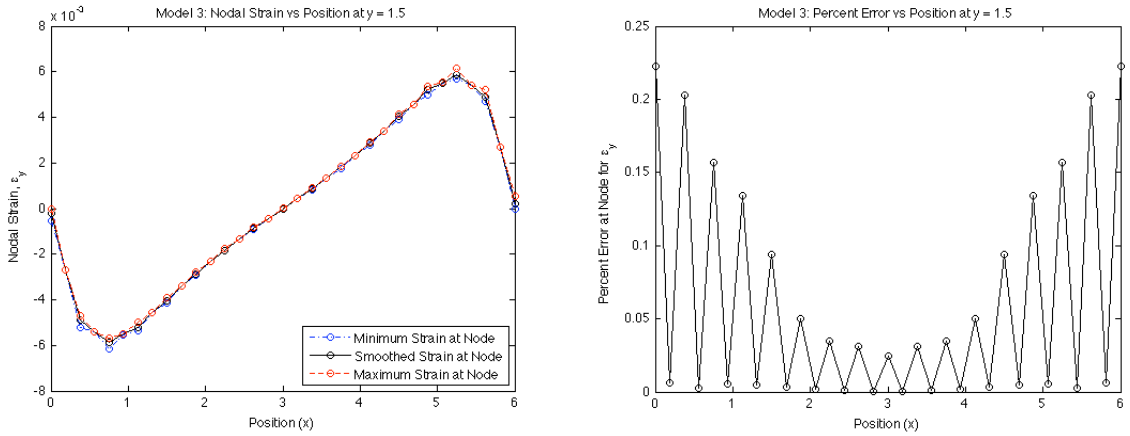

(a) Strain representation (b) Percent error

Figure 7.13 – Simple Load Case: Analysis of ε_y at Off-Center Line in Model 3

Figure 7.13a shows the strain representation at the off-center line of nodes for the third model. The finite element solution and the smoothed strain representation of this strain component are closer along the off-center line of nodes in the current model than in the two previous models of this loading condition. This is verified by observing that the magnitude of the inter-element jumps in this line of nodes is reduced in this model. The maximum percent

error has decreased to approximately 0.22 percent along this line of nodes, as shown in Fig. 7.13b.

Figure 7.14 shows the analysis of the third model at the center line of nodes.

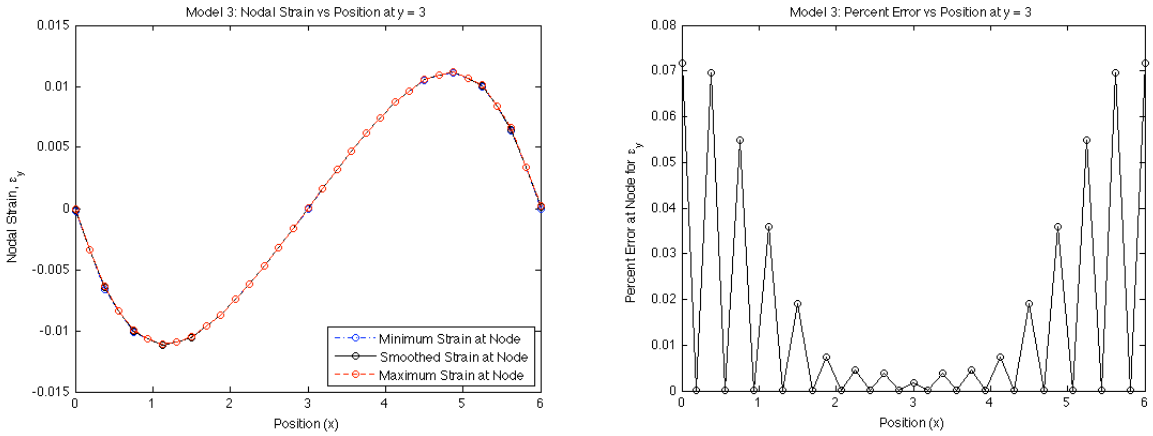

(a) Strain representation (b) Percent error

Figure 7.14 – Simple Load Case: Analysis of ε_y at Center Line in Model 3

Figure 7.14a shows the strain representation at the center line of nodes for the third model. The finite element solution and the smoothed strain representation of this strain component are closer along the center line of nodes in the current model than in the two previous models of this loading condition. This is verified by observing that the magnitude of the inter-element jumps in this line of nodes is reduced in this model and is approaching zero. The corresponding percent error has a maximum value of approximately 0.072 percent in this model, as shown in Fig. 7.14b.

It is shown in this subsection that the inter-element jumps decrease in magnitude as the model is improved for the strain in the y direction, ε_y. This result shows convergence in the strain representation for this strain component. In the next subsection, the capability of the three models to represent the behavior of the strain component in shear, γ_{xy}, is presented.

Modeling the shear strain component, γ_{xy}

In this subsection, the ability of the three successive models of the physical system to better represent the strain distribution in the shear direction, γ_{xy}, is examined. The capability of each model to capture this strain is observed by comparing the maximum and minimum strains that occur at the nodes from the finite element solution of the model to the smoothed strain representation. Again, the maximum absolute strain in each model is restated, since this quantity is the normalizing factor of the error estimator used in this work. The overall strain energy content in each model of this loading condition is not restated, as the model improvement is shown by the Rayleigh-Ritz criterion in the ε_x subsection.

The analysis of the first model of the physical system at the off-center line of nodes is shown in Fig. 7.15. The first model captures a maximum strain of 0.1583 units. This value of maximum strain does not appear in the figures presented for either line of nodes, as it occurs at a node located elsewhere in the model.

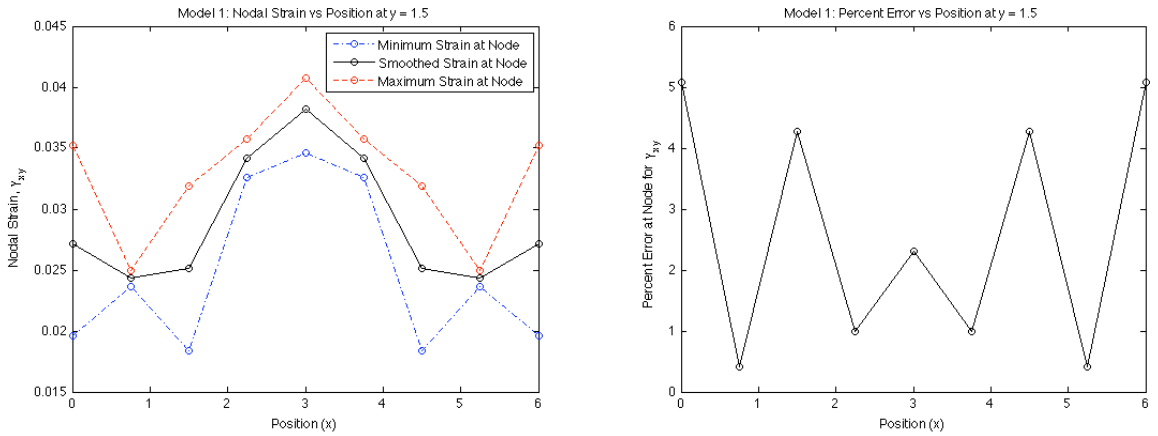

(a) Strain representation (b) Percent Error

Figure 7.15 – Simple Load Case: Analysis of γ_{xy} at Off-Center Line in Model 1

Figure 7.15a shows the strain representation at the off-center line of nodes for the first model. The minimum and maximum strains at each node are plotted against the smoothed strain result. The difference observed shows the modeling errors in the current model as inter-element jumps that occur at the nodes. The maximum absolute percent error at the nodes is shown in Fig.

7.15b. The maximum absolute percent error along this line of nodes is approximately 5.05 percent in this model.

The results at the center line of nodes are shown in Fig. 7.16.

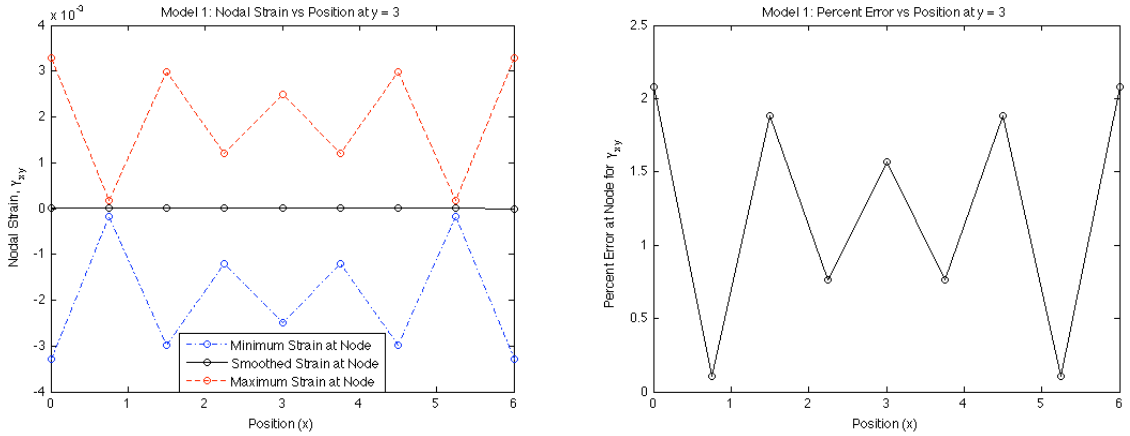

(a) Strain representation (b) Percent Error

Figure 7.16 – Simple Load Case: Analysis of γ_{xy} at Center Line in Model 1

As the center line of nodes is farther from the boundaries, the effects of the boundaries are reduced. Thus, the capability of the finite element solution to satisfy the governing differential equation at every point on the domain of an individual element, i.e., satisfy pointwise equilibrium, is more accurately represented. The finite element solution is closer to the smoothed strain representation for this line of nodes in the model, as shown in Fig. 7.16a, than for the off-center line of nodes. This is verified by observing that there is a reduction in the magnitude of the inter-element jumps along this line of nodes. The corresponding percent error has a maximum value of approximately 2.1 percent, as shown in Fig. 7.16b.

The analysis of the second model of the physical system at the off-center line of nodes is shown in Figure 7.17. This model captures a maximum strain of 0.1594 units. Again, this maximum strain is not represented in the associated figures as it occurs at a node located elsewhere in the model.

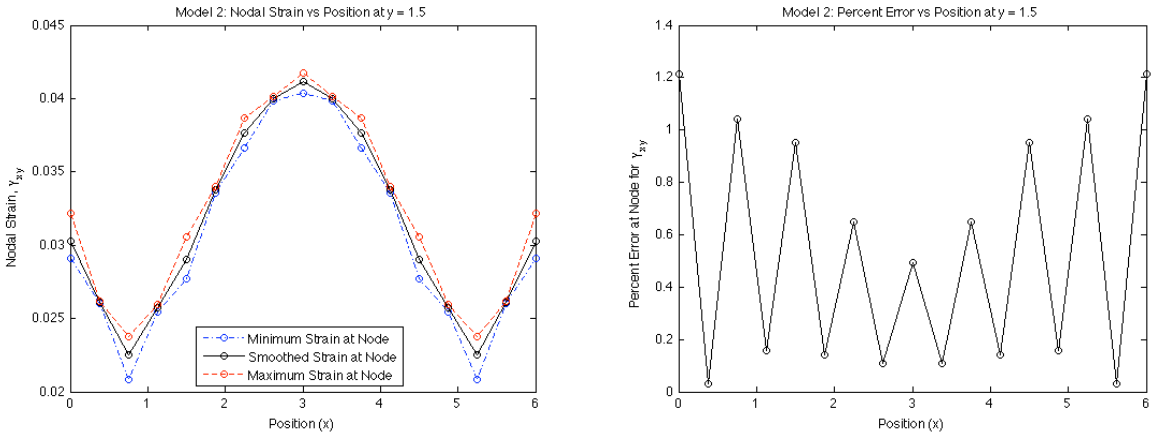

(a) Strain representation (b) Percent Error

Figure 7.17 – Simple Load Case: Analysis of γ_{xy} at Off-Center Line in Model 2

Figure 7.17a shows the strain representation at the off-center line of nodes for the second model. The finite element solution and the smoothed strain representation of this strain component are closer along the off-center line of nodes in the current model than in the initial model of this loading condition. This is verified through observing that the magnitudes of the inter-element jumps in this line of nodes are reduced in the current model. The maximum absolute percent error is reduced to approximately 1.2 percent along this line of nodes, as shown in Fig. 7.17b.

Figure 7.18 shows the analysis of the second model at the center line of nodes.

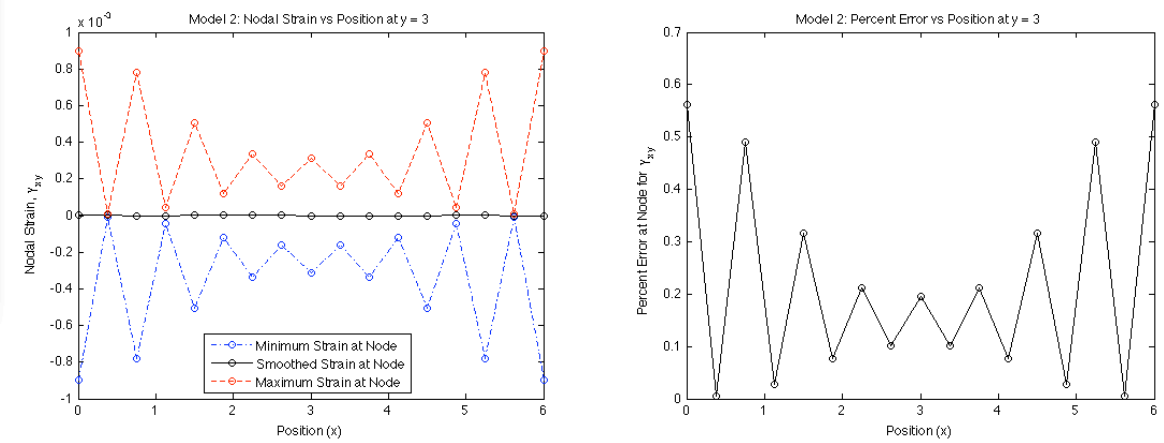

(a) Strain representation (b) Percent Error

Figure 7.18 – Simple Load Case: Analysis of γ_{xy} at Center Line in Model 2

Figure 7.18a shows the strain representation at the center line of nodes for the second model. The finite element solution and the smoothed strain representation of this strain component are closer along the center line of nodes in the current model than in the initial model of this loading condition. This is verified by observing that the magnitude of the inter-element jumps in this line of nodes is reduced in this model. The corresponding percent error has a maximum value of approximately 0.57 percent in this model, as shown in Fig. 7.18b.

The analysis of the third model of the physical system at the off-center line of nodes is shown in Fig. 7.19. The third model applied to the physical system captures a maximum strain of 0.1596 units. Again, this maximum strain is not represented in the associated figures as it occurs at a node located elsewhere in the model.

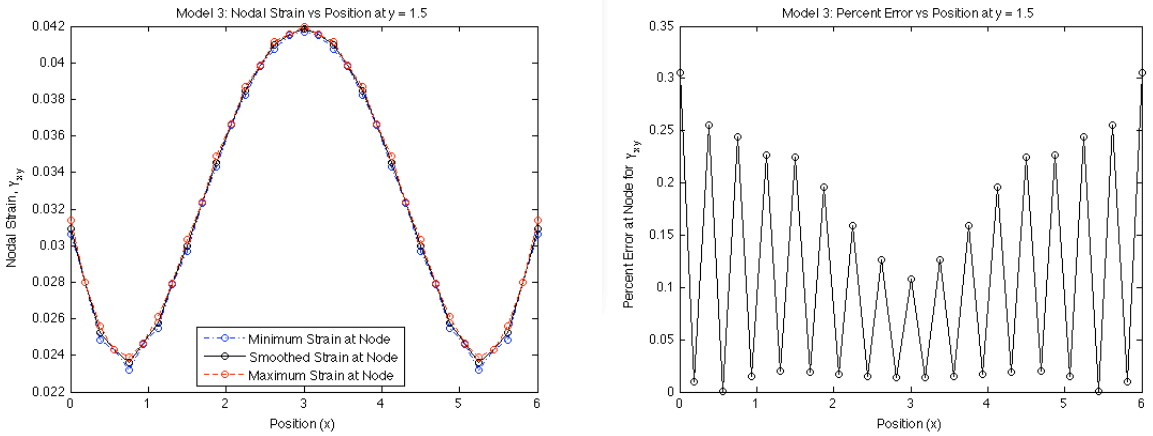

(a) Strain representation (b) Percent Error

Figure 7.19 – Simple Load Case: Analysis of γ_{xy} at Off-Center Line in Model 3

Figure 7.19a shows the strain representation at the off-center line of nodes for the third model. The finite element solution and the smoothed strain representation of this strain component are closer along the off-center line of nodes in the current model than in the two previous models of this loading condition. This is verified by observing that the magnitude of the inter-element jumps in this line of nodes is reduced in this model. The maximum absolute

percent error decreased to approximately 0.3 percent along this line of nodes, as shown in Fig. 7.19b.

Figure 7.20 shows the analysis of the third model at the center line of nodes.

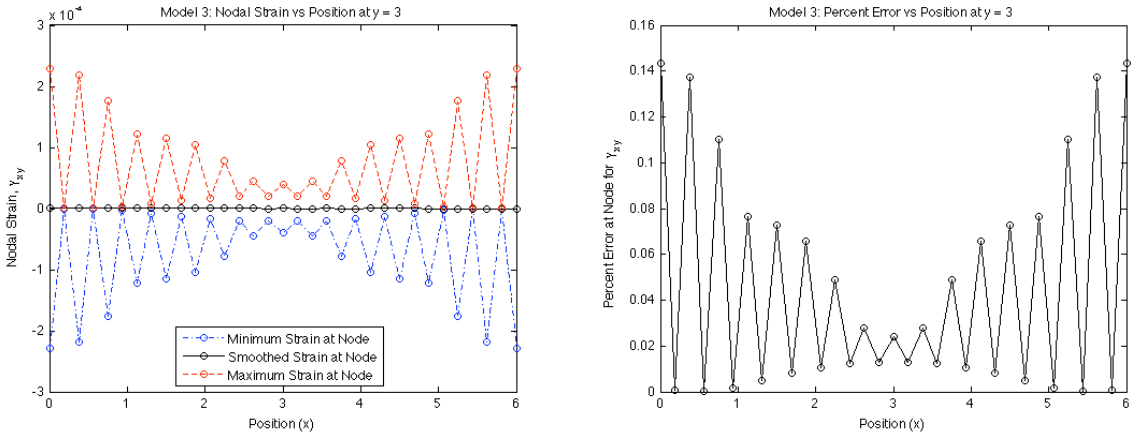

(a) Strain representation (b) Percent Error

Figure 7.20 – Simple Load Case: Analysis of γ_{xy} at Center Line in Model 3

Figure 7.20a shows the strain representation at the center line of nodes for the third model. The finite element solution and the smoothed strain representation of this strain component are closer along the center line of nodes in the current model than in the two previous models of this loading condition. This is verified by observing that the magnitude of the inter-element jumps in this line of nodes is reduced in this model and is approaching zero. The corresponding percent error has a maximum value of approximately 0.144 percent in this model, as shown in Fig. 7.20b.

It is shown in this subsection that the inter-element jumps decrease in magnitude as the model is improved for the strain in the strain direction, γ_{xy}. This result shows convergence in the strain representation for this strain component.

In the preceding subsections, the convergence of the finite element solution to the smoothed strain representation has been demonstrated for each of the three strain components.

The inter-element jumps were observed to decrease in magnitude as the model is improved. The corresponding percent error in each model was also mitigated.

7.3 - Model with Distributed Load and Runge Function Strain Distribution

The second loading condition in this demonstration is designed to produce displacements and an associated strain distribution that are Runge functions. This loading is chosen because a Runge function is difficult for a polynomial representation to capture. Thus, it is a severe test for the finite element model and the error estimator. For this example, the distributed load is applied in the x direction. The equivalent nodal loads are found for this loading condition and the model is analyzed. Again, it is noted that the interior nodes along the lines presented have an inter-element jump of zero.

The following subsection demonstrates the capability of the successive models to better represent the strain distribution of the component in the x direction, ε_x. It was shown in the previous Section that the inter-element jumps converge in each of the three strain components as the model is improved. It is for this reason that only the strain component in the x direction is presented here for this loading condition.

Modeling the x-direction strain component, ε_x

In this subsection, the ability of the three successive models of the physical system to better represent the strain distribution in the x direction is examined. The capability of each model to capture this strain is observed by comparing the maximum and minimum strains that occur at the nodes from the finite element solution of the model to the smoothed strain representation.

The analysis of the initial model of the physical system at the off-center line of nodes is shown in Fig. 7.21. This model captures a maximum strain of 0.0091 units. This value of

maximum strain does not appear in the figures presented for either line of nodes, as it occurs at a node located elsewhere in the model. The initial model has an overall strain energy content of 0.0168 units.

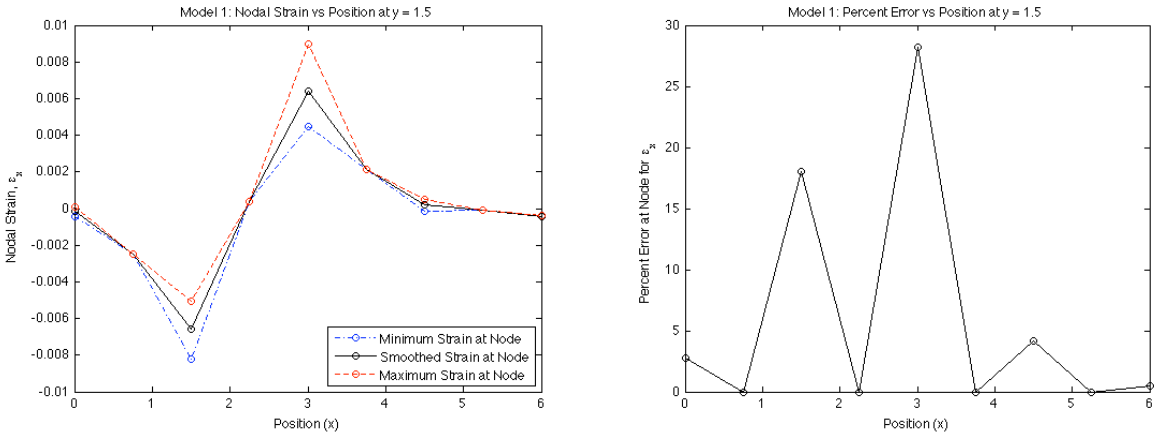

(a) Strain representation (b) Percent error

Figure 7.21 – Complex Load Case: Analysis of ε_x at Off-Center Line in Model 1

Figure 7.21a shows the strain representation at the off-center line of nodes for the first model. The minimum and maximum strains at each node are plotted against the smoothed strain representation. The difference observed shows the modeling errors in the current model as inter-element jumps that occur at the nodes. The maximum absolute percent error at the nodes is shown in Fig. 7.21b. The maximum percent error along this line of nodes is approximately 28 percent in this model. The errors contained in this model are higher than those for the model that is uniformly loaded. This is expected because this load produces large variation in the strain on the domain of the model.

The results at the center line of nodes of the model are shown in Fig. 7.22.

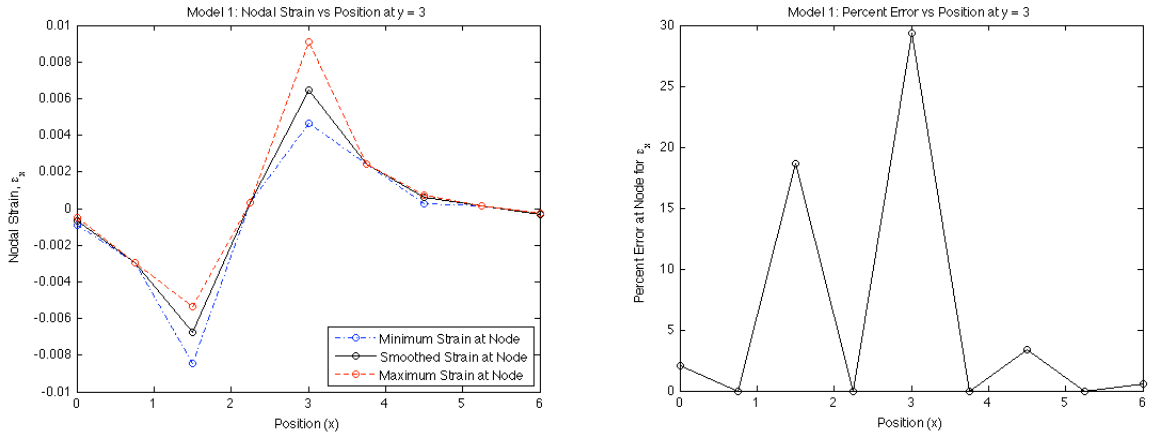

(a) Strain representation (b) Percent error

Figure 7.22 – Complex Load Case: Analysis of ε_x at Center Line in Model 1

The strain representation along the center line of nodes is shown in Fig. 7.22a. As this line of nodes is farther from the boundaries, the effects of the boundaries are reduced. Thus, the capability of the finite element solution to satisfy the governing differential equation at every point on the domain of an individual element, i.e., satisfy pointwise equilibrium, is more accurately represented. It is for this reason that a slight increase in the maximum absolute percent error, from approximately 28 percent at the off-center line of nodes to approximately 30 percent, as shown in Fig. 7.22b, at the center line of nodes is seen in the initial model of this loading condition.

The analysis of the second model of the physical system at the off-center line of nodes is shown in Figure 7.23. This model captures a maximum strain of 0.0130 units. Again, this maximum strain is not represented in the associated figures as it occurs at a node located elsewhere in the model. This model contains an overall strain energy content of 0.017350 units. This amount of strain energy is larger than that contained in the previous model, so the Rayleigh-Ritz criterion is satisfied.

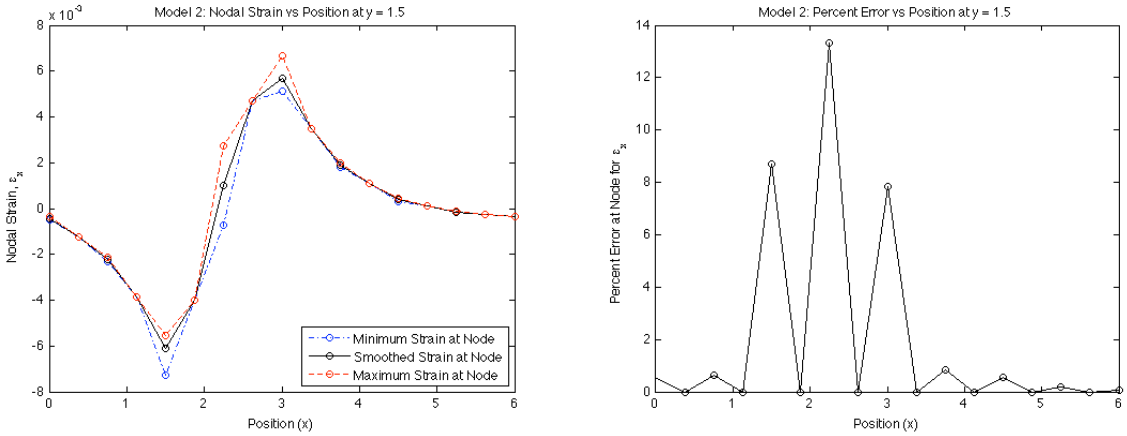

(a) Strain representation (b) Percent error

Figure 7.23 – Complex Load Case: Analysis of ε_x at Off-Center Line in Model 2

Figure 7.23a shows the strain representation at the off-center line of nodes for the second model. The finite element solution and the smoothed strain representation of this strain component are closer along the off-center line of nodes in the current model than in the initial model of this loading condition. This is verified through observing that the magnitudes of the inter-element jumps in this line of nodes are reduced in the current model. The maximum absolute percent error along this line of nodes is decreased to approximately 13 percent in this model, as shown in Fig. 7.23b.

Figure 7.24 shows the analysis of the second model at the center line of nodes.

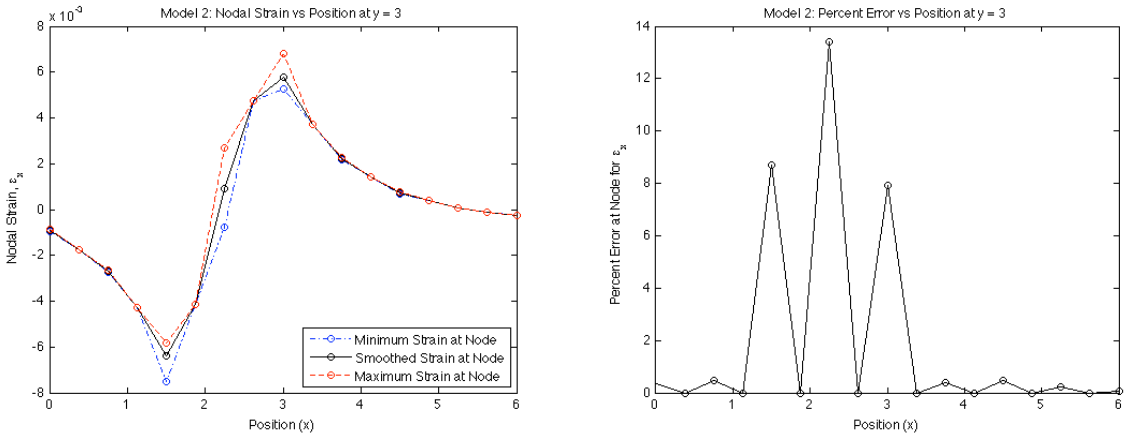

(a) Strain representation (b) Percent error

Figure 7.24 – Complex Load Case: Analysis of ε_x at Center Line in Model 2

Figure 7.24a shows the strain representation at the center line of nodes for the second model. The finite element solution and the smoothed strain representation of this strain component are closer along the center line of nodes in the current model than in the initial model of this loading condition. This is verified by observing that the magnitudes of the inter-element jumps in this line of nodes are reduced in the current model. The corresponding percent error has a maximum value of approximately 13 percent in this model, as shown in Fig. 7.24b.

The analysis of the third model of the physical system at the off-center line of nodes is shown in Fig. 7.25. The third model applied to the physical system captures a maximum strain of 0.0137 units. This maximum strain is not represented in the associated figures as it occurs at a node located elsewhere in the model. This model contains an overall strain energy content of 0.017433 units. Again, the Rayleigh-Ritz criterion is satisfied.

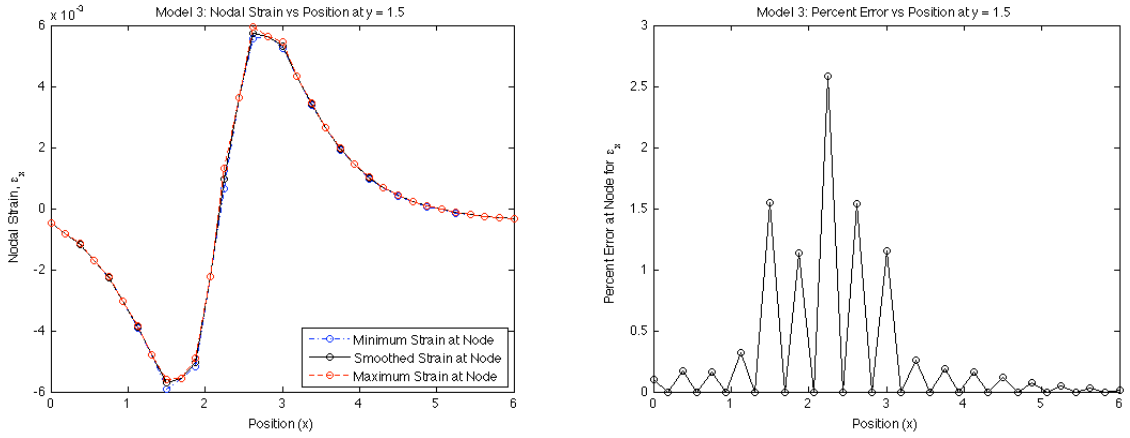

(a) Strain representation (b) Percent error

Figure 7.25 – Complex Load Case: Analysis of ε_x at Off-Center Line in Model 3

Figure 7.25a shows the strain representation at the off-center line of nodes for the third model. The finite element solution and the smoothed strain representation of this strain component are closer along the off-center line of nodes in the current model than in the two previous models of this loading condition. This is verified by observing that the magnitudes of the inter-element jumps in this line of nodes are reduced in the current model. The maximum

absolute percent error along this line of nodes is decreased to approximately 2.6 percent in this model, as shown in Fig. 7.25b.

Figure 7.26 shows the analysis of the third model at the center line of nodes.

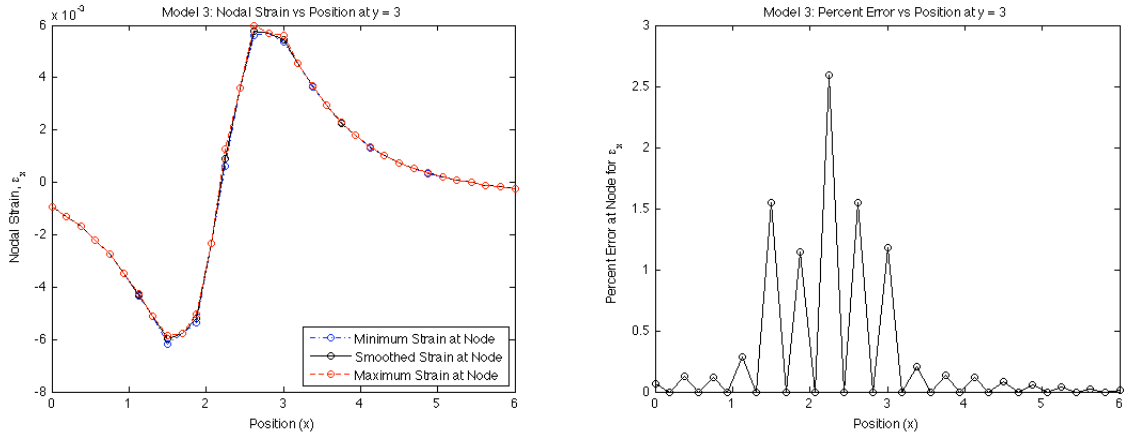

(a) Strain representation (b) Percent error

Figure 7.26 – Complex Load Case: Analysis of ε_x at Center Line in Model 3

Figure 7.26a shows the strain representation at the center line of nodes for the third model. The finite element solution and the smoothed strain representation of this strain component are closer along the center line of nodes in the current model than in the two previous models of this loading condition. This is verified by observing that the magnitudes of the inter-element jumps in this line of nodes are reduced in the current model. The corresponding percent error has a maximum value of approximately 2.6 percent in this model, as shown in Fig. 7.26b.

It is shown in this Section that the inter-element jumps decrease in magnitude as the model is improved for the strain component in the x direction, ε_x. This result shows convergence in the strain representation for this strain component.

7.4 - Summary and Conclusion

In Chapter 4, the failure of the finite element result to satisfy the governing differential equation was quantified by substituting the finite element result into the governing differential equation to form a residual for the one-dimensional case. This residual is a continuous function

over the domain of the element that can be treated as a distributed load. When this pseudo-distributed load is converted to nodal loads using the same process used to form the actual nodal loads, it quantifies the failure of the finite element result to satisfy the governing differential equation as nodal quantities.

When the nodal values of the residuals are assembled in the same manner as the equivalent nodal loads for the individual elements, the result is found to be equal to the inter-element jumps in the strains in the finite element solution. This means that an aggregated measure of the errors in the finite element model is available from the finite element solution itself. That is to say, the residuals for the individual elements, the equivalent nodal residuals, and the assembled residuals need not be computed.

The pointwise error estimator developed in Chapter 5 for one-dimensional problems was extended to a two-dimensional physical system in this Chapter. It was shown that this error estimator decreased as the finite element model was improved for two cases.

The first case modeled a constant distributed load. This loading condition was chosen because it produces a strain distribution that is simple for the finite element model to represent. The inter-element jumps were shown to converge in each of the three strain components, as the model was uniformly refined.

In the second case, the physical system was modeled under a more complex loading condition, which produces displacements and a strain distribution in the form of a Runge function. The inter-element jumps were demonstrated to converge for the strain component in the x direction, ε_x. As the inter-element jumps in the other strain components were shown to converge in the case of the constant distributed load, only the convergence of the strain

component in the x direction was presented in this demonstration. Convergence of the inter-element jumps also occurs in the other two strain components.

This convergence was shown through the reduction of the inter-element jumps in the finite element strain distribution with respect to the smoothed strain distribution. The reduction of the inter-element jumps occurs because the elements are more capable of satisfying the governing differential equation as the model is improved. The error estimator was shown to converge in each of the three strain components.

The key constituent of the adaptive refinement process centers on the error estimator driving the refinement. The error estimator presented in this Chapter was shown as being capable of determining locations of high and low levels of error in the finite element model. Thus, it can be concluded that a rational approach to the adaptive refinement of finite element models can be developed using this error estimator as a basis.

The results presented in this Chapter indicate that a metric found from the inter-element jumps can serve as an adequate termination criterion for the adaptive refinement process. There are two main advantages of this metric. The first advantage is that this metric is a physically useful measure. In other words, it is in terms of a quantity that is sought in the analysis and is meaningful to the analyst. The second advantage is that it is a pointwise error estimator. Therefore, there is no integration that is required in estimating the error.

CHAPTER 8

PERFORMANCE BASED REFINEMENT GUIDES

8.1 - Introduction

Two refinement guides that identify a level of refinement for individual elements that produce rapid convergence of finite element models are developed in this Chapter from first principles. The level of refinement for the individual elements is identified by first estimating the modeling deficiencies in the element and then finding the number of subdivisions needed to reduce the estimated errors in the smaller elements so that they satisfy the termination criterion. These approaches differ from the refinement guides presented earlier that are simply correlated to the error estimators that serve as termination criterion.

The two refinement guides developed here compute the *in situ* estimates of the modeling deficiencies using similar, but theoretically different, approaches. Both refinement guides first **form smoothed strain distributions** that are closer to the exact solution than is the discontinuous strain distribution produced by the finite element model. The smoothed strain distributions that serve as the basis for both refinement guides are formed by eliminating the inter-element jumps in the finite element strain representation. The theoretical difference in the two refinement guides is contained in the way in which the inter-element strain values are computed.

In the first approach, the discontinuous strain distribution is smoothed by forming an inter-element strain value by applying a central difference template to a set of displacements taken from the elements adjacent to the inter-element node. In the second approach, the smoothed solution is formed by averaging the elemental strain values that exist at the inter-

element nodes. This form of smoothing is used to create the smoothed solution used in the Zienkiewicz and Zhu (ZZ) error estimator presented in Chapter 6.

The objective of this Chapter is to develop and demonstrate the two refinement guides just described.

The rationale behind the two refinement guides developed here is shown graphically in Fig. 8.1. The smoothed solution contained in these figures is formed by applying finite difference templates to the augmented displacements of the individual elements. If nodal averaging were used to form the smoothed solution, the figures would contain the same ideas.

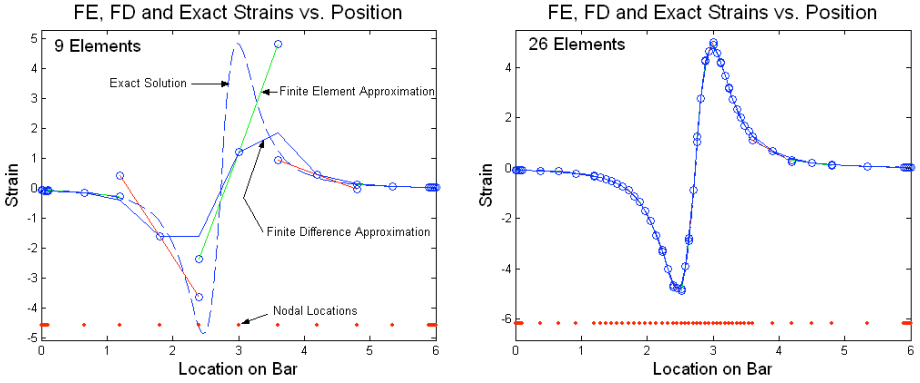

a) Initial Model b) Refined Model

Figure 8.1 – Finite Element, Exact and Smoothed Strain Representations

Figure 8.1a presents the finite element strain distribution for an inaccurate initial model of the control problem. The exact solution and the smoothed strain distribution are superimposed on the finite element result. As can be seen, the structure or shape of the smoothed strain distribution on the domain of the individual elements is more complex than the discontinuous finite element solution.

For the three-node elements shown in Fig. 8.1, the smoothed strain contains curvature, a complexity that does not exist in the finite element representation. It is this difference in

complexity between the smoothed solution and the finite element strain representation that is exploited in the refinement guides developed here.

The differences between the two strain representations approximate the modeling deficiency in the individual elements. The level of refinement is identified by determining the number of subdivisions of an element that are needed to represent the higher complexity of the smoothed solution with a finite representation that will satisfy the termination criterion.

The result of adaptively refining the initial model is shown in Fig. 8.1b. As can be seen, the three strain representations are nearly identical. That is to say, the higher complexity of the exact solution is closely represented by the additional elements introduced by the adaptive refinement process.

The two refinement guides developed here have three significant advantages over existing approaches. The level of refinement is directly related to the cause of the modeling errors. That is to say, an element is refined sufficiently so that the polynomial basis of the element is capable of representing the portion of the exact strain distribution that exists on the shortened element to the specified level of accuracy. The refinement guides are computed from pointwise quantities, so no integrals are involved in their formulation. Finally, the refinement guides are expressed in terms of quantities that are the focus of the analysis, namely, strains or stresses. This contrasts to other approaches where the refinements are related to the error estimators in terms of strain energy or an equivalent distributed load quantity [2, 3, 34, 35].

An overview of the development of the finite difference approach to smoothing is presented in the next Section. The theoretical background that provides the basis of this development is presented in the following two Sections. The development of the procedure for

quantifying the discretization errors and forming the refinement guides follows. Finally, the results for a series of illustrative examples are presented.

In Section 8.6, a refinement guide found from a higher-order strain distribution formed from the average nodal strains is demonstrated with the same set of examples used to demonstrate the finite difference approach. The procedures are identical except for the source of the nodal strain quantities that produce the smoothed solution. This approach has the additional advantage that it is computationally more efficient than the approach based on the finite difference approximation.

8.2 – Theoretical Overview for Finite Difference Smoothing

Modeling errors exist in finite element solutions when the polynomial basis for an individual finite element cannot capture the complexity of the exact result that exists on its domain. The refinement guide developed here compares the modeling capabilities of a single element to a higher-order smoothed strain approximation derived from the current finite element results. This refinement guide identifies the number of subdivisions an element needs to capture the higher-order strain approximation that exists on its domain to within the desired level of accuracy.

The most direct approach for extracting the higher-order strain representation is to place a higher-order finite difference template at the center of the element being evaluated. Then, the displacements for the element being evaluated and the displacements for selected interior nodes of the adjacent elements are introduced into the template in order to extract the higher-order strain terms. However, in this presentation a two-step process is used to find the higher-order strain quantities instead of this direct approach. This is done so the procedure for forming two refinement guides developed here are nearly identical.

In the examples presented here, the first step is to compute the inter-element strains by inserting the appropriate displacements into a three-node central difference template. Then, the nodal strains for the smoothed solution on the domain of the element being evaluated are inserted into a central difference template to estimate the higher-order strain terms for the finite element.

The estimates of the modeling deficiencies in the individual finite elements are computed as the differences between the smoothed and the finite element strain distributions. These differences are computed by subtracting the Taylor series representations of the two approximate strain representations from each other. In the three-node bar elements used in the examples presented here, the first three terms of the smoothed strain representation are subtracted from the two-term finite element strain representation over the domain of an individual finite element.

The strain representation contained in a three-node bar element consists of the following two Taylor series terms, namely, ε_x and $d\varepsilon_x/dx$. The finite difference representation of the smoothed strain used in these examples also contains the next term in the Taylor series expansion, namely, $d^2\varepsilon_x/dx^2$. This higher-order term represents the curvature that exists in the smoothed solution on the domain of the element being evaluated.

When this subtraction is performed, the estimated error in the finite element being evaluated is the following:

$$\Delta\varepsilon_x = \underbrace{\left((\varepsilon_x)_o + (\varepsilon_{x,x})_o\, x + (\varepsilon_{x,xx})_o\, x^2/2\right)}_{\substack{\text{Smoothed}\\ \text{Solution}}} - \underbrace{\left((\varepsilon_x)_o + (\varepsilon_{x,x})_o\, x\right)}_{\substack{\text{Finite}\\ \text{Element}}} \qquad \text{(Eq. 8.1)}$$

The derivative terms in Eq. 8.1 are expressed in the compact strain gradient notation where

$(\varepsilon_{x,x})_o = (d\varepsilon_x/dx)_o$ and $(\varepsilon_{x,xx})_o = (d^2\varepsilon_x/dx^2)_o$.

The constant strain terms are the same for both approximate representations because both expansions use the interior node of the three-node element as the local reference. The equality of

the strains at the local origin in the center of an element for the two approximate strain representations can be seen in Fig. 8.1.

As a result, the constant strain terms are eliminated when Eq. 8.1 is simplified. This reduces the difference between the two representations to the following:

$$\Delta\varepsilon_x = \left[\left((\varepsilon_{x,x})_o \right)_{\substack{\text{Smoothed} \\ \text{Solution}}} - \left((\varepsilon_{x,x})_o \right)_{\substack{\text{Finite} \\ \text{Element}}} \right] x + \left[\left((\varepsilon_{x,xx})_o \right)_{\substack{\text{Smoothed} \\ \text{Solution}}} \right] x^2 / 2 \qquad \text{(Eq. 8.2)}$$

The strain difference identified in Eq. 8.2 consists of the difference between the smoothed and the finite element slope representations and a term that the linear strain element cannot represent, namely, the curvature of the strain in the smoothed strain representation.

The three components of Eq. 8.2 are shown visually in Fig. 8.2 for the fourth element from the left in the finite element model. In this figure, the slopes of the finite element and the smoothed strain representation are identified for this element. The difference between these slopes is the coefficient of the linear term in Eq. 8.2. As can be seen in Fig. 8.2, there is a significant difference between the two slopes.

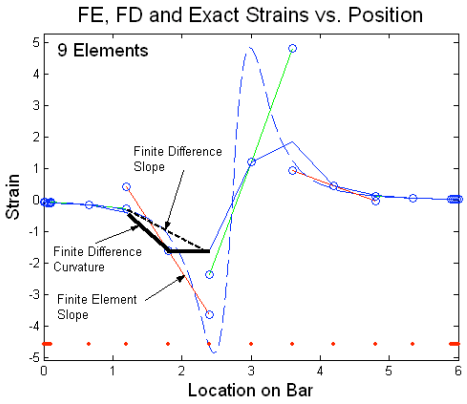

Figure 8.2 – Finite Difference Parameters

An approximation of the curvature in the smoothed strain representation is also shown for this element in Fig. 8.2. This approximation consists of the two heavy lines labeled as the finite difference curvature. Since curvature is related to the rate of change of the slope, the finite difference curvature for the finite element is computed as a function of the difference between the slopes of the two segments of the heavy line shown in Fig. 8.2.

The level of refinement given to an individual element is identified by relating the maximum difference between the two approximate solutions given by Eq. 8.2 to the termination criterion. This maximum difference is given by the following relationship:

$$\left|\Delta\varepsilon_x\right| = \text{abs}\left[\left((\varepsilon_{x,x})_{\text{o}}\right)_{\substack{\text{Smoothed}\\ \text{Strain}}} - \left((\varepsilon_{x,x})_{\text{o}}\right)_{\substack{\text{Finite}\\ \text{Element}}} \right] h + \text{abs}\left[\left((\varepsilon_{x,xx})_{\text{o}}\right)_{\substack{\text{Smoothed}\\ \text{Strain}}} \right] h^2/2 \qquad \text{(Eq. 8.3)}$$

where "h" is equal to one-half of the maximum length element that satisfies the termination criterion.

8.3 - Development of the Refinement Guide

The refinement guide developed here estimates the number of elements needed to reduce the difference between the smoothed and the finite element strain approximations to below the magnitude of the termination criterion. This level of refinement is designed to satisfy the termination criterion in a small number of iterations.

This refinement guide is very conservative. It is designed to verify the efficacy of this approach to model refinement. It has a rational basis and is not based on a correlation that is related to the termination criterion. A less conservative approach based on the same idea is developed and applied in a later Chapter. The later development is applied to models formed from four-node elements.

Equation 8.3 predicts the difference in the approximate representations as a function of the distance from the origin of the element. The refinement guide formed here identifies maximum length that will keep the difference between the two approximate solutions below the desired level of acceptable error, i.e., below the termination criteria.

That is to say, the refinement guide is formed as follows. The distance h from the origin for which the following relationship holds is found:

$$\Delta\varepsilon_x(h) < \text{Termination Criterion} \qquad \text{(Eq. 8.4)}$$

That is to say 2h is the largest length of an element for which the error will not exceed the termination criterion.

Thus, the number of elements that replaces the existing element is found by dividing the length of the n^{th} element by the length of an element that will possess an acceptable error for the polynomial that must be represented. That is to say, the element being evaluated is subdivided into the following number of elements:

$$N = \frac{L_n}{2h} \qquad \text{(Eq. 8.5)}$$

For example, let us say that Eq. 8.3 is satisfied when h is equal to one-fifth of the original length of the element. This means that the element being evaluated must be divided into $N = L_n / 2(L_n/5)$ elements. Since N for this case is equal to 2.5, this element will be divided into 3 elements in the refined model.

In this analysis, the termination criterion requires that the jumps in the inter-element strains be less than a specified percentage of the maximum absolute stress in the current finite element model. In the examples presented here, the termination criteria will be either two or four percent.

An example of the results produced by this refinement guide is presented in Table 8.1. This table contains the refinements applied to the initial model shown in Fig. 8.1a and Fig. 8.2, which is an augmented version of Fig. 8.1a. The contents of this table show that five elements are not subdivided and that two of the elements are divided into two elements. The element used as an illustration in Fig. 8.2 is subdivided into seven elements. As will be shown in the next Section, this element is spanning a region that contains one inflection point and the minimum point for the strain distribution. The linear strain element that is subdivided into ten elements

covers a region that contains two inflection points and the maximum point for the strain distribution.

Table 8.1 – Element Subdivisions for Initial Nine-Element Model

El. No.	1	2	3	4	5	6	7	8	9
No. Divisions	1	1	2	7	10	2	1	1	1

As can be seen in Fig. 8.1b, these refinements produced a new model with twenty-six elements that represent the exact solution very well. This model satisfied the termination criterion of four percent of the maximum absolute strain in the finite element model. That is to say, the performance of this refinement guide exceeded expectations. The initial model was sufficiently refined in regions with excessive discretization error so that a second iteration was not needed to get a result with an acceptable level of error.

8.4 - Problem Description

This Section describes the longitudinal bar problem with fixed ends being approximated in this Chapter. As can be seen in Fig. 8.1, the loading is such that the strains are nearly zero at the two ends of the bar. This loading condition is chosen so the boundary conditions have little if any affect on this problem.

In order to further reduce any boundary effects two very small elements are included in the model at both ends to absorb any small errors. As can be seen in Table 8.1, the small elements on the boundaries are performing as expected. None of the small elements have been subdivided. The presence of the elements designed to reduce any boundary effect make this model different from the control problem used in earlier Chapters. Three-node linear strain elements are used in all of the models presented here.

The problem is loaded with a distributed load that produces a displacement in the exact solution that is a Runge function. This loading condition is chosen because Runge functions are

difficult for polynomial representations to capture [36]. This difficulty results from the fact that Runge functions are rational polynomials, i.e., one polynomial divided by another polynomial. As such, these functions cannot be represented exactly by a finite number of polynomial terms.

The displacement in the exact solution is based on the following Runge function which is shown in Fig. 8.3: $f(x) = 300/(x + 30.0 / 2.0)^2$. As can be seen, this function is symmetric about the center of the domain. In order to make the problem a bit more complex, the symmetry in the displacement function is eliminated by moving the displacement slightly away from the center of the bar. The off-center displacement function is the following: $f(x) = 300/(x + 30.0/ 2.2)^2$.

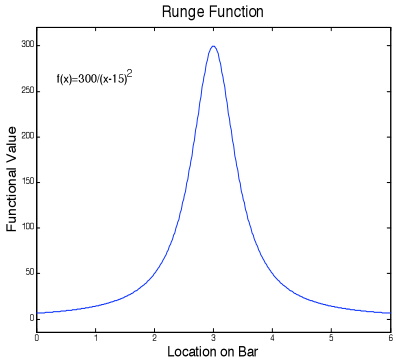

Figure 8. 3 – A Runge Function

The loading condition that produces the displacement given by this Runge function is found by integrating this displacement function twice. When these two integrations are performed, the "high-demand" loading condition is shown in Fig. 8.4a. The strain distribution produced by this loading is presented in Fig. 8.4b.

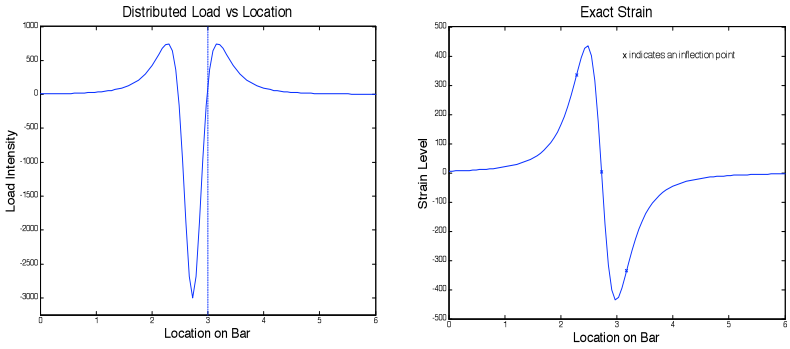

a) Load Shifted to the Left b) Resulting Strain Distribution

Figure 8.4 – A "High-Demand" Loading Condition and Resulting Strain Distribution

As can be seen in Fig. 8.4b, this complex strain distribution presents a difficult task for linear strain elements. This strain distribution contains three inflection points, a maximum point

and a minimum point. The inflection points are indicated by the "x's" in Fig. 8.4b. These modeling complexities are the reasons for choosing this problem to demonstrate this approach to adaptive refinement.

8.5 - Examples of Adaptive Refinement

This Section contains three examples of problems refined under the guidance of the approach developed here. The first objective of these examples is to demonstrate the effectiveness of this refinement guide. The second objective is to demonstrate the sensitivity of the refinement guide to the size of the discretization errors in a model and to the restriction imposed by the termination criterion.

The first example is the problem used in the Introduction to give an overview of this development. Figure 8.1 is reproduced here as Fig. 8.5 for the convenience of the reader. Figure 8.5a presents the finite element and the smoothed solution formed with finite difference strain approximations extracted from the finite element displacements for the initial nine-element model along with the exact strain distribution. As can be seen, there is a significant difference between these two approximate strain representations where they both vary greatly from the exact solution.

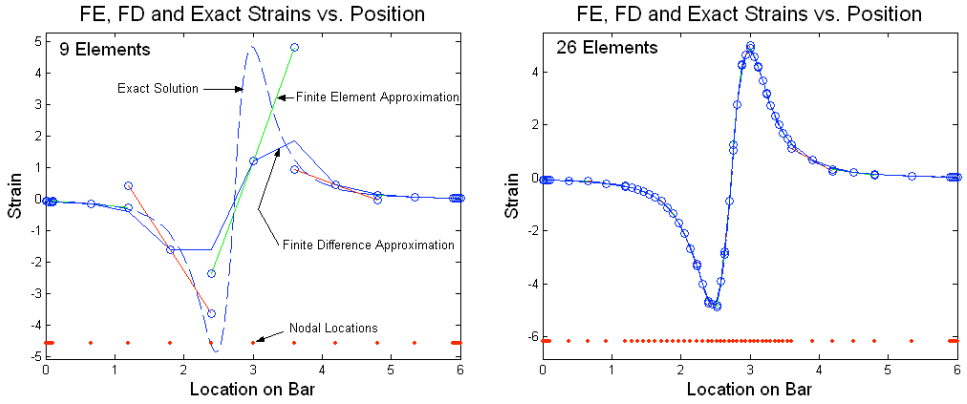

a) Initial Model b) Refined Model

Figure 8.5 – Initial and Refined Finite Element Models

The differences between the two approximate solutions computed with Eq. 8.3 and a termination criterion of four percent of the maximum strain in the finite element model are used in this example to form the refinement guides for the individual finite elements. The refinements for the individual elements for this problem are shown in Table 8.2. This table is identical to Table 8.1. It is reproduced here for the convenience of the reader.

Table 8.2 – Element Subdivisions for Initial Nine-Element Model

El. No.	1	2	3	4	5	6	7	8	9
No. Divisions	1	1	2	7	10	2	1	1	1

The contents of Table 8.2 indicate that five of the elements in the initial model satisfy the termination criterion and will not be subdivided. Two of the original elements will be subdivided into two elements. However, the two elements in the center of the model that have the most complex region to represent are subdivided into seven and ten elements, respectively.

Figure 8.5b contains the same three strain representations as Fig. 8.2b. As can be seen, the three strain representations are close to each other. That is to say, there are no significant differences between the finite element and the smoothed approximations and the exact result. The finite element strains in Fig. 8.5b satisfy the specified termination criterion of 4.0 percent.

The similarity of the three strain distributions is shown in detail for the regions of maximum and minimum strains in Fig. 8.6. Note that the structures of the two approximate solutions for both the maximum and the minimum points are similar in this close-up view. The slopes of the two approximate solutions are significantly different and the curvature in the finite difference representation is high. However, the inter-element jumps in the strain are small, so the finite element solution satisfies the termination criterion.

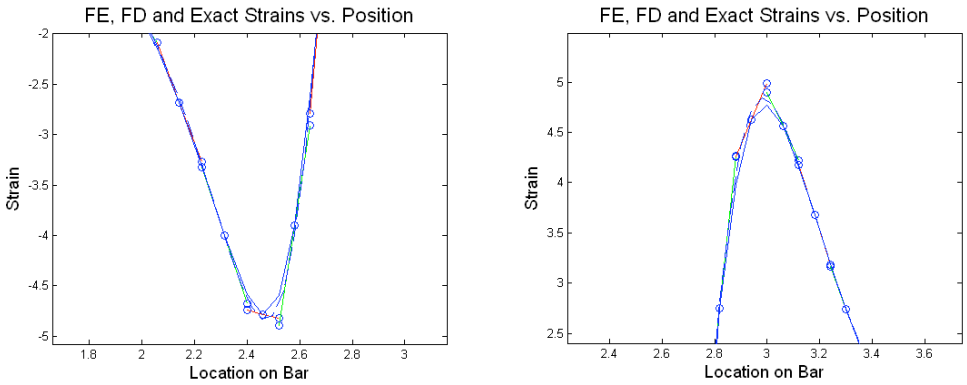

a) Minimum Strain Detail b) Maximum Strain Detail

Figure 8.6 – Strain Representations at the Extreme Points – 25-Element Model

The refinement guide will now be applied to an initial model that better represents the exact solution than the initial model for the first example. This model has 15 elements instead of the nine elements contained in the initial model for the previous example.

This example is designed to show the sensitivity of the refinement guides to the level of error in the elements being evaluated. The strain representations for the initial model are shown in Fig. 8.7a.

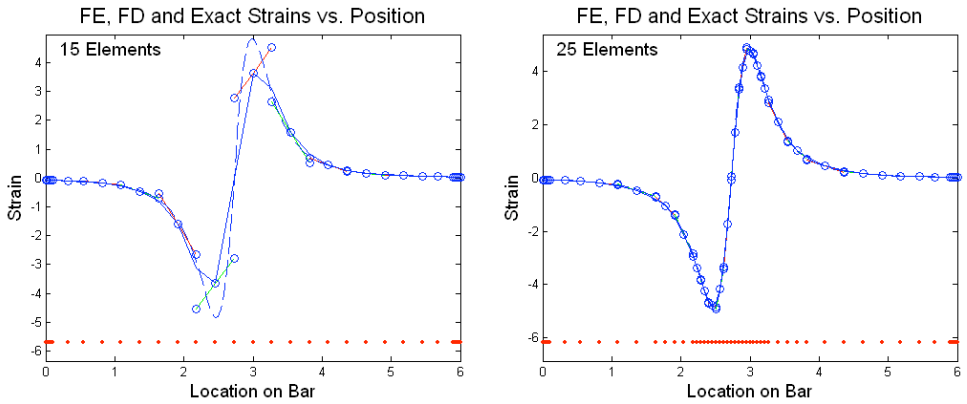

a) Initial Mesh b) First Iteration and Last

Figure 8.7 – Initial and Refined Finite Element Models

The refinements identified by the refinement procedure for this model are shown in Table 8.3. In this case, the refinement guide added ten new elements to the initial model. This contrasts to the seventeen elements that were added to the previous example.

Table 8.3 – Refinements for 15-Element Model, Termination Criterion of 4%

El. No.	1	2	3	4	5	6	7	8	9	10	11	12	13	14	15

No. Divisions	1	1	1	1	1	2	5	5	2	1	1	1	1	1	1

The strain results for the final model are shown in Fig. 8.7b. As can be seen when Fig. 8.7a is compared to Fig.8.7b, the elements were added in the regions that needed refinement. This model satisfies the termination criterion.

In the final example, the previous model with the fifteen elements in the initial model is evaluated with a more restrictive termination criterion. The termination criterion is reduced from 4 percent to 2 percent of the max absolute strain in the finite element model. The objective of this example is to demonstrate the sensitivity of the refinement guides to the termination criterion. The refinements identified for this case are presented in Table 8.4.

Table 8.4 – Refinements for 15-Element Model, Termination Criterion of 2%

El. No.	1	2	3	4	5	6	7	8	9	10	11	12	13	14	15
No. Divisions	1	1	1	1	1	2	9	9	2	1	1	1	1	1	1

The initial strain distribution is, of course, the same as that shown in Fig. 8.7a. The final strain distribution for the model with 33 elements is presented in Fig. 8.8a. As can be seen, elements are added only in the critical regions of the maximum and minimum strains. This final result is contrasted to the final result for the same initial model with the 4 percent termination criterion, which is presented in Fig. 8.8b.

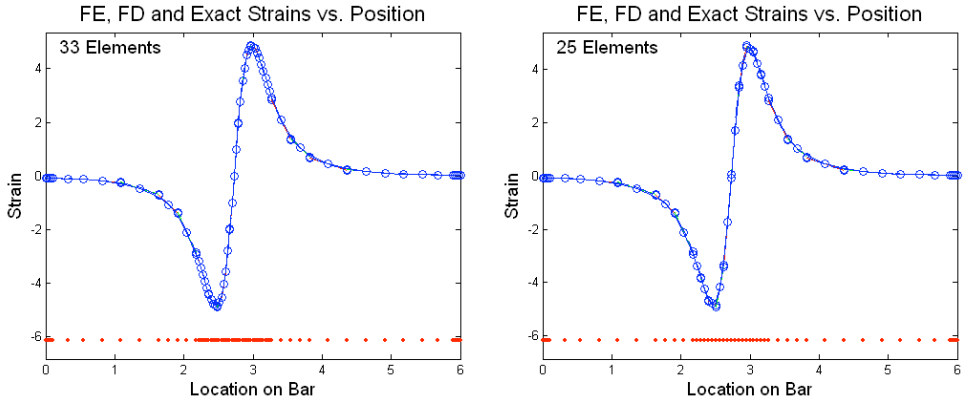

a) First Iteration and Last – 2% Error b) First Iteration and Last – 4% Error

Figure 8.8 – Refined Finite Element Models – Initially 15 Elements

The strain models for the critical points are shown with close-ups in Fig. 8.9. When these close-ups are compared to the magnified strains in the critical regions for the 25-element model shown in Fig. 8.6, the strain distributions in these regions more closely match the exact result than do the distributions for the coarser model shown in Fig. 8.6. This example has demonstrated that the refinement guides are sensitive to the termination criterion.

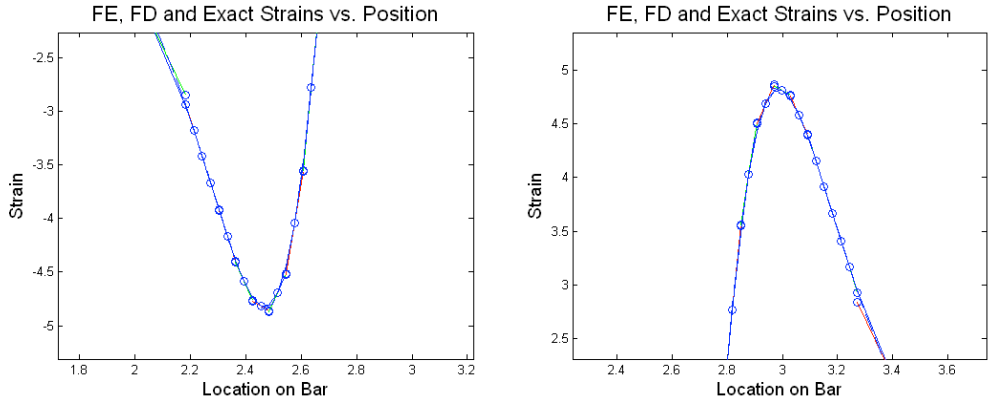

a) Minimum Strain Detail b) Maximum Strain Detail

Figure 8.9 – Strain Representations at the Extreme Points - 33 Element Model

8.6 – An Efficient Refinement Guide Based on Nodal Averaging

This Section presents and demonstrates a refinement guide that forms the smoothed solution using a simpler approach than that used in the refinement guide developed earlier. The smoothed strain representation is formed by averaging the strains at the inter-element nodes. This approach to smoothing is identical to that used in the Zienkiewicz and Zhu error estimator. Once the smoothed solution is formed, the procedure for generating this refinement guide is identical to the procedures presented in Section 8.2 and 8.3 for the refinement guide just demonstrated.

The approach presented in this Section has significant practical advantages, particularly in the case of multi-dimensional problems. When the nodal strains are found by applying a finite difference template to the nodal displacements, the locations of the nodes surrounding the point

of interest must be identified in order to form the necessary finite difference template. In the multi-dimensional case, this is **not** a minor bookkeeping problem.

In contrast, when the higher-order strain representations are formed from the average nodal strains, no such topological information is required. The nodal strain quantities for the individual elements are readily available. Similarly, the nodal coordinates of the individual elements needed to form the finite difference template at the local origin of the individual elements are part of the finite element model. As a result, the higher-order strain representation for the individual elements are readily available.

The efficacy of this approach is demonstrated by applying the refinement guide developed in this Section to the examples used earlier in the Chapter.

The strain distribution formed by connecting the averages of the nodal strain for the nine-element model evaluated earlier with straight lines is shown in Fig. 8.10a. The strain distribution formed using the finite difference templates is shown in Fig. 8.10b. As can be seen when Figs. 8.10a and 8.10b are compared, the two approaches have similarities and differences.

The two strain distributions are nearly identical when the finite element model accurately represents the exact solution. This is to be expected since both approximate solutions will converge to the exact solution in the limit. However, the averaged and the finite difference solutions can be very different when the finite element solution is highly inaccurate. The effect of this difference will be seen in the examples that follow.

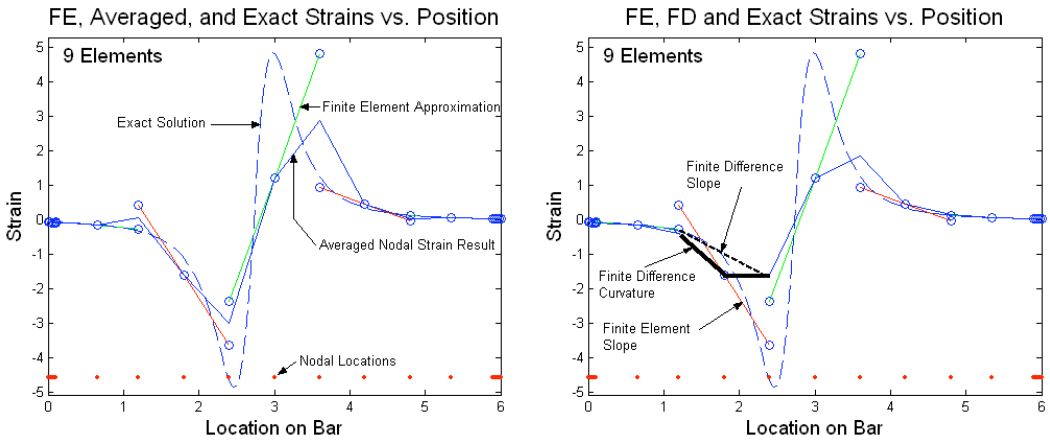

a) Averaged Nodal Strains b) Finite Difference Representation

Figure 8.10 – Smoothed Strain Comparison

When the refinement guide for the nine-element model is formed using the averaged nodal strain approach, the refinements produced by this approach are identified in Table 8.5. When the sub-divisions identified in row 2 of this table are summed, it is seen see that the refined model will contain 18 elements.

Table 8.5 – Element Subdivisions for Initial Nine-Element Model

El. No.	1	2	3	4	5	6	7	8	9
No. Divisions	1	1	2	2	4	5	1	1	1

When the results contained in Table 8.5 are compared to the refinements identified by the finite difference approach to smoothing contained in Table 8.2, which is reproduced here for the convenience of the reader, the similarities and differences just discussed can be seen.

The elements that are closely representing the exact solution at the two ends of the model are not refined or are only subdivided once. However, the elements in the center of the model that produce strain distributions that bear no resemblance to the exact solution are more highly refined with the refinement guide formed using finite difference smoothing. This iteration of the adaptive refinement process produces a model with 26 elements that satisfies the termination criterion.

Table 8.2 – Element Subdivisions for Initial Nine-Element Model

El. No.	1	2	3	4	5	6	7	8	9

No. Divisions	1	1	2	7	10	2	1	1	1

When the 18-element model identified by the refinements contained in Table 8.5 is solved, the strain distribution produced by this model is shown in Fig. 8.11a. As can be seen, there are significant inter-element jumps in the strain distribution. This model does not satisfy the termination criterion. This means that the adaptive refinement process must be applied again.

When the 18-element model is evaluated, the refinements are identified in Table 8.6. This produces a model with 22 elements. The strain distribution for this refined model is shown in Fig. 8.11b. This model does satisfy the convergence criterion. As can be seen, this refinement guide introduced new elements where they were needed.

When Fig. 8.11b is compared to Fig. 8.5b, it is seen that, although the smoothing formed using nodal averaging required two iterations of adaptive refinement, it produced an acceptable model with fewer elements.

Table 8.6 – Element Subdivisions for Initial 18-Element Model

El. No.	1	2	3	4	5	6	7	8	9	10	11	12	13	14	15	16	17	18
No. Divisions	1	1	1	1	1	2	2	2	2	1	1	1	1	1	1	1	1	1

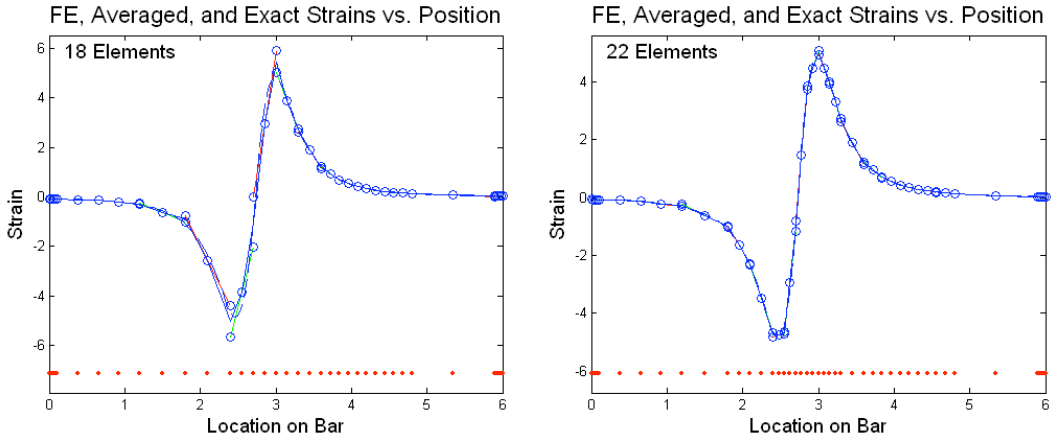

a) Initial Refinement of 9 Element Model b) Second Refinement

Figure 8.11 – Refinements of the Nine Element Model – 4% Termination Criterion

8.7 – Further Examples of the Efficient Refinement Guide

The results for refining the initial model with fifteen elements with two different termination criteria will now be presented for completeness. The initial models will be refined with termination criteria of four percent and two percent.

The strain distribution formed using the averaging approach and the finite difference approach are presented in Figs. 8.12a and 8.12b, respectively. In this case, the curvatures for the center three elements are seen to be larger for the averaged result than for the finite difference result. This observation will be verified by the difference in refinements that will be seen for the two refinement guides.

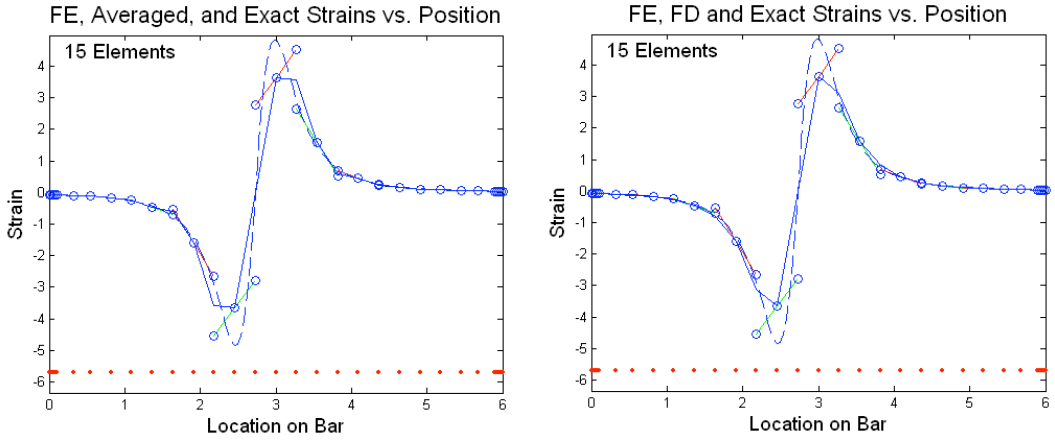

a) Averaged Nodal Strains b) Finite Difference Smoothing

Figure 8.12 – Smoothed Strain Comparison

When this initial model is refined with the nodal averaging approach and a termination criterion of 4 percent, the refinements identified for the individual elements are presented in Table 8.7. This produces a final model containing 29 elements. The strain distribution for this case is shown in Fig. 8.13a.

Table 8.7 – Element Subdivisions for Initial 15-Element Model – 4%

El. No.	1	2	3	4	5	6	7	8	9	10	11	12	13	14	15
No. Divisions	1	1	1	1	1	3	6	6	3	1	1	1	1	1	1

The adaptively refined model found using the finite difference refinement guide is presented in Fig. 8.13b. This model has 25 elements vs. 29 elements contained in the model

formed with the refinement guide based on the nodal average strains. This result is consistent with the observation made concerning the difference in the curvatures discussed with respect to Fig. 8.12, i.e., the discrete curvatures are larger for the averaged results.

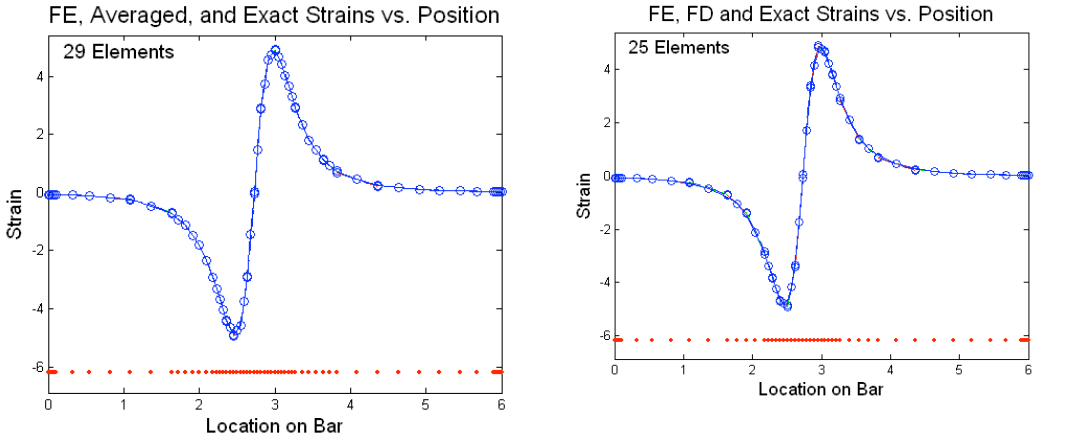

a) First and Final Refinement - Averaged b) First and Final Refinement – Finite Difference

Figure 8.13 – Refinement of the 15-Element Model – 4% Termination Criterion

When this initial model is refined with the nodal averaging approach and a termination criterion of 2%, the refinements identified for the individual elements are presented in Table 8.8. This produces a final model containing 43 elements. The strain distribution for this case is shown in Fig. 8.14a.

Table 8.8 – Element Subdivisions for Initial 15-Element Model – 2%

El. No.	1	2	3	4	5	6	7	8	9	10	11	12	13	14	15
No. Divisions	1	1	1	1	1	5	11	11	5	1	1	1	1	1	1

The adaptively refined model found using the finite difference refinement guide is presented in Fig. 8.14b. This model has 33 elements vs. 43 elements contained in the model formed with the refinement guide based on the nodal average strains. This result is consistent with the observation made concerning the difference in the curvatures discussed with respect to Fig. 8.12.

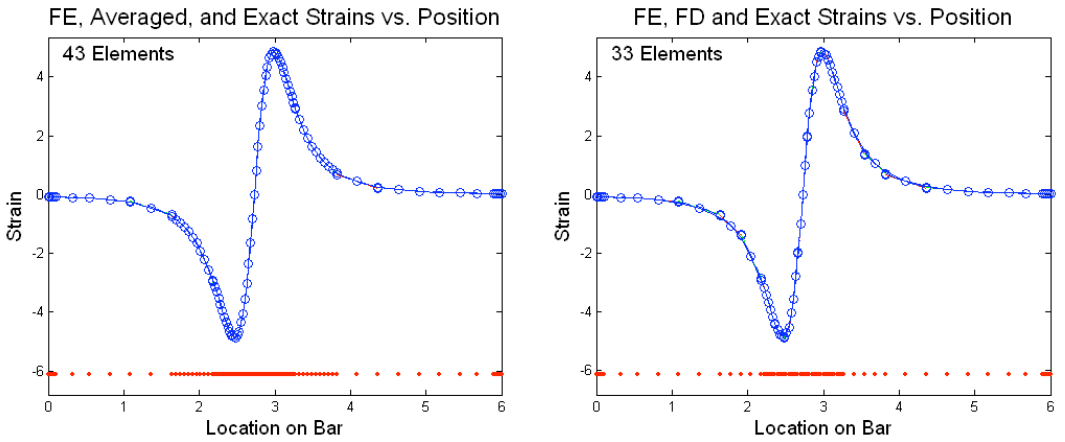

a) First and Final Refinement - Averaged b) First and Final Refinement – Finite Difference

Figure 8.14 – Refinement of the 15-Element Model – 2% Termination Criterion

8.8 - Summary and Conclusion

The development presented here forms refinement guides in a totally new way. This approach compares the modeling capability of an individual element to an approximation of a higher-order strain representation on the domain of the individual elements. The level of refinement depends on the differences between the finite element and the higher-order strain representation in the element and the termination criterion. The refinement guide attempts to identify the level of refinement needed to produce a model that satisfies the termination criterion.

This refinement guide is designed to provide a rational alternative to refinement guides that are correlated to the magnitude of the error estimator. In other words, the refinement guides developed here are based on the causes of the modeling errors and not on the effect of the errors. This, of course, means that the new approach opens the door to further developments, as is usually the case when the basic understanding of a problem emerges.

The higher-order strain representation is formed by applying finite difference templates to nodal strain quantities that differ from the strains in the finite element being evaluated. The alternate form of the nodal strains is formed in two different ways. In one approach, the nodal strains are found by applying finite difference templates to the nodal displacements of the

surrounding nodes. In the second approach, the alternate nodal strains are found by averaging the finite element strains at the nodes.

Both approaches produce rapidly converging results. The use of the averaging approach is computationally simpler, particularly for higher-dimension models.

The development of this refinement guide utilizes many of the improvements to computational mechanics that result from the use of physically interpretable notation:

1. The notation eliminates the separation between the solution technique and the problem being solved because the problem is expressed in terms of the quantities being sought in the analysis.
2. The modeling capabilities of individual elements can be identified during the formulation process.
3. The finite element and the finite difference methods can be formulated from the same basis so the finite difference method can be used to evaluate any finite element model; i.e., the finite difference method can be used to solve any problem that the finite element method can solve.

CHAPTER 9

CONCLUSION

The finite element method has evolved into a widely used and powerful technique for finding approximate solutions to the differential equations that occur in solid mechanics. In this method, a continuous problem is broken into a discrete physical representation consisting of a finite number of regions or finite elements. The equations for the discrete representation are formed by combining the stiffness matrices and the load vectors for the individual finite elements.

The process of breaking the continuum into finite regions introduces errors into the finite element approximation. These errors are called discretization errors. Discretization errors occur when the exact solution is too complex for the basis functions of the individual finite elements to represent. These errors are seen in the finite element result as inter-element jumps in the strain representation.

The objective of adaptive refinement is to iteratively reduce the level of the discretization errors below a specified limit. This is accomplished by evaluating the result for errors, by identifying any needed refinement to the finite element model if the model does not possess the desired level of accuracy and, then, modifying the finite element model in preparation for another cycle, if it is needed.

The key elements in the adaptive refinement process are the error estimator and the refinement guide. This work has developed and demonstrated improvements to both of these components of the adaptive refinement process.

The error estimator presented here is an improvement on the error estimator used in the Zienkiewicz and Zhu (ZZ) approach to adaptive refinement in two ways. The improved error estimator presented here is a pointwise quantity so its computation does not require integration, as is the case for the ZZ approach. In addition, the error estimator developed here is expressed in terms of strain components instead of strain energy. This means that the termination criterion can be expressed in terms that have specific meaning in solid mechanics. For example, this means that the termination criterion can be specified in terms of a failure criterion.

The refinement guide presented here changes the whole texture of adaptive refinement. The error estimator developed here does not define the level of refinement heuristically. That is to say, the refinement guide does not depend directly on the estimated error that is used as a termination criterion.

The refinement guide developed here is based on first principles. The modeling deficiencies in the individual elements are found by comparing an improved strain distribution to the strain distribution that actually exists in the finite element being evaluated. Then, the modeling deficiencies are related to the modeling capabilities of the element and the termination criterion to identify the level of refinement that will improve the existing finite element model.

In the case where the improved strain distribution is formed by averaging the inter-element nodal strains, the resulting error estimator can be viewed as integrating the two basic approaches to error estimation, the residual and the recovery approaches. This is the case because it is shown in this work that the inter-element jumps are directly due to the failure of the finite element solution to satisfy the governing differential equation being solved. This failure is quantified as a residual over the domain of the element. The smoothed solution, itself, can be

viewed as a component of the recovery approach. It is improved because a quantity that is directly related to the residuals in the individual elements is used to produce this improvement.

There are two distinct areas presented here that can fruitfully be extended. The rational, as opposed to heuristic, refinement guide that is developed here for one dimension can be extended to two dimensions. This work must investigate several possibilities. Can the refinement in the two directions be analyzed separately? What is a good metric for defining the refinement since three strain components are available in two dimensions?

The demonstration that the residuals and the inter-element jumps are directly related was presented for one dimension. This could be extended to two dimensions. This would be somewhat more involved for the two dimensional case. The displacements in the two directions found by the finite element analysis would have to be substituted into the governing differential equations to produce the residual quantities. The residuals must then be treated as distributed loads to form a set of equivalent nodal loads. These loads would then have to be applied to the existing finite element model. Finally, the resulting strains would have to be related to the inter-element jumps in the original problem. This result would insure that a smoothed solution formed by averaging the nodal strains would be an improved solution for the two dimensional problem.

BIBLIOGRAPHY

1. Zienkiewicz, O.C., Taylor, R.L. and Zhu, J.Z., *The Finite Element Method: Its Basis and Fundamentals*, 6th ed., Elsevier, New York, 2005.

2. Zienkiewicz, O. C. and Zhu, J. Z., "A Simple Error Estimator and Adaptive Procedure for Practical Engineering Analysis," *International Journal for Numerical Methods in Engineering*, Vol. 24, 1988, pp. 337-357.

3. Kelly, D. W., "The Self-Equilibration of Residuals and Complementary A-Posteriori Error Estimates in the Finite Element Method," *International Journal for Numerical Methods in Engineering*, Vol. 20, pp. 1491-1506, 1984.

4. Dow, J.O., Bodley, C.S. and Feng, C. C., "An Equivalent Continuum Representation of Structures Composed of Repeated Elements," AIAA/ASME/ASCE/AHS 24th Structures, Structural Dynamics and Materials Conference Proceedings, May 2-4, 1983, Lake Tahoe, Nevada, pp. 630-640.

5. Dow, J.O. and Huyer, S.A., "An Equivalent Continuum Modal Analysis Procedure for Space Station Lattice Structures," 5th International Modal Analysis Conference Proceedings, April 6-9, 1987, Imperial College of Science and Technology, London, England, Vol. II, pp.1060-1068.

6. Dow, J.O. and Huyer, S.A., "An Equivalent Continuum Analysis Procedure for Space Station Lattice Structures," AIAA/ASME/ASCE/AHS 28th Structures, Structural Dynamics and Materials Conference Proceedings, April 6-8, 1987, Monterey, Calif., Part 1, pp. 110-122.

7. Dow, J.O. and Huyer, S.A., "Continuum Models of Space Station Structures," *ASCE Journal of Aerospace Engineering*, Vol. 2, No. 4, Oct. 1989, pp. 212-230.

8. Dow, J.O. and Byrd, D.E., "The Identification and Elimination of Artificial Stiffening Errors in Finite Elements," *International Journal for Numerical Methods in Engineering*, Vol. 26, March 1988, pp. 743-762.

9. Dow, J.O. and Byrd, D.E., "The Elimination of Artificial Stiffening in Plate Elements," ASCE Engineering Mechanics Division Specialty Conference Proceedings, May 22-25, 1988, Blacksburg, VA.

10. Dow, J.O. and Byrd, D.E., "An Error Estimation Procedure for Plate Bending Problems," AIAA/ASME/ASCE/AHS 29th Structures, Structural Dynamics and Materials Conference Proceedings, April 18-20, 1988, Williamsburg, VA, Part II, pp. 901-910.

11. Dow, J.O., Harwood, S.A., Jones, M.S. and Stevenson, I., "A Finite Difference Error Analysis Procedure," AIAA/ASME/ASCE/AHS 31st Structures, Structural Dynamics

and Materials Conference Proceedings, April 2-4, 1990, Long Beach, CA, Part II, pp. 1010-1022.

12. Dow, J.O. and Byrd, D.E., "Error Estimation Procedure for Plate Bending Elements," *AIAA Journal*, Vol. 28, No. 4, April 1990, pp. 685-693.

13. Dow, J.O., Jones, M.S. and Harwood, S.A., "A Generalized Finite Difference Method for Solid Mechanics," *International Journal of Numerical Methods for Partial Differential Equations*, Vol. 6, No. 2, Summer 1990, pp. 137-152.

14. Dow, J.O., Jones, M.S. and Harwood, S.A., "A New Approach to Boundary Modeling for Finite Difference Applications in Solid Mechanics," *International Journal for Numerical Methods in Engineering*, Vol. 30, No. 1, July 1990, pp. 99-113.

15. Dow J.O., Harwood, S.A., Jones, M.S. and Stevenson, I., "Validation of a Finite Element Error Estimator," *AIAA Journal*, Vol. 29, No. 10, October 1991, pp. 1736-1742.

16. Dow, J.O., Hardaway, J.L., and Hamernik, J.D., "Combined Application of the Finite Element/Finite Difference Methods," AIAA/ASME/ ASCE/AHS 33rd Structures, Structural Dynamics and Materials Conference Proceedings, April 13-15, 1992, Dallas, TX, pp. 129-134.

17. Dow, J.O. and Hamernik, J.D., "A Point-Wise Error Estimator for Finite Element Stresses," AIAA/ASME/ASCE/AHS 33rd Structures, Structural Dynamics and Materials Conference Proceedings, April 13- 15, 1992, Dallas, TX, pp. 355-359.

18. Dow, J.O. and Hardaway, J.L., "The Validation of Finite Difference Boundary Condition Models for Solid Mechanics Applications," *AIAA Journal*, Vol. 30, No. 4, July 1992, pp. 1864-1869.

19. Dow, J.O. and Hardaway, J.L., "The Modeling of Multi-Material Interfaces in the Finite Difference Method," *International Journal of Numerical Methods for Partial Differential Equations*, Vol. 8, No. 5, Sept. 1992, pp. 493-503.

20. Dow, J.O. and Stevenson, I., "An Adaptive Refinement Procedure for the Finite Difference Method," *International Journal of Numerical Methods for Partial Differential Equations*, Vol. 8, No. 6, Nov. 1992, pp. 537-550.

21. Abdalla, J.E. and Dow, J.O., "An Error Analysis Approach for Laminated Plate Finite Element Models," *Computers and Structures*, Vol. 52, No. 4, August 1994, pp. 611-616.

22. Dow, J.O. and Abdalla, J.E., "Qualitative Errors in Laminated Composite Plate Models," *International Journal for Numerical Methods in Engineering*, Vol. 37, 1994, pp. 1215-1230.

23. Dow, J.O. and Sandor, M.J., "A Sub-Modeling Approach to Adaptive Mesh Refinement," *AIAA Journal*, Vol. 33, No. 8, August 1995, pp. 1550-1553.

24. Dow, J.O., *A Unified Approach to the Finite Element Method and Error Analysis Procedures*, Academic Press, New York, 1999.

25. Budynas, Richard G., *Advanced Strength and Applied Stress Analysis*, 2nd ed., WCB/McGraw-Hill, New York, 1999, pp. 235-238.

26. Scheid, Francis, *Numerical Analysis*, 2nd ed., McGraw-Hill, Inc, Schaum's Outline Series, 1989, p. 267.

27. Madson, J.C. and Handscomb, D.C., *Chebyshev Polynomials*, Chapman and Hall/CRC, Boca Raton, FL, 2003, p. 45.

28. Van Loan, C.F., *Introduction to Scientific Computing*, 2nd ed., Prentice-Hall, Upper Saddle River, NJ, 2000, pp. 90 – 91.

29. Siegfried, Amy K., Point-Wise Discretization Error Measures for Finite Difference Solutions, Master's Thesis, University of Colorado, 2003.

30. Hughes, Thomas, R. J., *The Finite Element Method*, Dover Publications, Mineola, NY, 2000, p. 112.

31. Argyris, J. H. and Kelsey, S., *Energy Theorems and Structural Analysis*, Butterworth, London, 1960 (originally published in a series of articles in Aircraft Engineering, 1954-55).

32. Taig, I. C., *Structural Analysis by the Matrix Displacement Method*, English Electric Aviation Report No. S017, 1961.

33. Zienkiewicz, O. C. and Zhu, J. Z., "The Superconvergent Patch Recovery and A-Posteriori Error Estimates, Parts I and II," *International Journal for Numerical Methods in Engineering*, Vol. 33, 1992, pp. 1331-1382.

34. Akin, J. E., *Finite Element Analysis with Error Estimators*, Elsevier, Oxford, 2005, Chapter 5.

35. Dow, J.O., Ho, T. H. and Cabiness, H. D., "A Generalized Finite Element Evaluation Procedure," *Journal of Structural Engineering*, ASCE, Vol. 111, No. ST2, pp. 435-452, February, 1985.

36. Van Loan, C.F., *Introduction to Scientific Computing*, 2nd ed., Prentice-Hall, Upper Saddle River, NJ, 2000, Chapter 2.